1994-03

The origins of acicular ferrite in gas metal arc and submerged arc welds

Brothers, Daniel G.

Monterey, California. Naval Postgraduate School

NAVAL POSTGRADUATE SCHOOL
Monterey, California

THESIS

THE ORIGIN OF ACICULAR FERRITE
IN
GAS METAL ARC AND SUBMERGED ARC WELDS

by

Daniel G. Brothers

March, 1994

Thesis Advisor: Alan G. Fox

Approved for public release; distribution is unlimited.

REPORT DOCUMENTATION PAGE

Form Approved OMB No. 0704

1. AGENCY USE ONLY	2. REPORT DATE	3. REPORT TYPE AND DATES COVERED
	24 March 1994	Master's Thesis

4. TITLE AND SUBTITLE THE ORIGIN OF ACICULAR FERRITE IN GAS METAL ARC AND SUBMERGED ARC WELDS

5. FUNDING NUMBERS

6. AUTHOR(S) *Brothers, Daniel Glenwood*

7. PERFORMING ORGANIZATION NAME(S) AND ADDRESS(ES)
Naval Postgraduate School
Monterey, CA 93943-5000

8. PERFORMING ORGANIZATION REPORT NUMBER

9. SPONSORING/MONITORING AGENCY NAME(S) AND ADDRESS(ES)

10. SPONSORING/MONITORING AGENCY REPORT NUMBER

11. SUPPLEMENTARY NOTES The views expressed in this thesis are those of the author and do not reflect the official policy or position of the Department of Defense or the U.S. Government.

12a. DISTRIBUTION/AVAILABILITY STATEMENT
Approved for public release; distribution is unlimited.

12b. DISTRIBUTION CODE
*A

13.

ABSTRACT The nature of weld metal inclusions in relation to the formation of acicular ferrite was investigated. Gas-metal arc welds (GMAW) on High Strength Low Alloy (HSLA) plate with varying amounts of oxygen and/or carbon dioxide added to the argon cover gas and submerged arc welds (SAW) on HY-100 plate with five different fluxes were analyzed. This analysis determined the effect of weld metal composition on non-metallic inclusion composition and the ultimate effects on the formation of acicular ferrite. Scanning and transmission electron microscopy with energy dispersive x-ray analysis were used to determine inclusion size distribution, concentration and composition. This investigation revealed that the inclusions were complex MnO-Al_2O_3-SiO_2-TiO_2 oxides which contain a titanium-rich compound, Pyrophanite ($MnTiO_3$), existing as a faceted particle in those inclusions promoting acicular ferrite formation. From these results and the research of others such as Grong/Matlock and Ramsay/Matlock/ Olson it is concluded that the formation of acicular ferrite does depend on non-metallic inclusion composition demonstrating the importance of weld wire composition for achieving welds with optimum mechanical properties.

14. SUBJECT TERMS
HY-100 steel,submerged arc welding, HSLA-100 steel, gas metal arc welding, non-metallic inclusions, acicular ferrite.

15. NUMBER OF PAGES 162

16. PRICE CODE

17. SECURITY CLASSIFICATION OF REPORT	18. SECURITY CLASSIFICATION OF THIS PAGE	19. SECURITY CLASSIFICATION OF ABSTRACT	20. LIMITATION OF ABSTRACT
Unclassified	Unclassified	Unclassified	UL

Approved for public release; distribution is unlimited.

THE ORIGINS OF ACICULAR FERRITE
IN
GAS METAL ARC AND SUBMERGED ARC WELDS

by

Daniel G. Brothers
Lieutenant Commander, United States Navy
B.S., Clarkson College of Technology, 1978

Submitted in partial fulfillment
of the requirements for the degree of

MASTER OF SCIENCE IN MECHANICAL ENGINEERING

from the

NAVAL POSTGRADUATE SCHOOL

March 1994

Author: [redacted]

Daniel G. Brothers

Approved by: [redacted]

Alan G. Fox, Thesis Advisor

[redacted]

Matthew D. Kelleher, Chairman
Department of Mechanical Engineering

ABSTRACT

The nature of weld metal inclusions in relation to the formation of acicular ferrite was investigated. Gas-metal arc welds (GMAW) on High Strength Low Alloy (HSLA) plate with varying amounts of oxygen and/or carbon dioxide added to the argon cover gas and submerged arc welds (SAW) on HY-100 plate with five different fluxes were analyzed. This analysis determined the effect of weld metal composition on non-metallic inclusion composition and the ultimate effects on the formation of acicular ferrite. Scanning and transmission electron microscopy with energy dispersive x-ray analysis were used to determine inclusion size distribution, concentration and composition. This investigation revealed that the inclusions were complex MnO-Al_2O_3-SiO_2-TiO_2 oxides which contain a titanium-rich compound, Pyrophanite ($MnTiO_3$), existing as a faceted particle in those inclusions promoting acicular ferrite formation. From these results and the research of others such as Grong/Matlock and Ramsay/Matlock/Olson it is concluded that the formation of acicular ferrite does depend on non-metallic inclusion composition demonstrating the importance of weld wire composition for achieving welds with optimum mechanical properties.

TABLE OF CONTENTS

LIST OF FIGURES

LIST OF TABLES

ACKNOWLEDGEMENT

This work could not have been completed without the assistance and support of my fellow students and the faculty of the Naval Postgraduate School. Much of the credit and a special thank you goes to my wife, Linda, and family for their support during the many long days of research and writing. Final credits go to Professor Alan Fox for his many hours of support, valuable assistance and for being an excellent sounding board for new ideas.

I. INTRODUCTION

The U.S. Navy's desire to certify high strength low alloy (HSLA) steels for shipbuilding programs has led to significant research to develop welding consumables that produce weld metal deposits with mechanical properties equivalent to the base metal. The bulk of this research has concentrated on achievement of weld metal deposits with maximum toughness and ductility for a desired strength by controlling weld metal microstructure. A microstructure consisting primarily of acicular ferrite provides the optimum weld metal strength and ductility by virtue of its small grain size and high angle grain boundaries. This microstructure of acicular ferrite is also desirable in the weld deposits of other steels, such as HY-100, used in Naval construction programs.

Recent research at the Naval Postgraduate School in Monterey, California has dealt primarily with how different fluxes in submerged arc (SA) welds or different cover gases in gas metal arc (GMA) welds have influenced the size distribution, concentration and composition of non-metallic inclusions in the weld metal and the effects of this on the weld metal mechanical properties. This research did not include an analysis of how the final weld metal composition affects the non-metallic inclusions, formation of acicular ferrite and ultimately the mechanical properties of the weld.

This analysis is necessary to reach the final goal of predicting weld metal mechanical properties by controlling weld metal composition through use of different fluxes or cover gases to control size distribution, concentration and composition of non-metallic inclusions to get the desired final microstructure of acicular ferrite.

This investigation uses weld metal deposits from GMA welds on HSLA-100 plate and SA welds on HY-100 plate to determine those characteristics of non-metallic inclusions that promote formation of acicular ferrite. Different fluxes and cover gasses were used to control weld metal composition. By determining which weld metal compositions optimize acicular ferrite formation the flux or cover gas can be optimised to obtain welds with desired mechanical properties.

II. BACKGROUND

A. CHARACTERISTICS OF HIGH YIELD (HY-100) STEELS

High yield (HY) steels are used in Naval construction programs because of high strength and good fracture toughness properties. HY-100 steel is a quenched and tempered martensitic steel with strength and toughness optimized through heat treatments and alloying. Carbon combined with other alloys such as chromium, manganese, molybdenum, nickel and vanadium are added to increase strength and hardenability. Composition specifications and nominal compositions are listed in Table 2.1. Heat treatments consist of austentizing at temperatures between 1550 to 1650 °F, water quenching and tempering near 1150 °F to precipitate carbides and stress relieve the martensitic microstructure.

Welding of HY-100 steel is difficult because the heat affected zone (HAZ) of the weld can vary between martensitic and bainitic microstructures for small changes in composition and/or cooling rates. This places significant limitations on plate thickness, interpass temperatures and heat input for welds to ensure that desired mechanical properties are achieved. Mechanical properties limits are listed in Table 2.2. HY-100 steel is also highly susceptible to hydrogen induced cracking (HIC). These welding limitations require

carefully controlled and costly preheat and postheat treatments to avoid HIC and ensure the desired microstructure is obtained.

B. CHARACTERISTICS OF HIGH STRENGTH LOW ALLOY (HSLA-100) STEEL

High strength low alloy (HSLA) steels provide an attractive alternative for Naval construction programs that results in lower fabrication costs and higher productivity. HSLA-80 steels were certified in the 1980's for surface ship structural applications and is currently used in CG-47 and DDG-51 class ship construction. A certification program for HSLA-100 steel is currently in progress.

Lower carbon HSLA-100 steel achieves its high strength through copper precipitation strengthening, grain refinement and solid solution strengthening. Alloying with elements such as chromium, manganese, molybdenum and nickel is used to raise the equivalent carbon content to the same level as HY steels thus improving hardenability. Specifications and nominal compositions of HSLA-100 steel are listed in Table 2.1. Mechanical properties have the same limits as the HY-100 steel listed in Table 2.2.

HSLA-100 steel has two significant advantages over HY-100 steel. The low carbon content of HSLA-100 steel ensures that it is not susceptible to HIC at any value of carbon equivalence. The Graville diagram in Figure 2.1 is an

illustration of the improved weldability of HSLA-100 steel. Additionally, the HAZ microstructure of HSLA-100 steel is not as susceptible to changes in microstructure from martensite to bainite for changes in cooling rate. This allows welding without costly preheat and postheat treatments lowering fabrication costs and improving productivity.

C. SUBMERGED ARC WELDING

Submerged arc welding (SAW) is an arc welding process in which metal joining is accomplished by heating with an arc between a bare consumable electrode and the workpiece. The arc and the welding area are shielded from the atmosphere by a blanket of granular, fusible material (flux) placed over the welding area ahead of the mechanized electrode. This granular flux is primarily composed of oxides, which when molten cleans the weld metal of impurities which then rise to the surface of the weld pool as slag. This slag acts both to protect the weld pool from atmospheric contaminants and to reduce heat losses thus refining the weld metal. With the flux covering the arc, high arc currents (900 amps or higher) can be used without getting a violent arc which leads to a high deposition rate. The slag also reduces heat losses to the surroundings thus increasing the efficiency of the welding process. SAW weldments are limited to flat position welding and circumferential welding (of pipes) due to relatively large

volumes of molten slag and weld pool. Figure 2.2 shows the setup for a typical submerged arc weld. [Kou, 1987]

The weld metal composition of a SAW weldment is controlled by either controlling the heat input of the weld thus affecting the dilution from the base metal or by adding alloying elements via the filler wire or the flux. Heat input is closely controlled in both root pass and other passes of HY-100 SAW weldments to minimize the dilution of carbon from the base plate, thereby limiting the likelihood of hydrogen induced cracking (HIC). A simple measure of heat input (HI) is given by:

HI = (weld current x weld voltage) / weld speed

Heat input directly affects the weld pool cooling rate which can change the final microstructure of the weld metal. Therefore small changes in weld current or voltage can adversely affect weld mechanical properties.

In general, proper weld metal chemical composition is obtained in SAW weldments by using mild steel (low carbon content) filler wire with an alloyed flux or an alloyed filler wire with a neutral flux. If an alloy flux is used, the efficiency of alloy transfer from the flux to the weld deposit will vary with the arc voltage [Flax, 1971]. In HY-100 steel welds the composition of the weld filler wire is closely controlled to ensure the weld metal chemistry stays within specifications. Required electrode chemistry from MIL-E-23765 is given in Table 2.3.

Another feature of the chosen flux, besides alloying, is its ability to maintain low oxygen levels in the weld metal. High oxygen levels in the weld metal, introduced from the oxides in the flux, can result in porosity which is undesirable from a strength and fracture toughness aspect. An optimum flux chemistry prevents porosity but leaves sufficient oxygen (typically 250 - 350 ppm) to form a quantity of non-metallic inclusions in the matrix to provide strength and fracture toughness by changing the final microstructure to acicular ferrite. Previous research shows basic fluxes are more effective at reducing oxygen in the weld metal than acidic fluxes. High basicity fluxes, however, are not chemically neutral and therefore alter the weld metal chemistry through slag - metal interactions. Basicity index (BI), which is a ratio of the basic oxides to the non-basic oxides, is a measure of the fluxe's ability to deoxidize the weld metal. Although several different expressions have been developed to define BI, a general equation is given as:

$$BI = \Sigma(\%\ \text{basic oxides}) \ / \ \Sigma(\%\ \text{non-basic oxides}).$$

Controlling the microstructure and mechanical properties of SAW weldments is a complicated process. The magnitude of heat input affects solidification, austentization, quenching, tempering and hydrogen diffusion as seen by changes in the position of the continuous cooling transformation (CCT) curves. The choice of flux affects the final microstructure and composition of the weld metal and ultimately the

mechanical properties of the weld. All these factors and others must be carefully considered when performing submerged arc welds.

D. GAS METAL ARC WELDING

Gas metal arc welding (GMAW), also known as metal inert gas (MIG) welding, is an electric arc welding process accomplished by heating with an arc established between a continuous filler wire (consumable) electrode and the workpiece. The arc and the welding area are shielded from the atmosphere by using an inert cover gas such as argon or helium. To maintain a stable arc, reactive gases such as carbon dioxide or oxygen, are added in small quantities to the cover gas. Direct-current reverse polarity (electrode positive) is used for most applications for stable arc, smooth metal transfer with low splatter and good weld penetration. [Kou, 1987] Figure 2.3 shows the setup for a typical gas metal arc weld.

Three basic types of metal transfer can occur in the GMAW process. In short-circuiting transfer, the filler metal is transferred to the weld pool by direct contact. In either globular or spray transfer, discrete metal drops travel across the arc gap under influence of gravity and/or electromagnetic forces. The mode of metal transfer is determined by the magnitude of welding current, size of the electrode and composition of the shielding gas. [Kou, 1987]

Unlike the SAW process, welding current for a GMAW weldment is much less, typically in the range of 100 to 400 amps. The molten weld pool is exposed to the cover gas therefore weld pool heat losses are higher with resulting weld efficiency lower than SAW. These factors limit heat input to the weld with resulting lower deposition rates as compared to SAW. Control of weld metal chemical composition is obtained by addition of alloying elements to the filler wire.

The addition of reactive gases such as carbon dioxide or oxygen to the cover gas for arc stabilization, results in oxygen dissolving into the molten weld metal and oxidization of some alloying elements. These oxides are lighter than the molten metal and float to the surface of the cooling weld pool, forming a slag. This slag does not protect the weld pool from atmospheric contaminants or reduce heat losses as in SAW. Some of these oxides become trapped in the weld metal as non-metallic inclusions. Large amounts of oxygen in the weld metal can adversely affect the mechanical properties of the weld in two ways. As oxygen forms with strong deoxidizers in the weld metal such as manganese (Mn), silicon (Si) or titanium (Ti) strength and/or fracture toughness can be reduced as the final microstructure is changed. Secondly, a large amount of dissolved oxygen can combine with carbon to produce carbon monoxide in the molten metal which creates porosity, again reducing strength and fracture toughness. By controlling weld metal oxygen levels to a range of 250 to 400 ppm, porosity can

be avoided and non-metallic inclusions are formed which can be beneficial to fracture toughness and strength by promoting the formation of acicular ferrite in the final weld metal microstructure. Strong deoxidizers such as Mn, Si, Ti and aluminum (Al) are added to the filler wire to prevent loss of alloy concentration and limit oxygen levels in the weld metal.

Final weld metal composition is the result of base metal, welding wire and cover gas compositions. Changes in heat input (such as weld current or weld speed) or cover gas composition can change weld metal composition affecting non-metallic inclusion size, shape, distribution and composition which change final weld metal microstructure and ultimately weld mechanical properties.

E. WELD POOL REACTIONS AND COOLING RATE

Weld metal composition is controlled by chemical reactions occurring in the weld pool at elevated temperatures. It is influenced by the choice of welding consumables (filler metal, flux, cover gas), base metal chemistry and operational conditions of the weld. Chemical interactions between the molten metal and the surroundings (atmosphere, slag) exhibit strong non-isothermal behavior, with reactions taking place within seconds in a small volume where temperature gradients on the order of 1000 K/mm and cooling rates of 1000 K/sec exist. Figure 2.4 is a schematic representation of the complex thermal cycle experienced by the liquid metal during transfer

from the electrode to the weld pool in GMAW. Additionally a lack of adequate thermodynamic data for the complex slag - metal reaction exists. However, within these restrictions, the development of weld metal compositions can be modeled using the basic principles of deoxidation. [Grong, 1986]

Grong and Christensen modeled the weld pool during arc welding as a simplified two-stage reaction for chemical interactions which assumes:

- a high temperature stage where at least some of the reactions approach a state of local equilibrium,
- a cooling stage, where the concentrations established during the initial stage tend to readjust by precipitation of new phases.

The high temperature stage comprises both gas - metal and slag - metal interactions occurring at the electrode tip, in the hot part of the weld pool beneath the root of the arc (temperature range 1600 to 2400 °C). The second stage starts following the passage of the arc and is characterized by deoxidation reactions (i.e. precipitation of non-metallic inclusions). [Grong, 1986]

Partial oxidation of the weld metal occurs as oxygen from the cover gas in GMAW or the flux in SAW reacts rapidly due to high temperatures and large interfacial contact area for interactions. The rate controlling step in weld metal deoxidation is the removal of the inclusion from the weld pool because of the limited time available for separation of the precipitated particles. Based on research by Grong and

Christensen it is concluded that final concentrations of oxygen, silicon and manganese in GMAW weldments are controlled by reactions in the hot part of the weld pool. From this conclusion it follows that all inclusions formed at temperatures below 1800 °C are trapped in the weld metal. [Grong, 1986]

A characteristic feature of the weld pool model is that the temperature does not appear to vary with time when observed from a point located in the heat source. A graphical representation of the temperature field around the moving source is given in Figure 2.5 [Grong, 1986]. This figure shows that temperatures in the forward part of the weld pool increase rapidly to a peak of about 2000 °C and characteristic temperature ranges where specific chemical and physical reactions occur during cooling. Since the retention time at a given temperature depends on the applied operational conditions, a change in heat input (HI) will not only effect the cooling rate through the critical temperature range during the austenite to ferrite transformation, but also influences the weld metal chemical composition, inclusion size distribution, solidification microstructure and prior austenite grain size [Grong, 1986]. A formula to determine the cooling rate based on heat input is given by:

$$CR = A\ (T-T_0)^2\ /\ HI$$

where A is a constant, T is the instantaneous temperature and T_0 is the base metal temperature [Kettel, 1993].

For welding of steel the cooling time from 800 to 500 °C ($dt_{8/5}$) is accepted as an adequate index for the thermal conditions under which the austenite to ferrite transformation occurs. This cooling time can be approximated by the equation:

$$dt_{8/5} \approx 5\ n\ E$$

where n is the welding efficiency (n = .6 to .8 for GMAW, n = .95 for SAW) and E is the gross heat input in KJ/mm (as given for HI previously). [Grong, 1986]

In actuality $dt_{8/5}$ depends on many factors including plate thickness and thermal conductivity. The microstructure formed after the austenite to ferrite transformation is directly related to the cooling time from 800 to 500 °C. Depending on the weld metal composition, the microstructure changes from martensite and/or bainite for $dt_{8/5}$ less than five seconds to acicular ferrite for $dt_{8/5}$ just greater than five seconds to other types of ferrite and pearlite as $dt_{8/5}$ increases to 100 seconds. [Grong, 1986]

F. NON-METALLIC INCLUSIONS

Non-metallic inclusions found distributed throughout high strength steel welds are the result of deoxidation and/or desulphurization reactions taking place within the weld pool [Court, 1985]. Extensive research during the past two decades has shown these inclusions, typically 0.2 to 2.0 microns in diameter, play an important role in determining the final microstructure of the weld metal. Of particular interest is

the role of these inclusions on the nucleation of acicular ferrite which is the microstructure generally accepted as the best for optimizing strength and fracture toughness.

1. Sources

Two types of inclusions are commonly found in steel weldments, exogenous or indigenous. Exogenous inclusions occur due to entrapment of welding slag and surface scale. These inclusions are always detrimental to the mechanical properties of the weld. Of significantly more importance for control of weld metal mechanical properties are indigenous inclusions. These inclusions are formed as a result of deoxidation reactions (oxides) or solid state precipitation reactions (nitrides, carbides). They are almost always heterogeneous in nature both with respect to chemistry (multiphase), shape and crystallographic properties as a result of the complex alloying systems involved [Haddock, 1988].

2. Size Distribution

As compared to normal cast steel, non-metallic inclusions in steel welds have a much larger number of inclusions that are smaller in size. This is due to the limited time during the weld pool solidification for growth and separation of the particles. A major factor in determining inclusion size in SAW weldments is flux basicity [Grong, 1986]. However variations in weld metal composition and weld heat input also strongly influence the inclusion size

distribution. The effects of heat input on inclusion size distribution are seen in the larger inclusions found in SAW weldments (high heat input) as compared to GMAW weldments (low heat input). This is attributed to the slower cooling rate for higher heat input allowing more time for growth of the inclusions.

3. **Oxygen**

Oxygen is introduced into the weld pool from the cover gas in GMAW and from the flux in SAW. This oxygen forms with the deoxidizers present in the weld pool and due to the short time involved for weld pool solidification, many become trapped. Large inclusions (> 2 micron) have an adverse affect on weld metal fracture toughness by acting as crack initiators and propagators. However, oxides in the form of small inclusions may affect the final microstructure in ways that are beneficial for weld metal mechanical properties.

For high weld metal oxygen concentrations (> 600 ppm), a large number of small inclusions (0.1 to 0.2 microns) form in the weld metal which effectively pin the prior austenite grain boundaries and restrict grain growth. The fine austenite grains give a large surface area to volume ratio providing more grain boundaries which promote ferrite nucleation at the grain boundaries. Grain boundary ferrite is not desirable in the weld metal from a strength and fracture toughness standpoint.

At low levels of weld metal oxygen (< 200 ppm) there is insufficient oxygen to form a large number of inclusions. Based on weld metal composition and cooling rate bainitic and/or martensitic microstructures are likely. While these microstructures provide good strength characteristics, fracture toughness is much less than for an acicular ferrite microstructure.

Medium concentrations of oxygen (250 to 400 ppm) in the weld metal can create a size and distribution of non-metallic inclusions that is optimum for formation of acicular ferrite. These inclusions are large enough (0.3 to 1.0 microns) such that austenite grain boundaries are not pinned and the inclusions are overgrown by the austenite grains leaving them intragranular. These intragranular inclusions provide the initial nucleation sites for acicular ferrite. An optimum size distribution results in an optimum inclusion density within the austenite grains controlling both the volume fraction of grain boundary ferrite and acicular ferrite. The optimum size distribution would lie somewhere between the curves for high and low weld deposit oxygen shown in Figure 2.7 [Olson, 1990].

4. Deoxidizers

High levels of oxygen in the weld metal are detrimental to strength and fracture toughness due to porosity

and adverse affects on the final microstructure. To control weld metal oxygen concentration and prevent loss of alloys from the base metal, deoxidizers are added to the weld metal from the weld wire and/or the flux. These elements combine with the oxygen to form oxides that float to the top of the molten weld pool as slag. Those oxides unable to float out of the weld pool due to the rapid solidification become trapped and form the non-metallic inclusions that can be beneficial for weld mechanical properties. The combination of deoxidizers used can significantly affect the inclusion size distribution and the ability of the inclusions to act as nucleation sites for acicular ferrite.

The roles of metal deoxidants and the molten slag - metal interface in the formation of inclusions are relatively well understood for the near equilibrium case of molten steel. Using thermodynamic data and/or quartenary and ternary phase diagrams steel makers are able to predict inclusion composition [Philbrook, 1977]. Using a simple model, assuming only a single deoxidizing agent exists, the reaction equilibrium constant (K) can be calculated as:

$$K = \{a(M) \times a(O)\}^{-1}$$

where a(M) and a(O) are the oxide activities. Assuming low alloy steels the activities could be considered as equivalent to their weight percent (wt-%) changing the equation to:

$$K = \{(\%M) \times (\%O)\}^{-1}$$

Figure 2.6 could now be used to predict the phases in the inclusion based on weld metal chemical composition. In the actual case of multiple deoxidizers the activities would require corrections by using interaction coefficients which are based on equilibrium conditions. [Harding, 1986]

In the non-equilibrium conditions in the weld pool, where melting and solidification are rapid, these reactions are much more complex. Additionally for SAW weldments there is considerable debate on slag - metal interactions and the release of oxygen and metal ions in the molten weld pool [Dowling, 1986]. Consequently a model for predicting the origins and phases of weld metal inclusions has not been developed. This requires that any discussion of inclusion composition be based on qualitative analysis of experimental data. The effects of the most common deoxidizers are discussed below.

a. Aluminum

Of the elements added to the weld metal for control of weld metal oxygen, aluminum is the most reactive. The beneficial effects of aluminum containing inclusions on the formation of acicular ferrite have been observed by many researchers [Saggese 1983, Bhatti 1984]. The work of Bhatti suggests that those inclusions that contain large amounts of aluminum are efficient acicular ferrite nucleation sites. More recent work by Terashima and Hart shows that aluminum in high

concentrations in the weld metal has a detrimental effect on weld metal properties if oxygen levels are low, as a shift from acicular ferrite to ferrite with aligned second phases occurs [Terashima, 1984]. An important result of Terashima's research is that an optimum inclusion field for formation of acicular ferrite existed if the ratio of [wt-% AL]/[wt-% O]^2 equals 28. Figure 2.8 clearly shows how the inclusion size and density varies with this ratio and the effect on fracture toughness as the amount of acicular ferrite in the final microstructure changes [Terashima, 1984]. As this ratio increases above 28, inclusion diameter increases due to clustering and the inclusion density decreases rapidly, resulting in a shift from an acicular ferrite microstructure [Grong, 1986].

b. Titanium

Titanium is the second most effective deoxidizer added to the weld metal. At high concentrations of aluminum in the weld metal, titanium seems to have little or no effect on the ability of an inclusion to nucleate acicular ferrite. However, at low weld metal aluminum concentrations, titanium seems to play an active role in nucleation of acicular ferrite [Grong, 1986]. Saggese shows in his research that high volume fractions of acicular ferrite are always achieved when sufficient amounts of titanium are in the weld metal, irrespective of aluminum content (Figure 2.9) [Saggese, 1983].

Titanium in very high concentrations (typically > 0.05 wt-%) can lead to deterioration in fracture toughness caused by precipitation of finely dispersed coherent TiN particles in the ferrite which overshadows the beneficial effects of titanium on the gross microstructure.

c. Silicon

Silicon is added to high strength metals as a solid solution strengthener. Silicon lowers the austenite to ferrite transformation temperature which increases hardenability. Silicon is also an effective deoxidizer. Another beneficial aspect of silicon is that it increases the fluidity of the molten weld pool allowing oxides scavenged in the weld pool to more easily escape to the surface [Shackleton, 1972].

In general silicon is considered detrimental to the fracture toughness even in small concentrations as a result of the formation of martensite and/or austenite microphases and an increase in weld strength level. This tends to overshadow any beneficial effects that silicon has on the development of an acicular ferrite microstructure [Grong, 1986]. However, as silicon levels are lowered to levels less than 0.5 wt-% some improvements in weld metal fracture toughness are achieved. In GMAW weldments a correlation between decreasing inclusion volume fraction and an increase in the [wt-% Mn]/[wt-% Si] ratio in the weld metal has been observed. This observation indicates that increasing silicon concentration at a constant

manganese concentration increases the inclusion volume fraction which can improve weld metal mechanical properties. [Abson, 1986]

Although the effects of silicon are complex, optimum silicon contents for SAW weldments appear to lie in a range of 0.2 to 0.5 wt-% [Abson, 1986]. The low figure is appropriate for weld deposits with low oxygen and/or high aluminum. The high figure is appropriate for weld deposits of high oxygen and/or low aluminum. For GMAW weldments silicon levels near 0.3 wt-% are acceptable.

d. Manganese

After carbon, manganese is probably the most important alloying element used to increase strength and hardenability of high strength steels. As an austenite stabilizer, manganese lowers the austenite to ferrite transformation temperature which tends to promote the formation of acicular ferrite in the weld metal as well as a general refinement of the microstructure. Although a weak deoxidizer, the concentration of manganese in the weld metal is normally much higher than the other deoxidizers allowing it to take part in the deoxidation process. Manganese also acts as a solid solution strengthener allowing a reduction in carbon content while maintaining high strength. Thus manganese is normally found in the base metal in excess of 1.0 wt-% and

is added to the filler wire or the flux to prevent loss of strength due to the oxidation process.

Besides its contribution to strength and deoxidation, manganese is also important for desulphurizing the weld metal. By precipitating MnS vice FeS, the tendency for hot crack formation along grain boundaries is eliminated. This is accomplished by maintaining a ratio of [wt-% Mn]/[wt-% S] greater than 50. [Grong, 1986]

Manganese generally has a greater strengthening effect in weld metals than can be accounted for simply in terms of solid solution hardening [Abson, 1986]. Research by Evans demonstrated that the amount of manganese in the weld metal is critical for obtaining maximum amounts of acicular ferrite. At low manganese concentrations (< 1.0 wt-%), with other conditions optimized, only 30 % acicular ferrite was achieved. At manganese concentrations of 1.35 to 1.8 wt-% the amount of acicular ferrite in the weld metal was increased to 75 % [Evans, 1993]. This increase in acicular ferrite is probably due to the increased hardenability from the increased manganese which lowers the austenite to ferrite transformation temperature to a value optimum for acicular ferrite formation. Other research [Bhatti 1984, Dowling 1986] shows that a strong manganese dependence with aluminum and titanium exists for forming inclusions that promote the formation of acicular ferrite.

5. Inclusion Composition

The affect of inclusion composition on the formation of acicular ferrite is unclear. Early researchers [Dolby 1976, Kirkwood 1978, Abson 1978, Pargeter 1981] believed the controlling factors in determining the effectiveness of inclusions as nucleants were volume fraction and size distribution. Others [Farrar 1979, Harrison 1981] concentrated on the indirect effect that inclusion chemistry may have on hardenability, with the view that acicular ferrite developed based on manganese concentration exceeding 1.1 wt-%. More recent research [Bhatti 1984, Ramsey 1988, Evans 1993] shows that inclusion chemical composition is an important factor for nucleation of acicular ferrite. Since all these factors appear to have some affect on the nucleation of acicular ferrite the exact mechanism for nucleation of acicular ferrite is clearly not well understood. [Bhatti, 1984]

Multiple phases have been identified in most inclusions. Of these phases the most prominent are a titanium rich phase, aluminum manganese phase, manganese sulfide phase and a silica phase [Dowling, 1986]. Separation of the diffraction patterns obtained from the TEM for the multiple phases is a difficult process. Therefore multiple combinations of these phases may exist. For this reason the MnO-Al_2O_3-SiO_2 ternary diagram is often used for assessing the inclusion composition. Since a titanium rich phase also exists a quaternary phase diagram containing TiO_2 would be appropriate

for evaluation. A literature review has failed to show the existence of this phase diagram.

Although diffraction information is inconclusive, significant information has been gained from research of inclusion composition. TEM analysis of carbon replica samples by Ramsey and Bhatti in different research projects has shown that acicular ferrite only nucleates on inclusions that have at least one flat or faceted face. This face appears in inclusions that are either rich in titanium (>10 %) or inclusions that contain more aluminum than manganese. Although manganese appears to be an important component for inclusion formation, it produces a spherical smooth inclusion that does not appear to nucleate acicular ferrite. Bhatti found that maintaining weld metal composition such that the ratio of [wt-% Mn]/[wt-%Al] (in the inclusions) less than 0.24 formed inclusions rich in aluminum which promoted formation of acicular ferrite [Bhatti, 1984]. Evans found that manganese levels above 1.35 wt-% were optimum for acicular ferrite, but the amount of acicular ferrite formed became sensitive to the amount of titanium present as manganese concentration in the weld metal increased above 1.0 wt-% [Evans, 1993]. In both these research projects the weld metal contained only significant amounts of titanium or aluminum but not both. Ramsey, working with weld metal low in both titanium ($\leq$ 0.011 wt-%) and low in aluminum ($\leq$ 0.009 wt-%) found that inclusions formed only on faceted inclusions but could make no conclusion

on required aluminum or titanium concentrations. Peters, using auger analysis on a SEM, determined that the titanium phase in the inclusions was TiN. While possible, there is ample evidence that the titanium phase in the inclusions is more likely a titanium oxide.

Based on these observations it can be concluded that the composition of the inclusion is important for nucleation of acicular ferrite. Inclusions must be rich in aluminum or titanium to form inclusions with flat faces which act as nucleation sites for acicular ferrite. Aluminum concentrations of 0.025 to 0.035 wt-% were adequate for formation of good inclusions with titanium concentrations less than 0.005 wt-% or concentrations of 0.030 wt-% of titanium are adequate regardless of aluminum concentration. Therefore if the other factors for acicular ferrite formation are met then maintaining weld metal composition with a combined (wt-% Al) + (wt-% Ti) equal to 0.03 should be adequate to form non-metallic inclusions which will nucleate acicular ferrite.

G. ACICULAR FERRITE

A weld that achieves both strength and fracture toughness equivalent to the base metal is desirable. The formation of large proportions of upper bainite, martensite,ferrite side plates or grain boundary ferrite is detrimental to fracture toughness since these microstructures provide preferential crack propagation paths. By virtue of its small grain size

(typically 1 to 3 micron) and high angle grain boundaries, a microstructure of acicular ferrite slows crack propagation and optimizes both strength and fracture toughness. Figure 2.10 shows how acicular ferrite inhibits crack growth better in acicular ferrite as compared to bainite and/or martensite. Since a microstructure of acicular ferrite optimizes weld metal mechanical properties, welding consumables and procedures are designed to maximize the proportion of final microstructure that is acicular ferrite.

Acicular ferrite is a phase formed by the transformation of austenite during cooling of the weld deposit. It forms in a temperature range where diffusional transformations become relatively sluggish and displacive transformations such as Widmanstatten ferrite, bainite and martensite dominate [Yang,1989]. Its morphology consists of non-parallel plates of ferrite, nucleated intragranularly on inclusions in the coarse austenite grains. Multiple plates can nucleate on a single inclusion and subsequent plates can nucleate sympathetically on inclusion nucleated plates creating the basketweave pattern that identifies acicular ferrite.

The mechanism for transformation of acicular ferrite is not well understood, however, its formation seems to depend on complex interactions between several variables such as:

- total weld metal alloy content
- concentration, chemical composition, and size distribution of non-metallic inclusions

- prior austenite grain size
- weld thermal cycle.

Each of these variables are complex and are discussed in more detail. [Grong, 1986]

1. Total Alloy Content

Alloying elements present in the weld metal are introduced through the filler wire and/or flux or from dilution of the base metal. Additions of alloys serve to ensure desired strength requirements by solid solution or precipitation strengthening or control of the microstructure by modifying the austenite to ferrite transformation temperature. The ability of an alloy to accomplish these goals is often measured by a steels hardenability. When many alloys are used the carbon equivalence is used as a hardenability index, ranking the influence of the various alloy elements on the steel transformation behavior relative to carbon [Grong, 1986]. Although the carbon equivalents were originally developed to evaluate base metal cold cracking susceptibility, they also prove useful to clarify the complex relationships between weld metal composition and the resulting transformation behavior of the weld deposit. A number of carbon equivalent (CE) have been developed with frequently used equations by Graville (see Figure 2.1) and the Ito-Bessyo equivalent given by:

$$P_{CM} = C + (Mn+Cr+Cu)/20 + Si/30 + V/10 + Mo/15 + Ni/60 + 5B$$

where the value of each of the elements is given in weight percent [Grong, 1986].

Figure 2.11 shows that the effect of increasing carbon equivalence, and thereby increasing the hardenability, is to shift the continuous cooling curves to the right. This lowers the austenite to ferrite transformation temperature promoting higher strength microstructures for a given cooling rate [Olson, 1990]. Transformation temperatures less than 500 °C favor bainite or martensite microstructures. Transformation temperatures greater than 650 °C favor ferrite side plates or grain boundary ferrite as the transformation temperature continues to increase. To optimize hardenability for the formation of acicular ferrite the carbon equivalence should be at a medium level with transformation temperatures in the range of 500 to 650 °C. [Abson,1986] This clearly shows why controlling the amount of manganese is important to the formation of acicular ferrite. Note that the above analysis assumes that the other variables are also optimized for formation of acicular ferrite.

2. Non-metallic inclusions

a. Qualitative Analysis

The details of non-metallic inclusions were discussed in the previous section. This discussion will concentrate on a qualitative analysis of previous research as it pertains to the formation of acicular ferrite. To maximize

the opportunity for formation of large proportions of acicular ferrite in the weld metal optimum non-metallic inclusion concentration, composition and size distribution must be obtained.

The concentration of inclusions includes both the volume fraction and the distribution of the inclusions. If the volume fraction of inclusions is small, then although ferrite may nucleate on the inclusion, it will not achieve the small basket-weave pattern associated with acicular ferrite. If the distribution is not uniform, clustering of the inclusions exists, then the formation of acicular ferrite will be localized and the proportion of the weld metal with an acicular ferrite microstructure is reduced.

Large inclusions (> 2 microns) act to degrade the fracture toughness of the weld by acting as crack initiators and/or propagators. Large numbers of small inclusions (<0.2 microns) tend to pin prior austenite grain boundaries promoting the formation of grain boundary morphologies rather than acicular ferrite. Typically inclusion size distributions that have many smaller inclusions, but greater than 0.1 micron, with an average inclusion size near 0.5 microns seem to be the best to promote the formation of acicular ferrite.

As previously discussed, the composition of the inclusions is also important for nucleating acicular ferrite. TEM analysis of samples from different steels and welding processes has shown that acicular ferrite nucleates only on

inclusions that form with one or more flat or faceted faces. Only those inclusions that have an adequate amount of titanium rich or aluminum rich phases meet this requirement.

A qualitative analysis of previous research indicates that an optimum inclusion field is obtained through control of weld metal chemical composition. In general, to form an optimum inclusion field the amount of five elements, oxygen, manganese, silicon, aluminum and titanium, must be controlled. Oxygen in the weld metal must be in the range of 250 to 400 ppm to control inclusion size distribution. Manganese concentrations must be greater than one percent such that when combined with 0.3 percent silicon the correct hardenability for a transformation temperature near 600 °C exists. If a combination of aluminum plus titanium concentration is 300 to 400 ppm then the inclusions will have faceted edges as required to nucleate acicular ferrite.

b. Nucleation Mechanisms

Three mechanisms for acicular ferrite nucleation at the inclusions have been proposed. All three mechanisms are based on the classical theory of heterogeneous nucleation, nucleation by low mismatch interfaces between the inclusion and the ferrite, nucleation at a high energy inert substrate and nucleation in a region of high strain energy [Dowling, 1986]. Since little is actually known about the formation of inclusion phases, it is difficult to pinpoint the actual

nucleation mechanism, however, analysis of previous research does provide some possibilities.

An investigation of acicular ferrite nucleation as a result of the strain field around an inclusion created due to differences in thermal expansion between the phases of the inclusion and the ferrite is difficult. Although large differences in thermal expansion coefficients exist between ferrite and $Al_2O_3 \cdot MnO$ or TiO phases, other factors make the analysis complex. Angular phases such as $Al_2O_3 \cdot MnO$ and TiO form as solids in the molten weld pool. Other lower melting temperature phases would exist as liquids after solidification of the weld metal. In addition some of the aluminum-manganese spinels undergo phase transformation as they cool. [Dowling, 1986] Therefore there are too many unknown variables to determine an accurate value for the strain field created by the inclusion. Dallam and Olson have attempted a qualitative analysis by simulating the thermal-mechanical conditions of a weld. They found that the influence of the strain fields generated was insignificant to weld metal ferrite formation, suggesting that this nucleation mechanism is not a major factor for nucleation of acicular ferrite. [Ramsey,1988]

TEM analysis of inclusions has shown that ferrite nucleation only occurs on flat or faceted phases. This would suggest that an epitaxial relationship may exist which is responsible for some phases being better nucleation sites than others. Titanium oxide (TiO) which has been proposed as the

titanium rich phase found in inclusions has been observed to be an excellent phase for acicular ferrite nucleation. This phase which is a FCC structure would have a low mismatch relationship with ferrite supporting this theory for acicular ferrite nucleation. However, of the multiple TEM samples analyzed by Dowling and others no conclusive evidence of epitaxial relationships were found [Dowling, 1986]. In addition, many of the inclusions observed lacked well defined crystallographic faces, making epitaxial relationships unlikely. Considering the difficulties of TEM diffraction analysis of multiphase inclusions and the uncertainties of the actual phases present in inclusions, this nucleation model cannot be completely discounted.

The most widely accepted explanation for nucleation of acicular ferrite is that the inclusion acts as an inert substrate. The inclusion is a favorable nucleation site if a high-energy interface exists, thus lowering the energy barrier for nucleation. Using a general assumption that surface energy increases with melting temperature, then phases such as TiO, $Al_2O_3 \cdot MnO$, SiO_2 and MnS would have high surface energies and be good nucleation sites. Manganese silicates would be less efficient nucleation phases. This nucleation theory seems plausible with the exception that MnS phases in inclusions have been identified as very poor nucleation sites. This is probably because the MnS inclusion is spherical and soft which

would would not provide a suitable site for nucleation of the ferrite.

In review, TEM examination of inclusions has provided evidence that supports and refutes all three nucleation theories. The answer to this important question, what nucleation mechanism promotes ferrite nucleation, will probably remain a mystery until more is known about the composition of the inclusions.

3. Prior Austenite Grain Size

The formation of acicular ferrite requires large austenite grains (typically > 45 micron). Smaller austenite grains provide a large surface area to volume ratio of grain boundaries, providing large amounts of energy for transformation. This facilitates grain boundary ferrite nucleation at small undercoolings. Weld deposits with large concentrations of oxygen (> 600 ppm) normally have large volume fractions of grain boundary ferrite.

4. Weld Thermal Cycle

In addition to weld deposit hardenability, the cooling rate of the weld pool is of major significance when considering solid-state transformation reactions. Cooling rate controls the time available for atomic diffusion and nucleation/growth of the transformation products. For welding of steels, the time to cool the weld from 800 to 500 °C ($dt_{8/5}$) is considered to be a controlling factor for weld

metal microstructure. For long periods ($dt_{8/5} \approx 100$ seconds), sufficient time for diffusion and nucleation/growth exists and the final microstructure will be predominately grain boundary ferrite. For $dt_{8/5} < 5$ seconds insufficient time for diffusion exists so the final weld metal microstructure will consist of bainite and/or martensite which depend on displacesive rather than diffusion transformations. For HSLA steels a $dt_{8/5}$ near 15 seconds will produce a predominately acicular ferrite microstructure in the weld metal [Olson,1990].

The effects of changing the cooling rate in the weld pool is not limited to solid-state transformations. Upon decreasing the cooling rate, larger delta-ferrite grains will form in the delta phase which tends to make larger austenite grains upon cooling [Olson, 1990]. This effect can also optimize the weld metal transformation for acicular ferrite formation.

In summary, the variables that affect the nucleation of acicular ferrite are complex and have interdependencies that make formation of accurate prediction models difficult to formulate. For this reason, qualitative analysis of weld metal deposits and conditions continues to be the most valuable tool for understanding how welding parameters affect the formation of acicular ferrite.

H. SCOPE OF THE PRESENT WORK

The purpose of the present work was to determine how weld metal composition affects the composition, size distribution and concentration of non-metallic inclusions and ultimately the formation of acicular ferrite. This research is in support of the research and development program aimed at certifying HSLA-100 steel for shipbuilding, currently being conducted by the Naval Surface Warfare Center, Carderock Division, Annapolis Detachment.

Submerged arc welds on HY-100 steel with different fluxes and gas metal arc welds on HSLA-100 steel with varying cover gases were used to produce weld deposits with varying amounts of alloys and oxygen concentrations. Previous work on these samples at the Naval Postgraduate School concentrated on how the different fluxes and cover gases affected the non-metallic inclusions and ultimately the weld mechanical properties. The present research used the results of these investigations [Kettel 1993, Seraiva 1993] and probed further into the reasons the resulting weld metal compositions influenced the final weld metal mechanical properties. In addition, procedural changes were introduced for SEM EDX analysis which correct the composition of the inclusions found in the previous research.

Different weld metals and weld types were used for this analysis so that traits common to both weld types would be indicative of parameters that could be used to predict optimum

weld mechanical properties. This project concentrates on predicting a weld metal chemical composition that enhances formation of acicular ferrite by a qualitative analysis. The "how to" of obtaining this optimum weld metal composition is left to others.

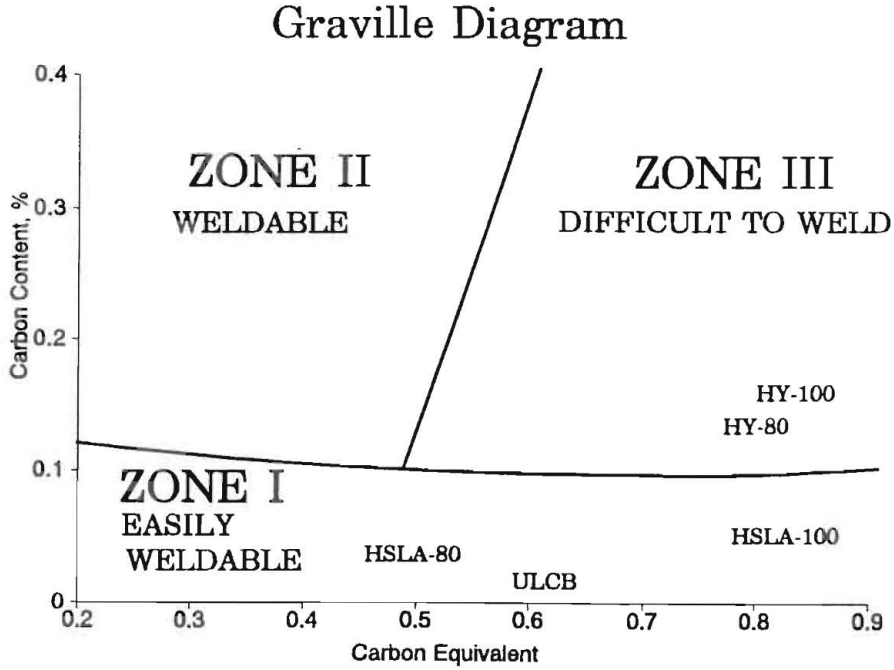

$$CE = C + \frac{Mn+Si}{6} + \frac{Ni+Cu}{15} + \frac{Cr+Mo+V}{5}$$

Figure 2.1
Graville Diagram [Graville, 1978]

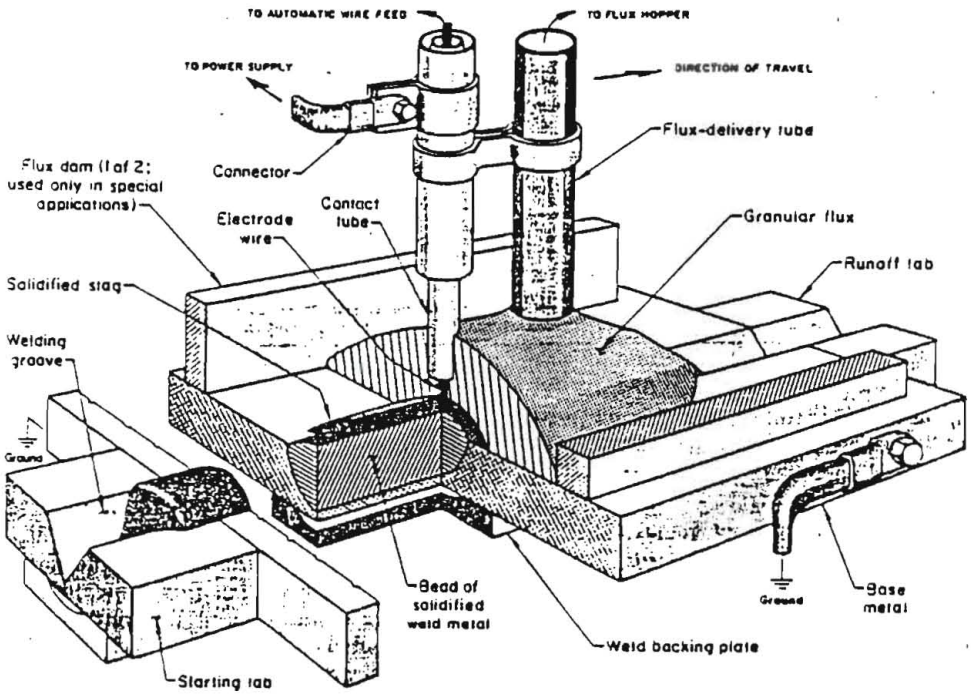

Figure 2.2
SAW Process [Metals Handbook, 1983]

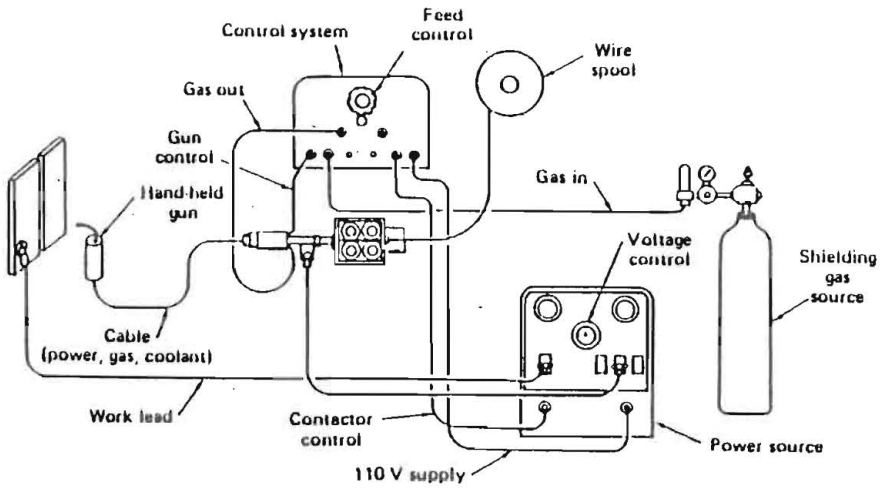

Figure 2.3
GMAW Process [Metals Handbook, 1983]

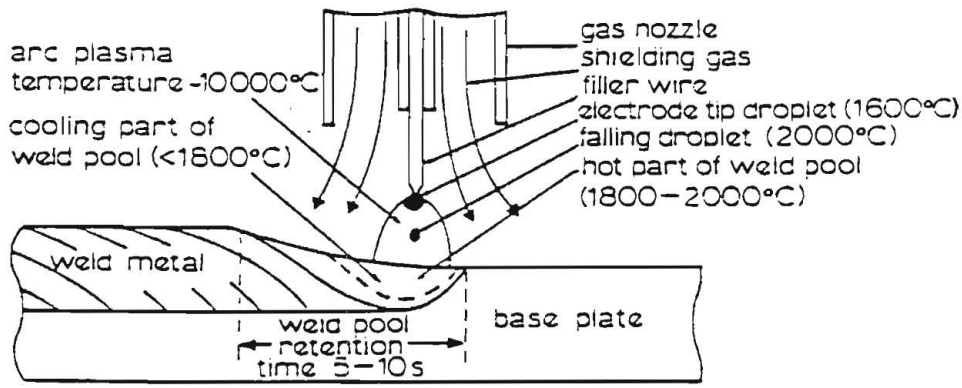

Figure 2.4
Schematic diagram of the main process stages in GMA welds. Characteristic temperatures for each stage are given in parenthesis. [Grong, 1986]

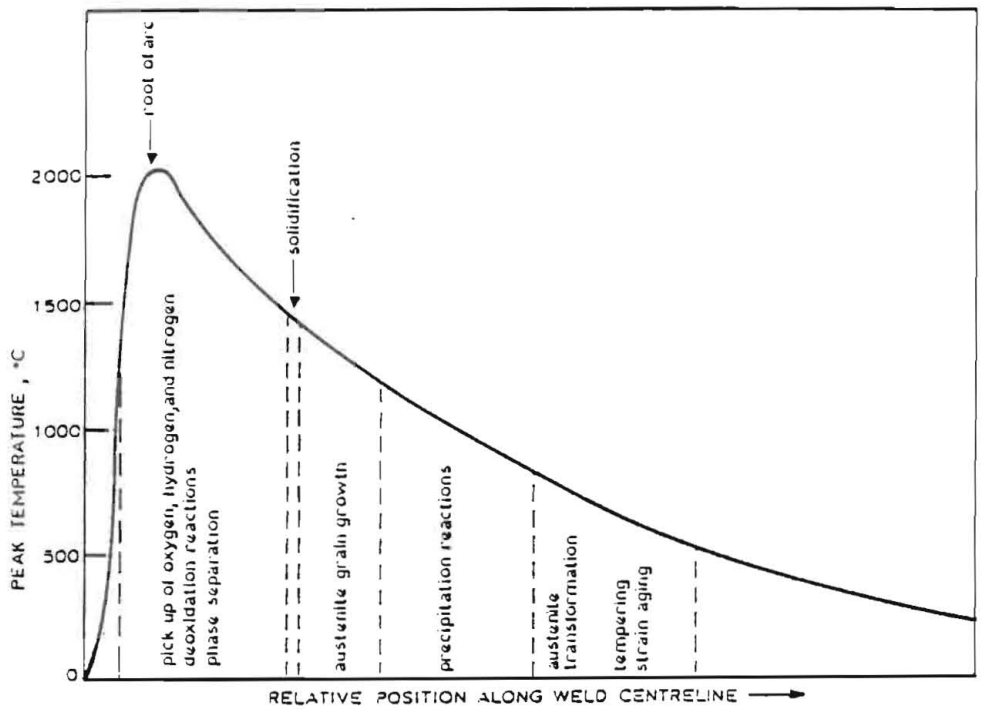

Figure 2.5
Schematic diagram illustrating weld centerline peak temperatures as a function of distance from the root arc. Includes characteristic temperature ranges for chemical and physical reactions. [Grong, 1986]

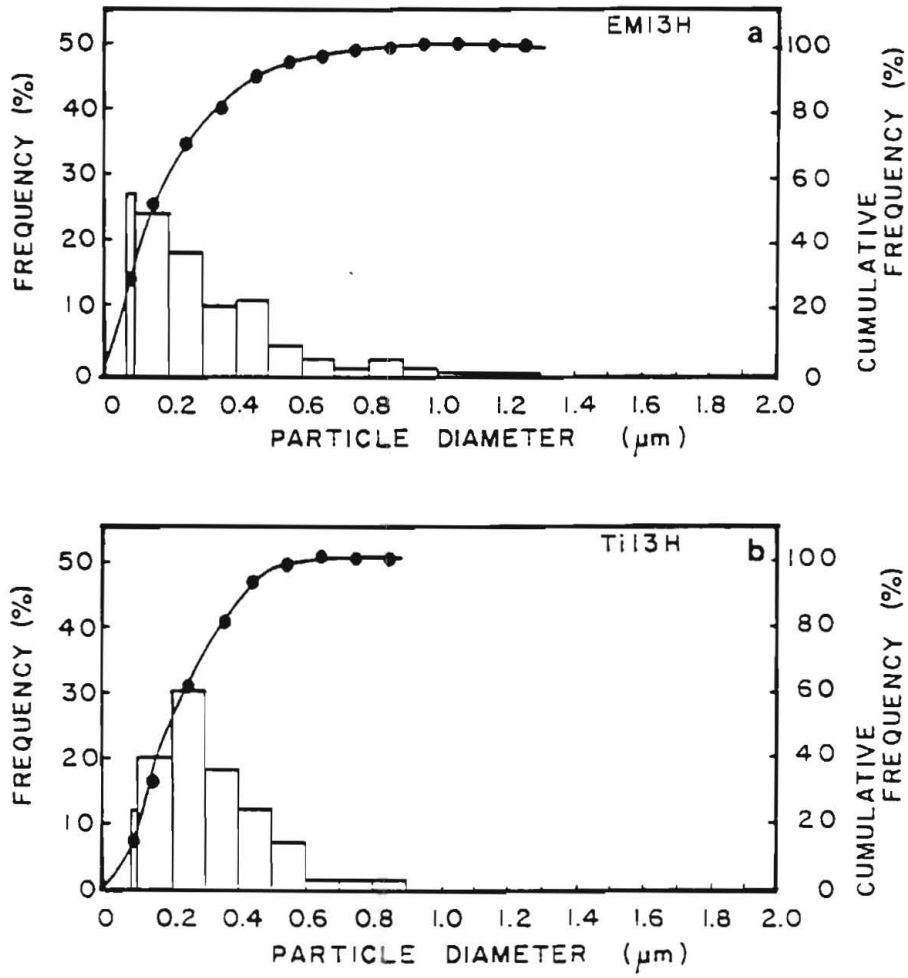

Figure 2.6
Size distribution of inclusions extracted from (a) high-oxygen weldment; (b) low oxygen weldment. [Olson, 1990]

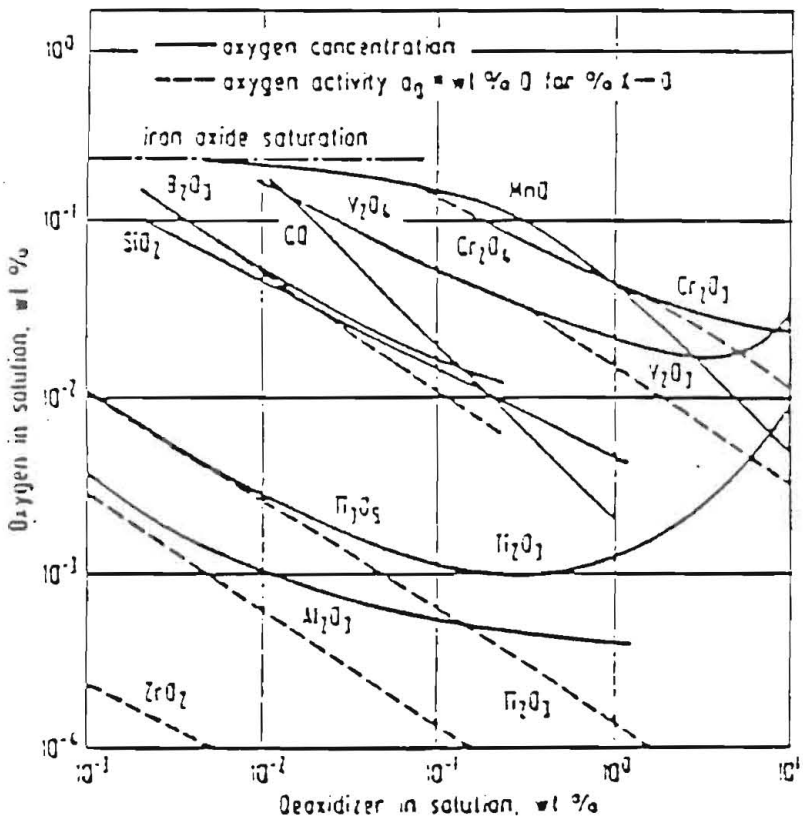

Figure 2.7
Deoxidation equilibria in liquid iron at 1600 °C.
[Haddock, 1988]

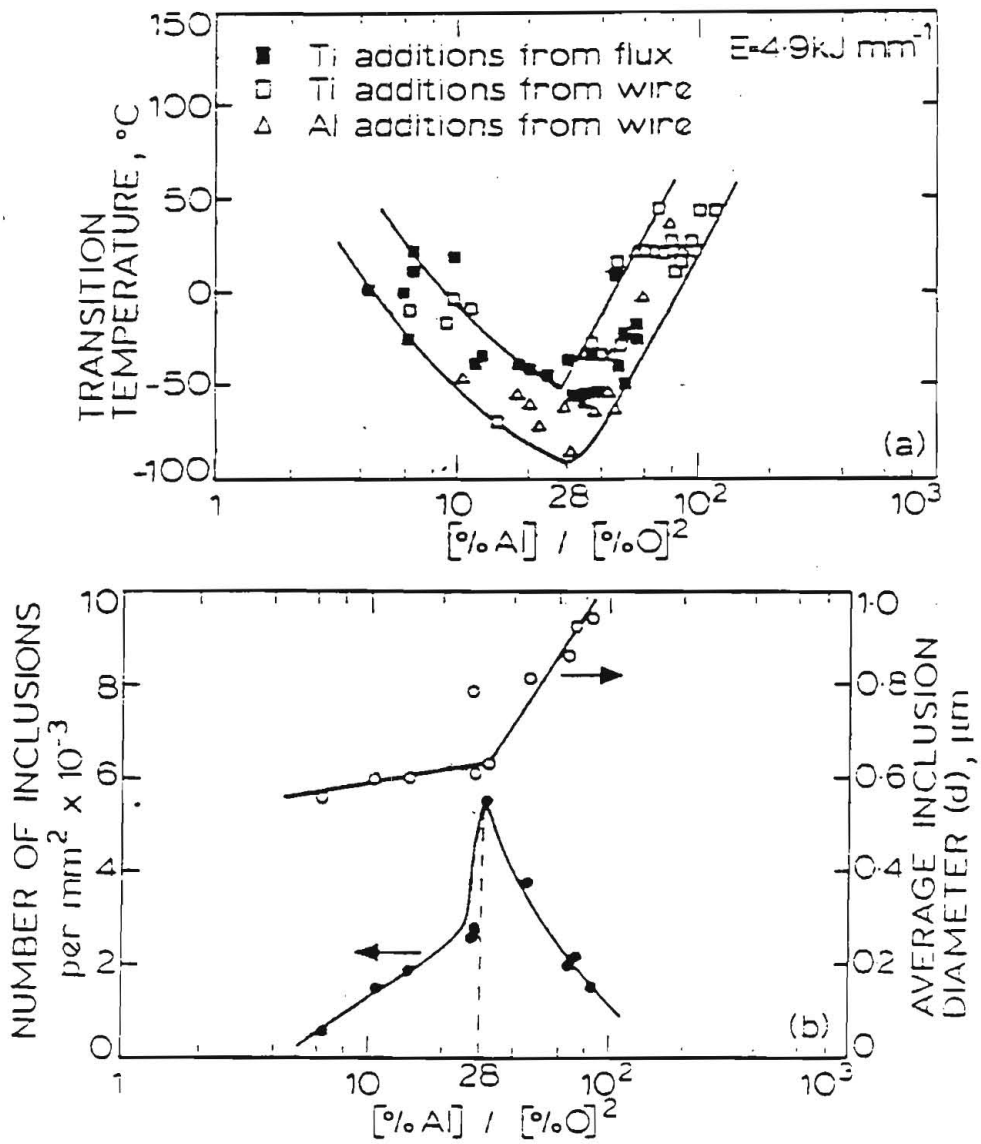

Figure 2.8
Relationship between weld deposit [wt% Al]/[wt% O]^2 ratio and (a) 35 J charpy transition temperature; (b) inclusion size distribution for microalloyed Si-Mn-Al-Ti deoxidized steel welds; data from Terashima and Hart. [Grong, 1986]

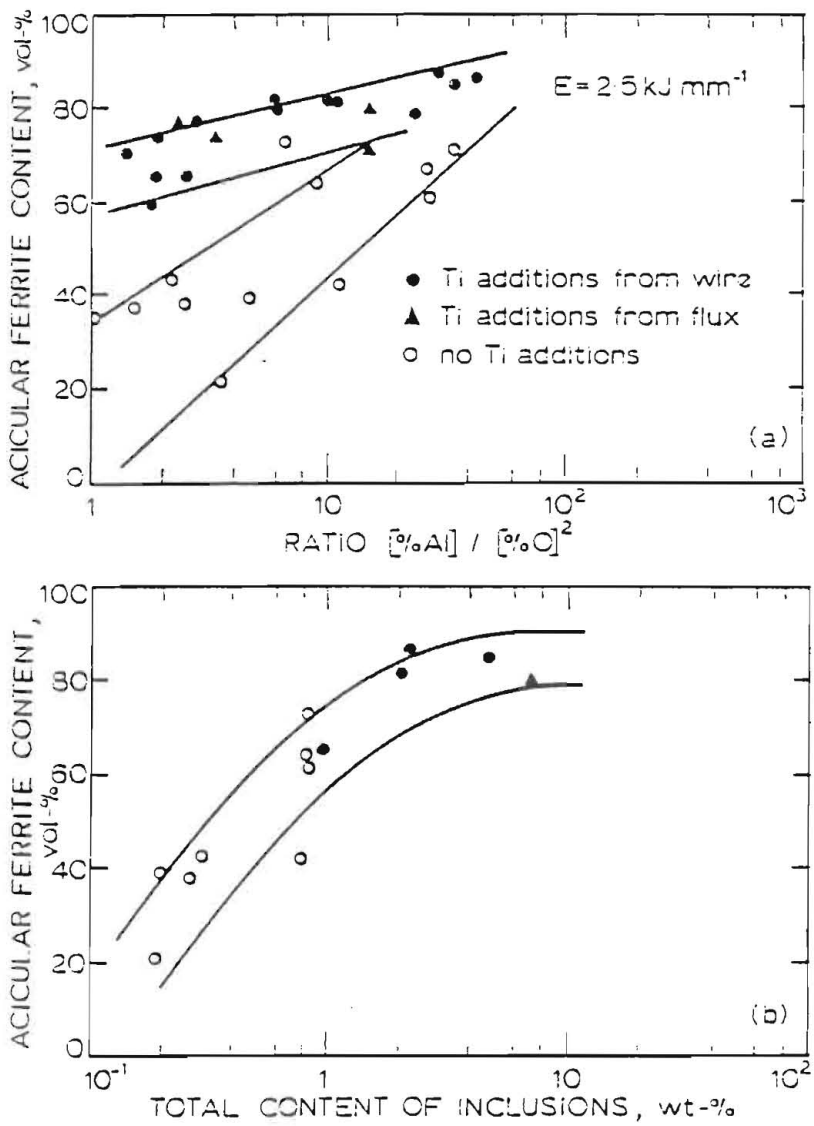

Figure 2.9
Weld metal acicular ferrite vs (a) weld metal [wt% Al] /[wt% O]^2 ratio for different levels of titanium from wire or flux and (b) titanium concentration in inclusions. [Grong, 1986]

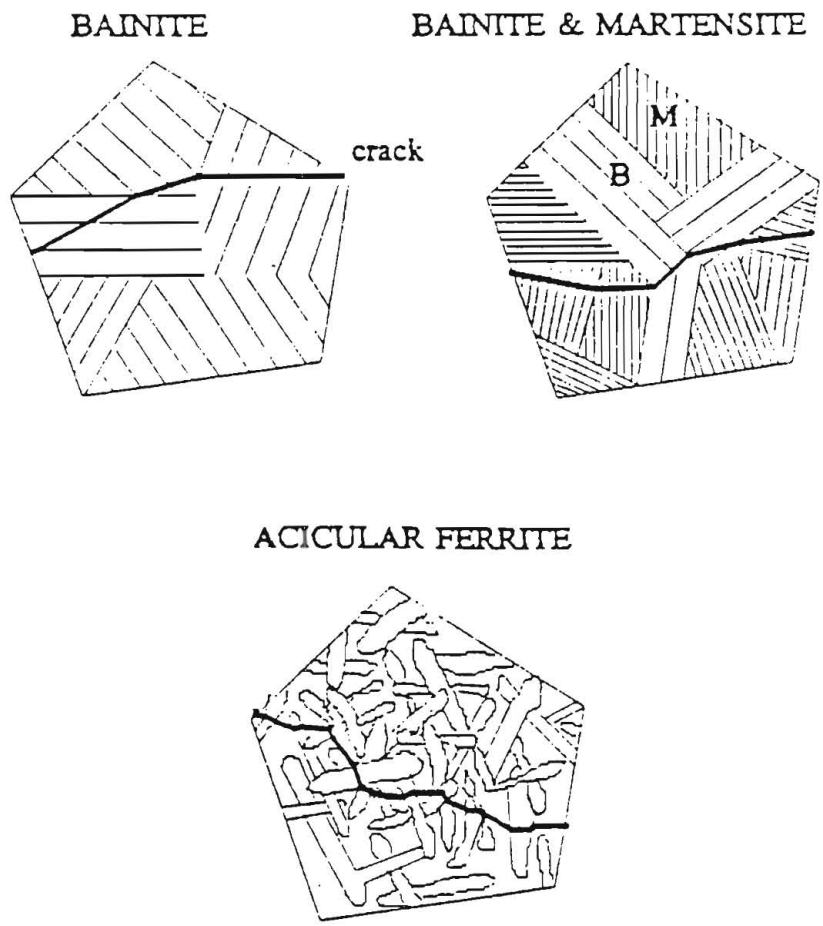

Figure 2.10
Schematic diagram showing crack propagation through various microstructures. [Edmonds, 1990]

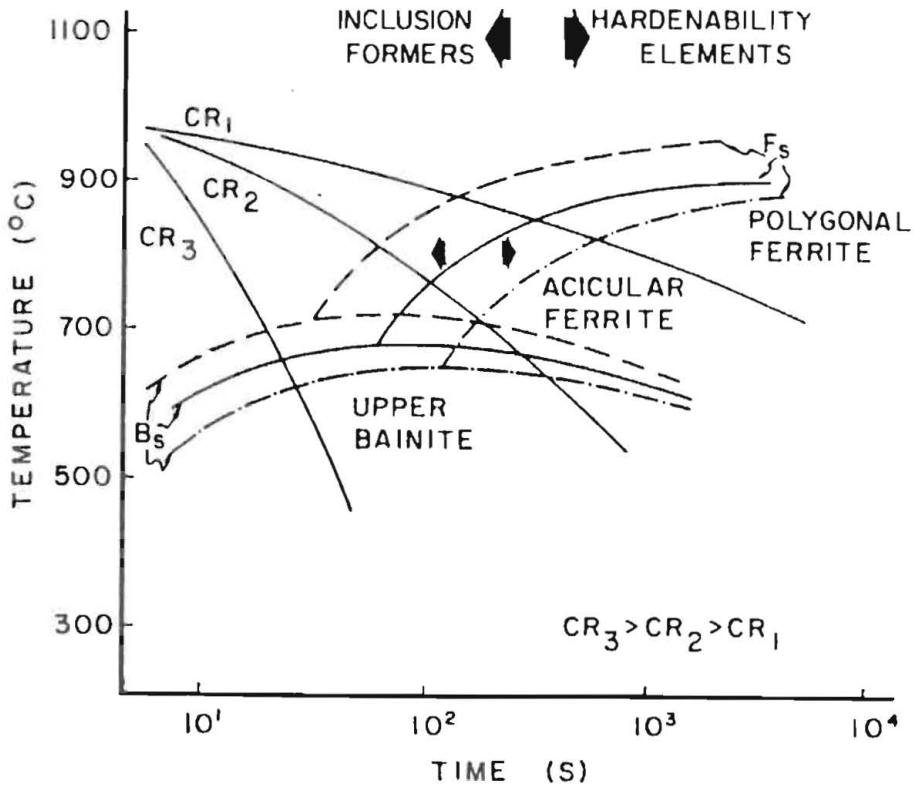

Figure 2.11
Continuous cooling transformation (CCT) diagram showing the effects of alloying elements, inclusion formers and cooling rate on weld metal microstructure. [Olson, 1990]

TABLE 2.1 COMPOSITION OF HIGH STRENGTH STRUCTURAL STEELS

[Czyryca, 1990]

	HY-100 MIL-S1621K	HSLA-100 MIL-S24645A	HY-100 Nominal	HSLA-100 Nominal
C	0.14-0.20	0.06	0.17	0.04
Mn	0.10-0.40	0.75-1.05	0.25	0.90
P	0.015	0.015	0.01	0.01
S	0.008	0.006	0.01	0.005
Si	0.15-0.38	0.40	0.25	0.25
Ni	2.75-3.50	3.35-3.65	2.90	3.50
Cr	1.40-1.80	0.45-0.75	1.40	0.60
Mo	0.35-0.60	0.55-0.65	0.40	0.60
Cu	0.25	1.45-1.75	0.05	1.60
Cb	nil	0.02-0.06	-	0.03
V	nil	nil	0.01	-
CE			0.81	0.81

Carbon equivalent (CE)

$$CE = C + (Mn+Si)/6 + (Ni+Cu)/15 + (Cr+Mo+V)/5$$

TABLE 2.2 MECHANICAL PROPERTIES LIMITS OF HIGH STRENGTH STRUCTURAL STEELS

[MIL-E-23765/2D(SH),1990]

PROPERTY	LIMIT
Yield strength	min. 102 Ksi max. 122 Ksi
Percent Elongation	14 %
Charpy Impact Toughness (-30 °F)	min. ave. 45 ft-lb
Charpy Impact Toughness (0 °F)	min. ave. 60 ft-lb
Dynamic Tear Toughness (-20 °F)	min. ave. 400 ft-lb
Dynamic Tear Toughness (30 °F)	min. ave. 575 ft-lb

TABLE 2.3 HY-100 SAW ELECTRODE CHEMISTRY

[MIL-E-23765]

	C	Mn	Si	P	S	Ni	Mo
min	-	0.90	-	-	-	1.00	0.30
max	0.09	2.35	0.60	0.012	0.008	3.00	1.00
	Cr	**V**	**Al**	**Ti**	**Zr**	**H**	
min	-	-	-	-	-	-	
max	0.80	0.03	0.10	0.10	0.10	5.5	

All limits in weight percent except H which is ml/100 gr

III. EXPERIMENTAL PROCEDURES AND RESULTS

A. WELD DEPOSITS

1. SAW Samples

Five, one inch HY-100 base plates were welded by the Annapolis Detachment of the Carderock Division of Naval Surface Warfare Center (NWSC) using a single-vee butt weld geometry. Heat input was restricted to 55.3 KJ/in (2.177 KJ/mm) to achieve the desired tensile strength in the weld metal and to avoid proeutectoid ferrite formation. Cooling rates in the weld pool were measured using chromel-alumel thermocouples which provided good readings on 50 % of the weld passes. Measured cooling rates showed close agreement to calculated cooling rates. Weld conditions were controlled to optimize the analysis of flux influence on the weld metal mechanical properties. Weld control parameters are listed in Table 3.1. The calculated basicity index for each of the fluxes used are listed in Table 3.2. Additional information on flux types and compositions is found in the Master's Thesis of K.W. Kettel from the Naval Postgraduate School [Kettel, 1993]. Resulting weld metal deposit chemical composition was determined for NSWC by Luvak Incorporated laboratories. The methods of analysis and confidence levels for the results are listed in Table 3.3. The chemical compositions of the

filler wire, HY-100 base plate and weld deposits are listed in Table 3.4 [Kettel, 1993].

2. GMAW Samples

Fourteen bead-on-plate automated GMAW weldments on HSLA-100 one inch plates were made by Annapolis Detachment, Carderock Division of NSWC. Welding parameters were kept constant with the exception of the cover gas composition. Weld control parameters are listed in Table 3.1. A three component simplex experimental design was chosen to aid in analyzing each sample as a function of shielding gas composition. A diagram of the simplex experiment design showing the relative positions of the argon (Ar), oxygen (O_2), and carbon dioxide (CO_2) gases used is provided in Figure 3.1. Shielding gas compositions (in wt-%) used were as follows:

- 100% Ar (Ar)
- 5% CO_2 / 95% Ar (C-5)
- 10% CO_2 / 90% Ar (C-10)
- 2% O_2 / 98% Ar (M-2)
- 4% O_2 / 96 % Ar (M-4)
- 50% C-10 / 50% M-4 (C-10/M-4)
- 33.3% Ar / 33.3% C-10 / 33.3% M-4 (MIDPT).

To minimize weld metal contamination, electrodes were stored in a heated cabinet and the base plate was sandblasted and cleaned with acetone prior to welding. [Gibson, 1992]

Resulting weld metal chemical composition was determined for NWSC by Luvak Incorporated laboratories. Methods of analysis and confidence levels are listed in Table 3.3. Six samples of the electrode, base metal and weld deposits were analyzed. The average value of the chemical composition analysis are listed in Tables 3.5 and 3.6. [Gibson, 1992]

Multi-pass GMAW weldments with the same weld control parameters as the single bead-on-plate welds were analyzed for percent acicular ferrite and percent columnar grains for comparison with fracture toughness data. The interpass temperature for these welds was 150 °C.

B. SAMPLE PREPARATIONS

Each of the weld deposits examined were sectioned and prepared for analysis in three phases. First the samples were surface ground, hand sanded on 240, 320, 500, 1000 and 2400 grit silicon sanding papers and then polished to one micron using diamond paste on polishing wheels. This provided the samples with a flat surface for SEM and EDX inclusion analysis. After completion of SEM and EDX analysis the samples were etched in a 5% nital solution for optical analysis of the microstructure and calculation of the proportion of microstructure in the weld metal that was acicular ferrite and percent columnar grains.

The final phase of sample preparation was preparing carbon replicas of the samples for TEM analysis. This involved deep etching the samples for 25 seconds in the 5% nital solution. The etched surface was then carbon coated using a EFFA Mk II carbon coater to a thickness of 200 angstroms (three carbon strands). The carbon coated surface was then scribed to produce three millimeter squares. The carbon was loosened from the sample by immersing it in a 5% nital solution for five minutes. The sample was then transferred to a beaker of methanal to remove the carbon that had not floated free in the nital. The small carbon samples were transferred with tweezers to a 20% by volume acetone in water solution. The surface tension of this solution causes the curled carbon to straighten. The carbon is then floated onto a 400 mesh carbon grid for TEM analysis.

C. SCANNING ELECTRON MICROSCOPY (SEM)

A Cambridge Stereo Scan S200 scanning electron microscope with a LaB_6 filament energized to 20,000 volts was used for non-metallic inclusion analysis. To determine the size distribution and concentration of the inclusions, the SEM was used to view 100 random fields of view with inclusion size and number recorded for each field. For this analysis the SEM was used in the backscatter mode to enhance the resolution of the inclusions versus the background. GMAW samples were analyzed at 4000 times magnification at a working distance of eight

millimeters resulting in each field of view representing 500 square millimeters. SAW samples were analyzed at 7040 times magnification at a working distance of nine millimeters resulting in each field of view representing 180 square millimeters. From this data a statistical analysis for average inclusion size and volume calculations were made. The results of this analysis were available from the previous research and can be seen in Tables 3.7, 3.8 and 3.9 [Kettel 1993, Seraiva 1993]. Typical inclusion fields are presented in Figures 3.2 and 3.3.

Inclusion composition was determined using a Kevex 8000 Energy Dispersive X-ray (EDX) analysis spectrometer. For this analysis working distance was increased to 18 mm with a spot size five. The most accurate representation of inclusion elemental makeup was achieved using the RASTER function to frame the inclusion, vice using the spot controls. Each inclusion was counted for 100 seconds at a count rate of 1000 to 1500 counts/second. An analysis of the background matrix near the inclusion was made with total counts matching those from the inclusion analysis. This background was then subtracted from the inclusion count using the matrix stripping routine leaving only those elements from the inclusion in the final analysis. This background subtraction accounts for the elements from the matrix were included in the analysis due to the bulb of interaction being larger than the inclusion. Figure 3.4 shows how a typical electron beam produces x-rays

in the inclusion and the matrix. Typical analysis displays after removing the background are presented in Figures 3.5 and 3.6.

At this point the resulting spectrum was analyzed on the Kevex 8000 to determine the atomic percent of each element normalized to 100%. This analysis also corrects for the effects of differences in atomic number on the x-ray analysis. It was noted that using the Gaussian fit method to determine the relative intensities of the elements present resulted in the small manganese beta peak dominating and most of the large alpha peak being neglected. Since little or no secondary interference existed for the elements found, the simple integration processing technique eliminated this problem, resulting in a more accurate representation of the amount of manganese present. A minimum of 20 inclusions were analyzed in this manner for each sample. The results of this analysis for each sample are listed in Tables 3.10 through 3.21.

The use of the backscatter mode of operation on the SEM visually revealed multiple phases with a light angular phase often found at the edge of the inclusion. The x-ray mapping mode of the Kevex was used to verify that this lighter phase was rich in titanium (Figures 3.7 and 3.8). The spot size on the SEM was changed to a spot size seven to minimize the bulb of interaction for further EDX analysis. Several inclusions

with the titanium rich phase near the center (Figures 3.8 and 3.9) were probed to determine the composition of the phase. Results of this analysis are listed in Table 3.22.

Samples were then lightly etched in a 5% nital solution for optical analysis. The SEM in a backscatter mode was used to visually record how acicular ferrite nucleates on the inclusions. Figure 3.10 shows how multiple inclusions nucleate ferrite and form the basketweave microstructure, acicular ferrite. Figure 3.11 shows that without a network of inclusions, ferrite will nucleate intragranularly, but the resulting microstructure will be primarily bainite or martensite.

D. OPTICAL MICROSCOPY

Etched samples were examined at various magnifications using a Zeiss ICM 405 optical microstructure. Ten pictures at random locations in the weld metal were taken to analyze the microstructure. A statistical analysis of the proportion of acicular ferrite in the weld metal microstructure was conducted using a five square millimeter grid for each of the ten micrographs and averaging the results. Figure 3.12 is an example of an optical micrograph used for this analysis. The results of this analysis is presented in Table 3.23. Low magnification micrographs were taken of the entire weld deposit and analyzed for percent columnar grains. Figure 3.13 shows a typical GMAW weld deposit micrograph. Kettel

previously conducted this analysis for the SAW samples [Kettel, 1993]. The results of this analysis are reported in Table 3.23.

E. TRANSMISSION ELECTRON MICROSCOPY (TEM)

A JEM-100 CX II transmission electron microscope with a LaB_6 filament energized to 120,000 volts was used for final analysis of the samples. The inclusions in the carbon replica samples were too thick to provide any useful spot patterns for diffraction analysis. In addition, because of the thickness EDX analysis using the thin foil analysis is inaccurate showing more of the lighter elements such as Al and Si than really exists in the inclusion. A typical EDX spectrum from the TEM analysis, which is accurate, is presented in Figure 3.14. The TEM EDX spectrum is nearly the same as the SEM EDX spectrum (Figure 3.5) providing verification of the SEM inclusion analysis. Micrographs, taken at a magnification of 100,000 times, show the acicular ferrite nucleated on flat faces of the inclusions (Figure 3.15). These non-metallic inclusions were rich in the titanium phase providing the angular part of the inclusion.

A 1.5 million volt Kratos type EM 1500 (EM7 Mark III) high voltage electron microscope (HVEM) with a tungston filament energized to one million volts was used to overcome the inclusion thickness difficulties encountered with the 120,000 volt TEM. The HVEM presented its own unique problems in that

an inclusion oriented to the zone axis had to be found, as the time required to tilt the inclusion to the zone axis resulted in radiation damage from the high electron flux. A diffraction pattern from a one micron inclusion is shown in Figure 3.16. Note that the diffraction pattern is from a multi-phase inclusion making accurate analysis difficult.

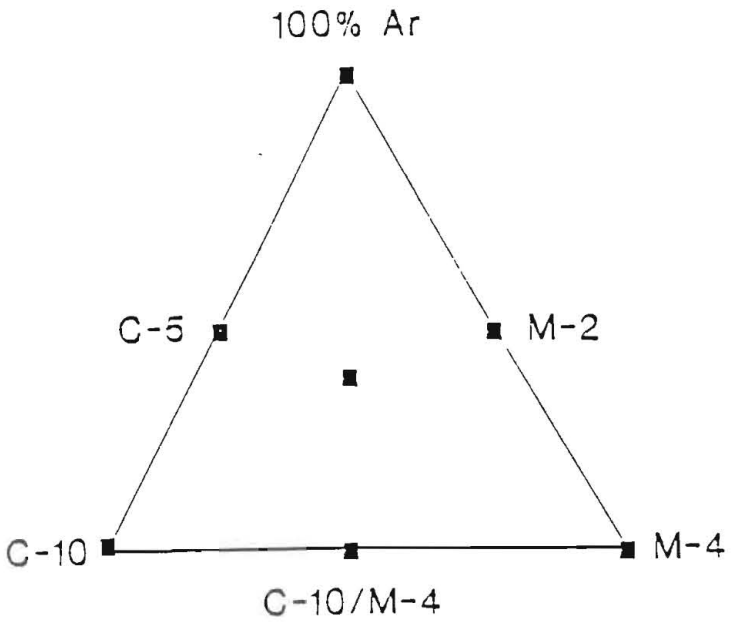

Figure 3.1
Diagram of the simplex design used for shielding gas composition selection.

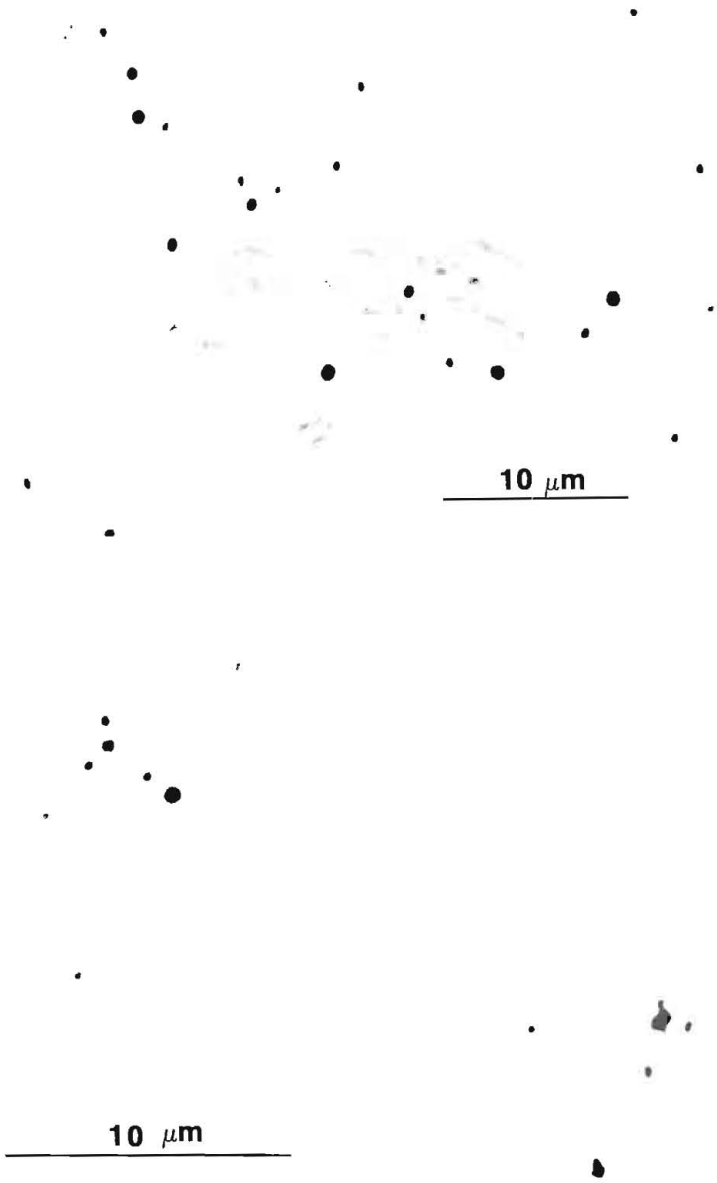

Figure 3.2
Typical inclusion field in GMAW samples, top 2.60 KX, bottom 4.02 KX. Note the clustering of the inclusions shown in the bottom photograph.

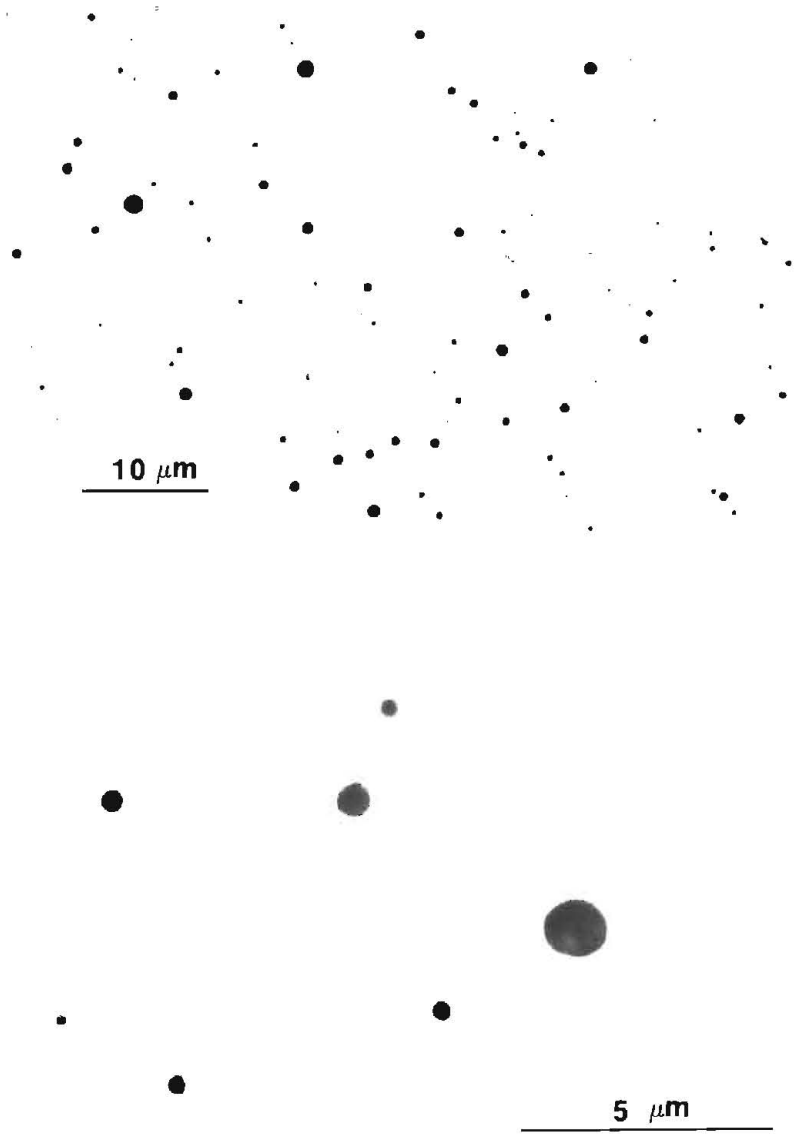

Figure 3.3
Inclusion field in SAW sample F296, top 2.02 Kx, bottom 7.04 Kx. This sample has a very even distribution of inclusions throughout the weld metal. Multiple phases can be seen in the large inclusion on the bottom.

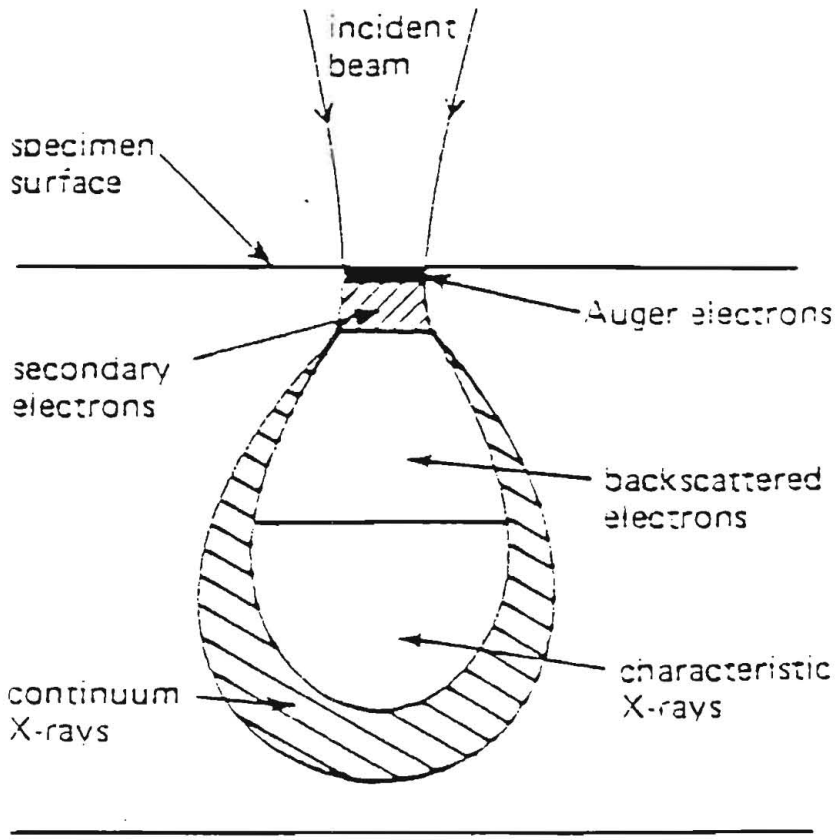

Figure 3.4
Bulb of interaction for an electron beam.

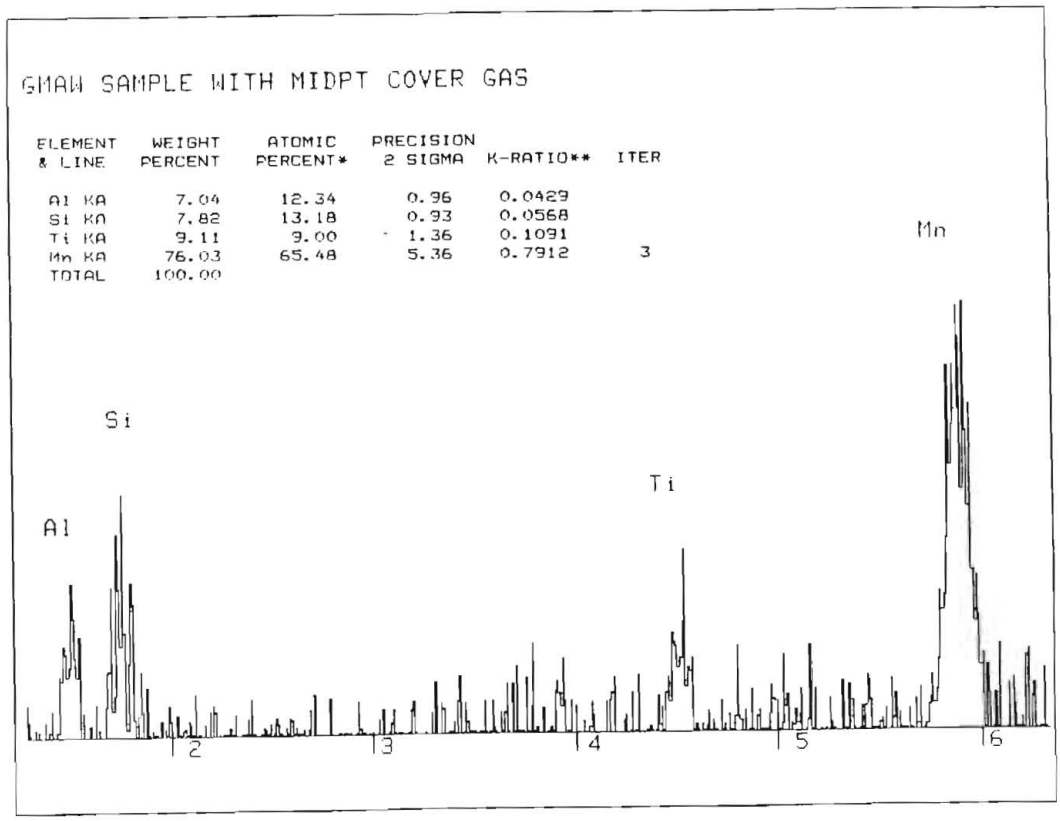

Figure 3.5
SEM EDX spectrum of GMAW non-metallic inclusion

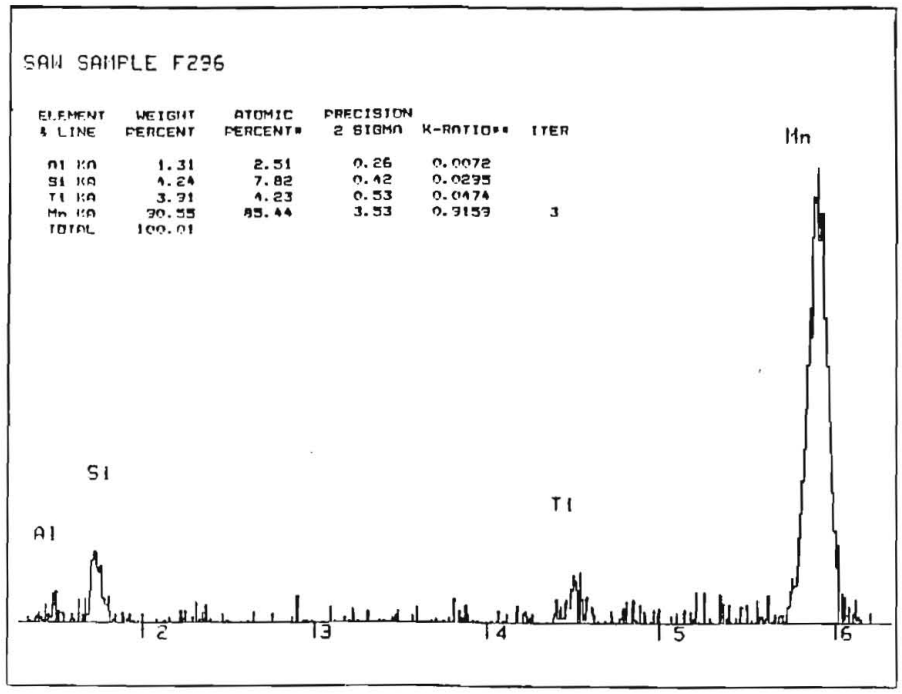

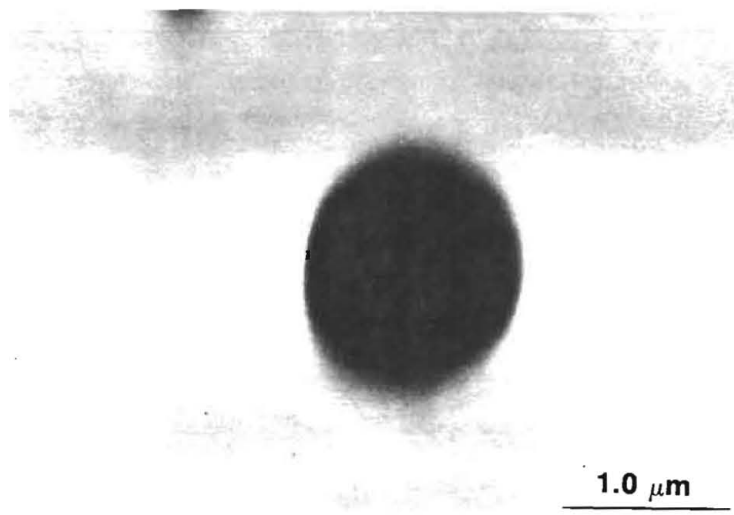

Figure 3.6
SEM EDX spectrum of SAW non-metallic inclusion (top), Photograph of the 1.2 micron inclusion (25.3 Kx). Note that the inclusion is spherical with no flat faces and the spectrum indicates that the composition is primarily manganese.

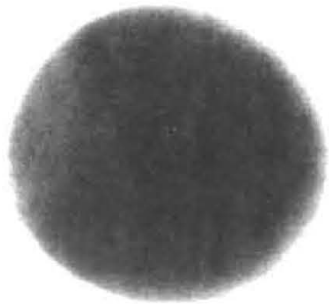

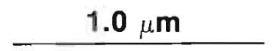

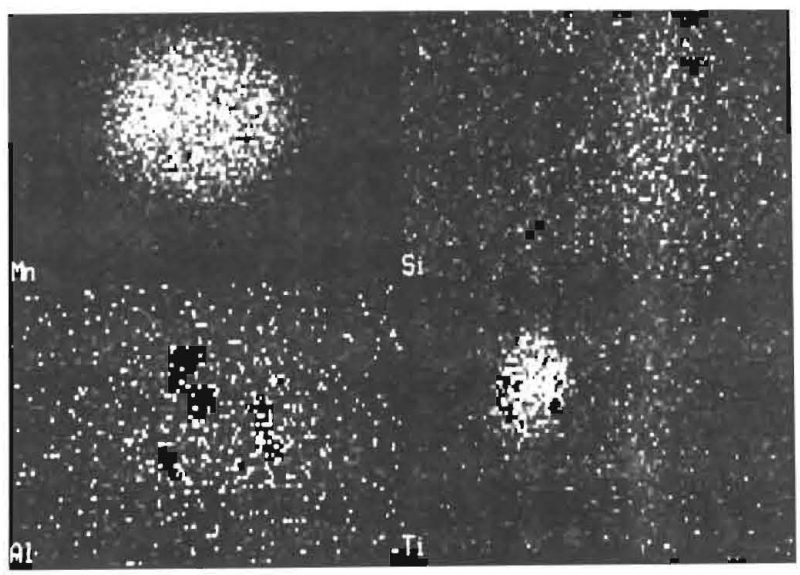

Figure 3.7
1.37 micron inclusion (35.0 Kx) showing titanium rich phase (top). Kevex x-ray map showing the light phase to be rich in titanium and manganese (bottom).

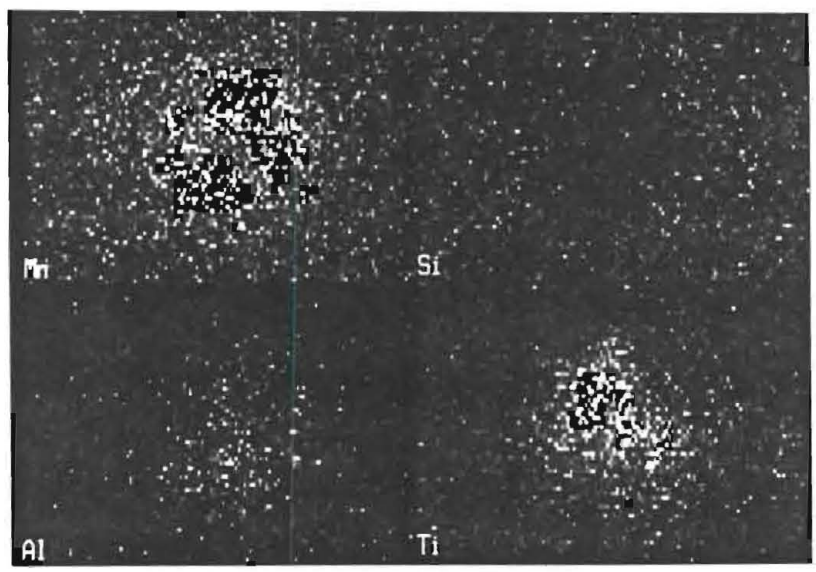

Figure 3.8
0.7 micron inclusion (50.1 Kx) with titanium rich phase in the center (top). Kevex x-ray map of the inclusion (bottom).

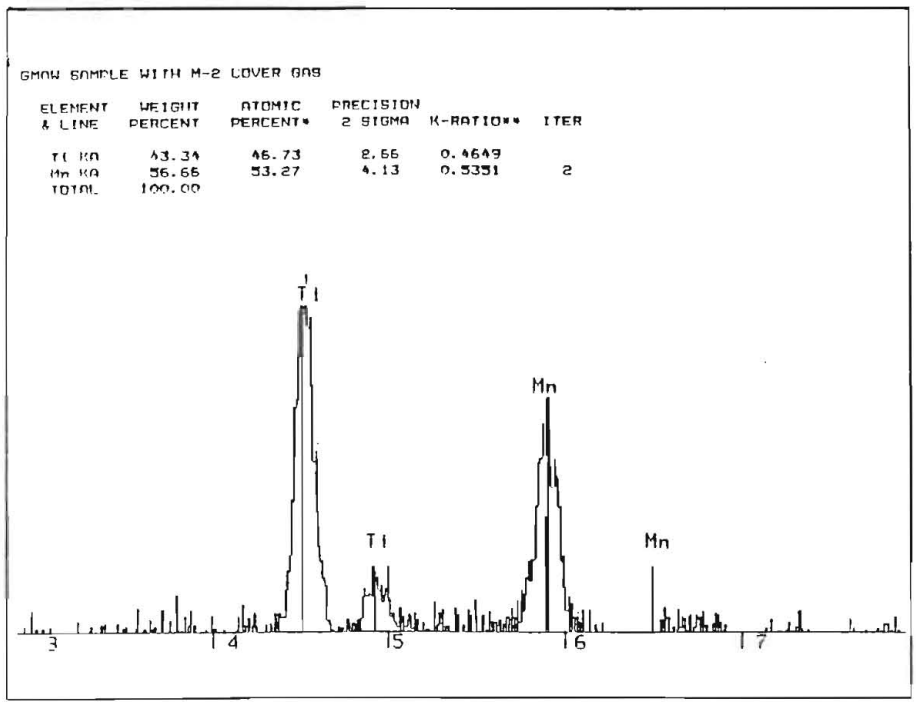

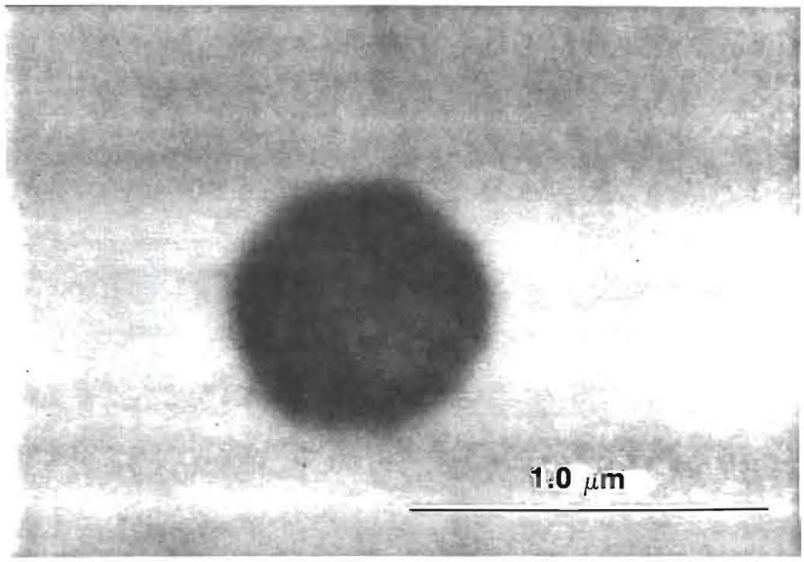

Figure 3.9
SEM EDX spectrum of titanium rich phase of a GMAW sample (top). Photograph of 0.7 micron inclusion (50.9 Kx) showing the titanium rich phase in the center of the inclusion (bottom).

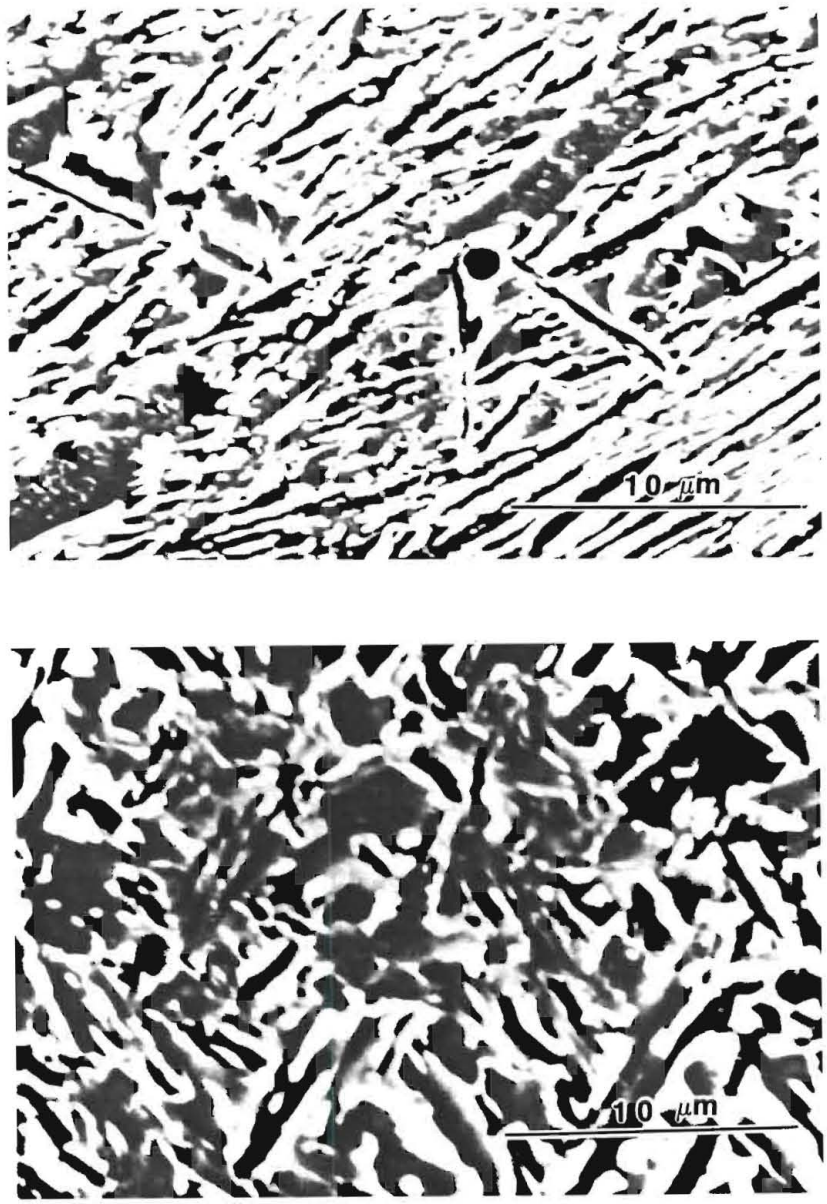

Figure 3.10
SEM photograph (4.02 Kx) of GMAW (M-2 cover gas) sample etched in 5% nital showing acicular ferrite formed by nucleation on multiple inclusions (top). SAW (F296) sample (4.02 Kx) etched in 5% nital showing same results (bottom).

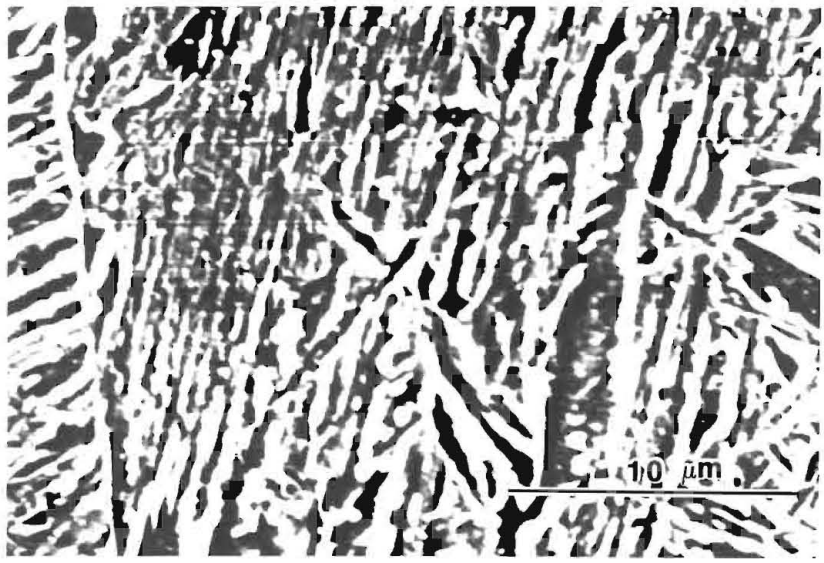

Figure 3.11
SEM photograph (4.02 Kx) of GMAW (M-2 cover gas) sample showing ferrite nucleated on an inclusion but a predominately bainite microstructure due to the small concentration of inclusions.

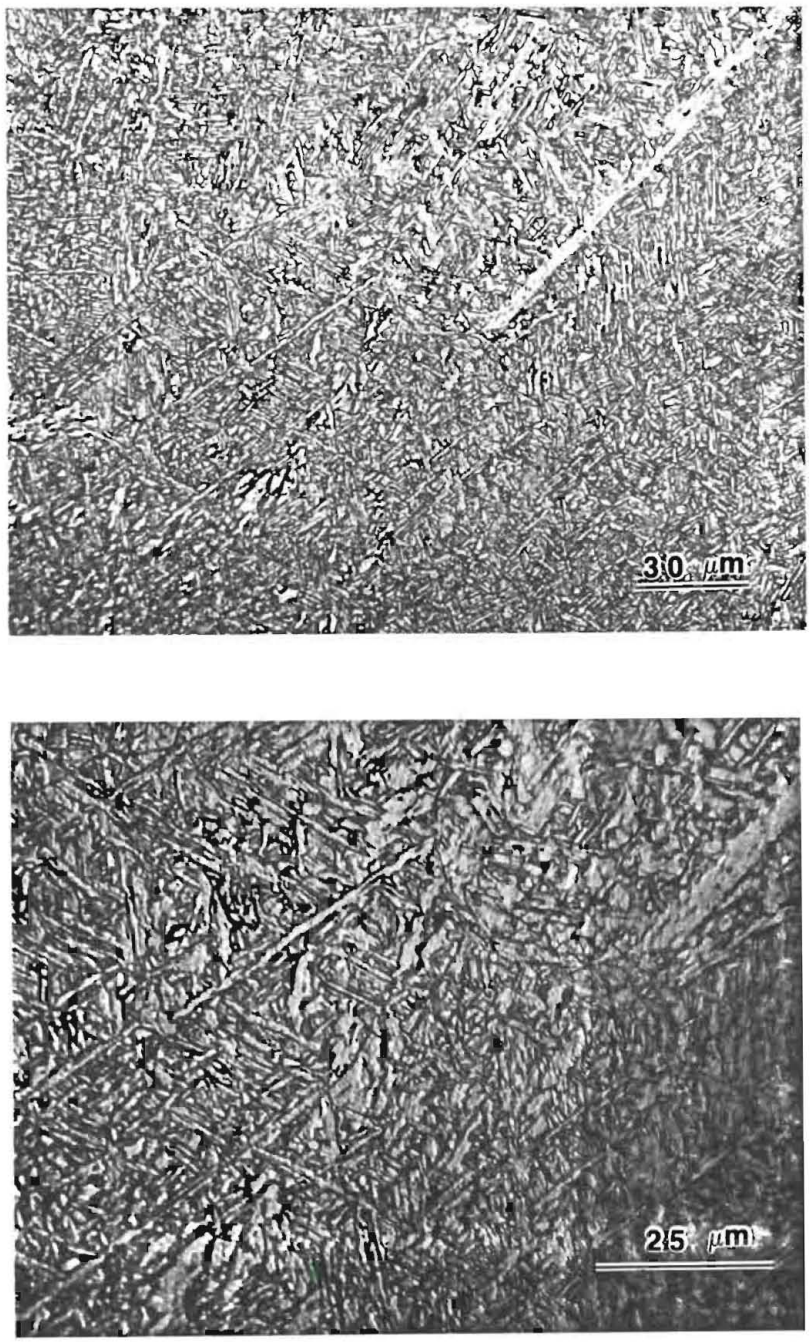

Figure 3.12
Optical photograph of SAW sample F296,top 500 x, bottom 1000 x. These are typical of the photographs used to find % acicular ferrite in the weld metal microstructure.

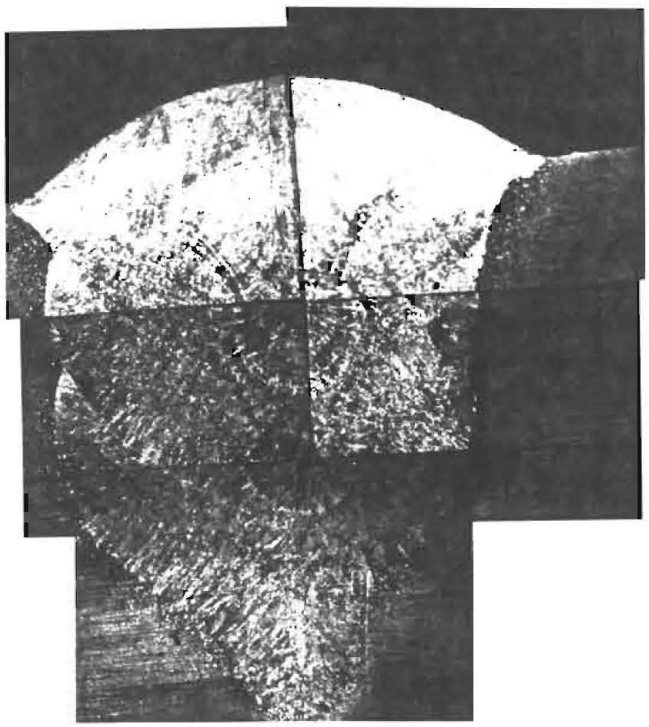

Figure 3.13
GMAW multi-pass weldment used for percent columnar grain calculations.

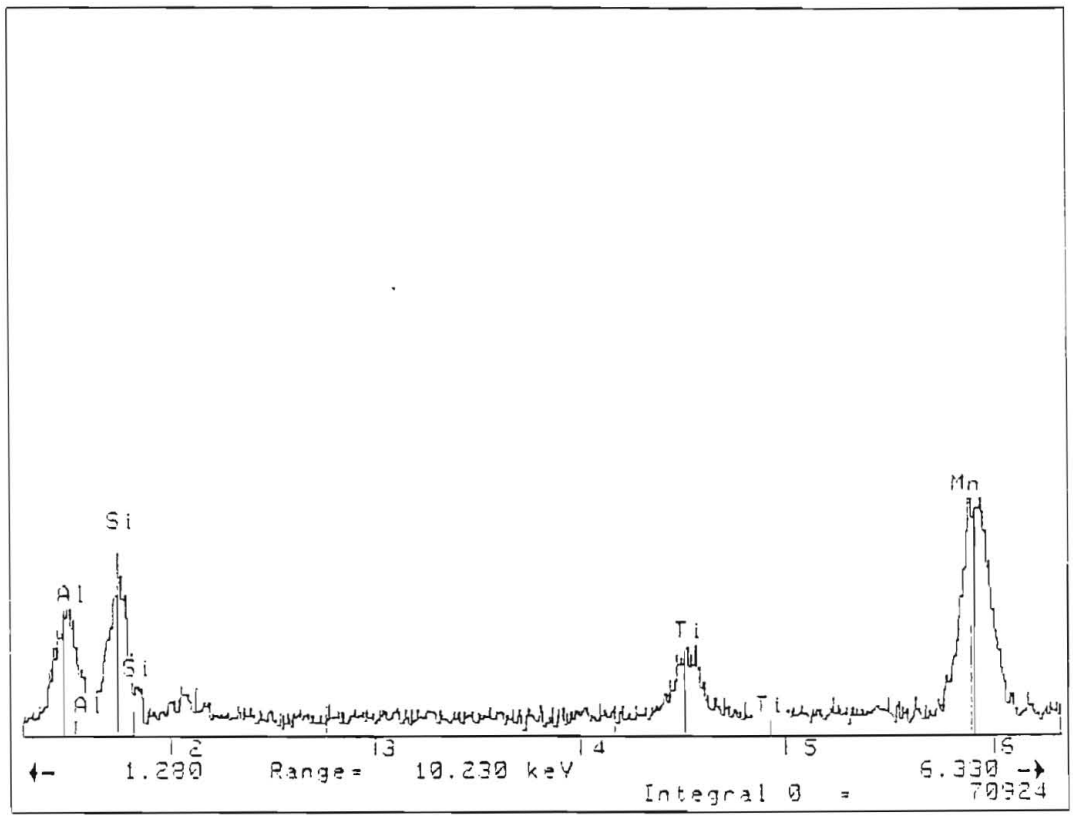

Figure 3.14
TEM EDX spectrum from a typical inclusion in a GMAW sample with M2 cover gas. Note that the spectrum is similar to the SEM EDX spectrum in Figure 3.5.

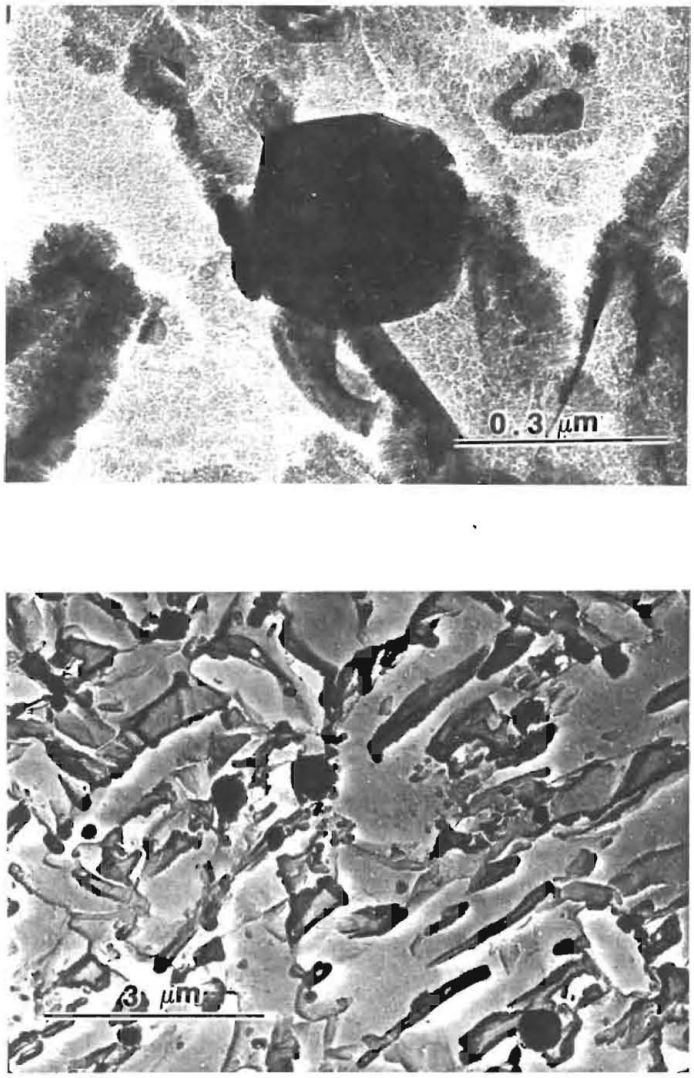

Figure 3.15
TEM micrographs (100 Kx) showing acicular ferrite nucleated on a flat face of an inclusion (top). Acicular ferrite formed by multiple inclusions (bottom).

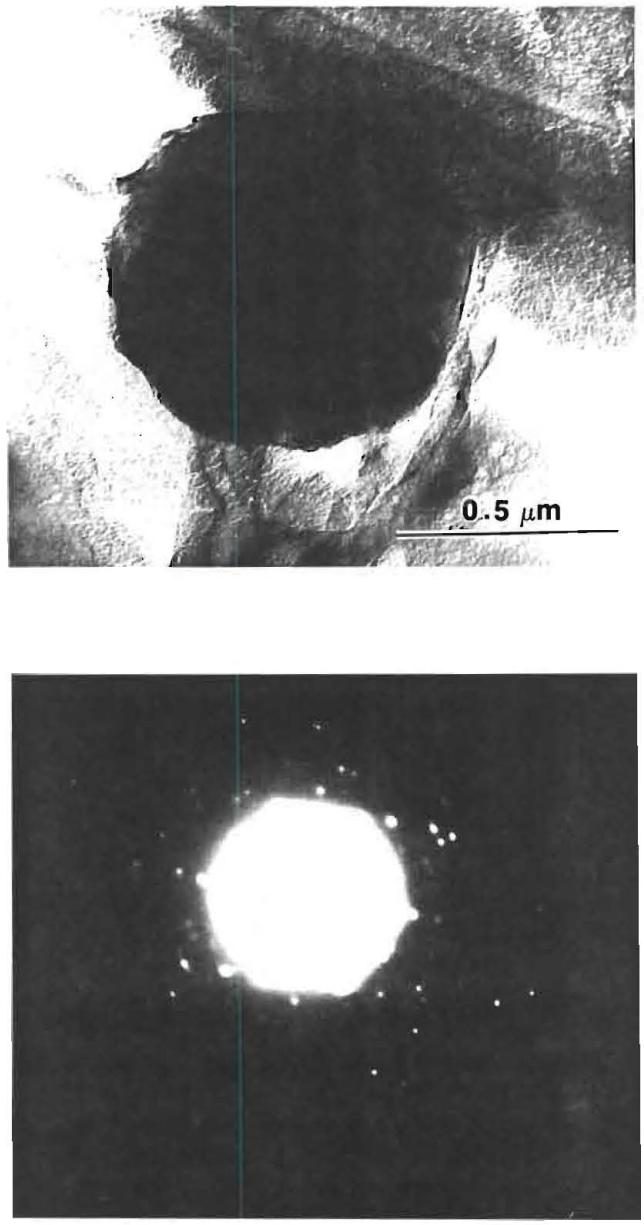

Figure 3.16
HVEM image and diffraction pattern of an inclusion from SAW sample F296.

TABLE 3.1 WELDING CONTROL PARAMETERS

[Kettel 1993, Seraiva 1993]

	SAW	GMAW
Base Plate Type	HY-100	HSLA-100
Plate Thickness	1 inch	1 inch
Number of Passes	21 or 24	1
Wire Type	L-TEC 120 (HT 120022)	Airco 140-S (HT 14005)
Wire Diameter	3/32 inch	1/16 inch
Current	500 amps, DCRP	260 amps
Voltage	35 volts	28 volts (29 v for argon)
Weld Speed	19 in/min	9 in/min
Heat Input	55.3 KJ/in	43.6 KJ/in
Preheat/Interpass Temperature	250-275 °F	Room Temp
Cooling Rate	18-23 °F/sec at 1000 °F	-
Shield Gas Flow Rate	None	50 ft^3/hr

TABLE 3.2 BASICITY INDEX FOR SAW FLUXES

[Kettel,1993]

SAMPLE	BI (w/o CaF_2)	BI (w CaF_2)
F289	1.74	2.65
F292	1.87	2.83
F293	2.14	2.75
F295	1.93	2.63
F296	2.04	2.97

$$BI = \frac{CaO+(CaF_2)+MgO+Na_2O+K_2O+Li_2O+0.5(MnO+FeO)}{SiO_2+0.5(Al_2O_3+TiO_2+ZrO_2)}$$

BI based on Easterling and Eagar relationships [Kou, 1987].

TABLE 3.3 CHEMICAL ANALYSIS METHODS

[Gibson, 1992]

ELEMENT	METHOD OF ANALYSIS	CONFIDENCE LIMIT +/- wt-%
Carbon	Combustion Infrared	0.001
Manganese	Plasma Emission	0.02
Silicon	Plasma Emission	0.01
Phosphorus	Plasma Emission	0.002
Sulfur	Combustion Automatic Titration	0.001
Nickel	Plasma Emission	0.05
Molybdenum	Plasma Emission	0.01
Chromium	Plasma Emission	0.02
Vanadium	Plasma Emission	0.001
Aluminum	Plasma Emission	0.002
Titanium	Plasma Emission	0.001
Zirconium	Plasma Emission	0.001
Copper	Plasma Emission	0.001
Oxygen	Inert Gas Fusion, TC136	0.001
Nitrogen	Inert Gas Fusion, TC136	0.001
Boron	Plasma Emission	0.001
Hydrogen	Vacuum Hot Extraction	0.00001
Niobium	Plasma Emission	0.001

Information provided by Luvak, Inc.

TABLE 3.4 SAW SAMPLES CHEMICAL COMPOSITION

[Kettel, 1993]

	FILLER	BASE	F289	F292	F293	F295	F296
C	.081	.157	.062	.062	.056	.064	.064
Mn	1.57	.33	1.45	1.49	1.28	1.51	1.54
Si	.40	.30	.38	.46	.42	.28	.34
P	.004	.003	.007	.005	.004	.015	.008
S	.006	.005	.010	.006	.006	.011	.007
Ni	2.25	2.79	2.33	2.56	2.51	2.34	2.34
Mo	.42	.36	.46	.52	.47	.47	.49
Cr	.28	1.46	.25	.43	.40	.47	.50
V	.001	.006	.003	.003	.002	.004	.003
Al	.012	.018	.013	.020	.011	.011	.014
Ti	.014	.004	.006	.008	.004	.005	.006
Zr	.012	0.0	.003	.003	.003	.002	.004
Cu	.011	.097	.020	.023	.017	.021	.026
O	.003	.0054	.030	.027	.034	.035	.032
N	.004	.016	.007	.006	.006	.009	.006
B	.004	.001	.004	.003	.004	.004	.001
H*	2.8	1.1	0.2	0.4	0.4	0.3	0.8

* All values given in weight percent (wt-%) except H in ppm.

Note that 0.03 wt-% equals 300 ppm.

TABLE 3.5 GMAW BASE/WIRE CHEMICAL COMPOSITIONS

[Gibson, 1992]

	FILLER WIRE	BASE
C	.079	.075
Mn	1.518	.793
Si	.428	.365
P	.005	.010
S	.002	<.001
Ni	2.518	3.307
Mo	.852	.587
Cr	.746	.543
Nb	<.001	.024
V	.003	.003
Al	.007	.020
Ti	.016	.004
Zr	.005	<.001
Cu	.034	1.633
O	.014	.002
N	.004	.011
B	.004	.003
H*	NA	.3

* All values in weight percent (wt-%) except H in ppm.

Note that .014 wt-% oxygen is 140 ppm.

TABLE 3.6 GMAW WELD DEPOSIT CHEMICAL COMPOSITIONS

[Gibson, 1992]

	Ar	M2	MIDPT	C5	M4	C10	M4/C10
C	.068	.066	.070	.069	.064	.070	.066
Mn	1.193	1.132	1.098	1.072	1.033	1.032	1.045
Si	.412	.383	.366	.353	.325	.332	.342
P	.008	.009	.009	.008	.008	.008	.006
S	.0002	.0005	.001	.0002	.0008	.001	<.001
Ni	2.873	2.787	2.895	2.882	2.812	2.915	2.858
Mo	.78	.765	.757	.765	.768	.760	.737
Cr	.698	.665	.682	.690	.653	.682	.670
Nb	.016	.015	.015	.016	.014	.015	.015
V	.003	.003	.003	.003	.003	.003	.003
Al	.015	.011	.010	.011	.008	.010	.010
Ti	.013	.008	.007	.007	.006	.006	.006
Zr	<.001	<.001	<.001	<.001	<.001	.001	<.001
Cu	.74	.713	.72	.767	.688	.823	.800
O	.003	.019	.019	.026	.022	.026	.024
N	.006	.008	.008	.008	.008	.009	.008
B	.004	.004	.004	.004	.004	.004	.005
H*	.35	.45	.412	.40	.40	.417	.383

* All values in weight percent (wt-%) except H in ppm.

Note that .014 wt-% oxygen is 140 ppm.

TABLE 3.7 INCLUSION STATISTICS

[Kettel 1993, Seravia 1993]

	SAMPLES	Inclusion Count	Mean Inclusion Size (micron)	Volume Fraction Inclusions (%)
S A W	F289	483	0.320	0.216
	F292	297	0.378	0.185
	F293	408	0.322	0.185
	F295	364	0.323	0.165
	F296 *	1237	0.423	0.966
G M A W	AR	88 (32)	1.294	0.231
	M2	548 (197)	0.800	0.551
	MIDPT	723 (260)	0.668	0.507
	C5	592 (213)	0.879	0.718
	M4	749 (270)	0.765	0.689
	C10	626 (225)	0.667	0.437
	M4/C10	567 (204)	0.821	0.600

Numbers of inclusions counted based on 100 fields of view of 180 square microns for SAW samples and 500 square microns for the GMAW samples. Numbers in paraenthesis correct for this area difference.

* Results listed for sample F296 are different than those used by Kettel. These numbers are from a second sample supplied by NSWC for verification of results [Kettel, 1993].

TABLE 3.8 SAW INCLUSION SIZE DISTRIBUTION DATA

	F289	F292	F293	F295	F296
0.15	161	84	163	130	265
0.3	146	74	110	115	440
0.4	100	55	62	45	161
0.5	40	35	25	34	126
0.6	18	20	14	18	74
0.7	8	11	14	10	63
0.8	3	5	10	7	23
0.9	3	3	3	1	22
1.0	0	3	2	1	19
1.1	0	4	4	3	9
1.2	2	1	0	0	6
1.3	1	0	1	0	10
1.4	1	1	0	0	0
1.5	0	1	0	0	3

Sample F296 has 16 inclusions larger than 1.5 micron.
The largest inclusion is 3.3 micron.

TABLE 3.9 GMAW INCLUSION SIZE DISTRIBUTION DATA

	Ar	M2	MIDPT	C5	M4	C10/M4	C10
0.1	0	0	0	0	0	0	0
0.2	0	0	0	0	0	2	1
0.3	0	0	0	2	4	38	0
0.4	3	8	51	5	18	60	5
0.5	18	58	133	36	62	154	23
0.6	0	145	203	98	172	76	112
0.7	0	143	138	145	136	115	132
0.8	28	0	118	0	162	36	172
0.9	0	104	28	115	58	50	56
1.0	16	56	33	85	74	12	76
1.1	0	22	5	57	28	16	20
1.2	3	8	14	22	19	2	12
1.3	0	2	0	15	9	2	0
1.4	3	0	0	0	2	2	6
1.5	0	0	0	8	5	2	0
1.6	2	0	0	4	0	0	8
1.7	0	2	0	0	0	0	0
1.8	0	0	0	0	0	0	4
1.9	0	0	0	0	0	0	0
2.0	3	0	0	0	0	0	9

TABLE 3.10 INCLUSION COMPOSITION SAW F289

ATOMIC PERCENT				OXIDE WEIGHT PERCENT		
Mn	Ti	Al	Si	MnO	Al_2O_3	SiO_2
74.96	8.94	8.85	7.25	84	8	8
70.75	10.11	8.86	10.28	80	8	12
81.71	9.09	6.19	3.02	91	6	3
67.63	9.56	14.01	8.80	77	13	10
68.59	9.86	11.01	10.54	78	10	12
66.73	12.42	8.66	12.19	77	9	15
69.79	9.35	13.26	7.60	79	12	8
71.80	11.61	10.78	5.81	83	11	7
74.01	8.94	13.13	3.92	84	12	4
77.30	5.77	10.47	6.46	85	9	6
54.33	11.16	23.63	10.88	62	24	13
76.98	10.67	9.29	3.06	88	9	3
65.36	10.93	13.18	10.53	75	13	12
84.07	10.70	4.08	1.15	95	4	1
54.36	16.52	13.08	16.04	62	15	22
78.27	10.2	4.95	6.58	88	5	7
70.08	9.43	12.32	8.18	79	12	9
75.95	11.96	6.23	5.86	87	6	7
66.57	9.66	16.0	7.78	75	15	9
62.80	9.27	13.92	14.01	71	13	16
Ave						
70.60	10.31	11.10	7.99	80	10.8	9.2

Calculation of oxide weight percent for Mn-Al-Si phase assuming that pyrophanite ($MnTiO_3$) forms as the titanium rich phase.

TABLE 3.11 INCLUSION COMPOSITION SAW F292

ATOMIC PERCENT				OXIDE WEIGHT PERCENT		
Mn	Ti	Al	Si	MnO	Al_2O_3	SiO_2
54.83	27.03	17.33	.81	68	30	2
65.35	15.53	14.29	4.82	78	16	6
61.42	18.89	18.17	1.52	75	23	2
62.87	22.93	12.17	2.03	79	17	3
72.67	22.18	3.49	1.66	93	5	3
56.92	18.33	21.19	3.55	68	27	5
53.19	21.03	25.25	.53	63	36	1
62.78	23.07	8.44	5.71	78	12	10
64	19.46	15.09	1.44	79	19	2
59.32	18.02	22.17	.49	72	28	1
62.75	16.75	17.38	3.12	75	20	4
62.55	16.84	17.17	3.44	75	20	5
61.79	18.89	18.83	.50	75	24	1
52.54	16.79	25.31	5.36	61	31	8
45.83	16.55	30.48	7.15	51	38	11
48.71	14.67	29.05	7.57	56	34	10
55.45	12.64	25.92	5.99	64	28	8
64.29	18.42	14.14	3.14	78	17	5
57.81	19.56	20.72	1.91	70	27	3
42.78	13.88	35.41	7.93	47	42	11
Ave						
58.39	18.53	19.60	3.48	70.4	24.6	5.0

Calculation of oxide weight percent for Mn-Al-Si phase assuming that pyrophanite ($MnTiO_3$) forms as the titanium rich phase.

TABLE 3.12 INCLUSION COMPOSITION SAW F293

ATOMIC PERCENT				OXIDE WEIGHT PERCENT		
Mn	Ti	Al	Si	MnO	Al_2O_3	SiO_2
67.86	8.82	12.05	11.27	75	11	12
54.51	13.53	11.32	20.65	62	12	26
64.29	8.65	12.68	14.39	72	12	16
77.44	5.59	9.03	7.94	84	8	8
67.51	10.37	11.16	10.95	77	11	12
77.47	6.82	8.11	7.60	85	7	8
82.39	7.02	4.95	5.64	90	4	6
79.71	6.19	5.77	8.33	87	5	8
80.16	9.43	6.02	4.39	90	5	5
77.49	8.63	6.4	7.48	85	6	8
70.89	7.45	9.09	12.57	79	8	13
65.59	7.62	12.02	14.77	78	11	16
72.20	9.47	8.53	9.80	81	8	11
69.43	8.37	10.93	11.27	78	10	12
73.27	7.85	8.66	10.22	81	8	11
70.43	8.38	8.963	12.57	79	8	13
76.20	5.6	12.49	5.71	84	11	6
77.42	8.08	7.13	7.36	86	6	8
71.98	5.36	11.52	11.15	79	10	11
72.46	6.13	9.13	12.27	80	8	12
Ave						
72.44	7.97	9.28	10.31	80.5	8.4	11.1

Calculation of oxide weight percent for Mn-Al-Si phase assuming that pyrophanite ($MnTiO_3$) forms as the titanium rich phase.

TABLE 3.13 INCLUSION COMPOSITION SAW F295

ATOMIC PERCENT				OXIDE WEIGHT PERCENT		
Mn	Ti	Al	Si	MnO	Al_2O_3	SiO_2
81.15	5.82	7.10	5.92	88	6	6
86.74	4.92	4.30	4.04	93	3	4
81.7	6.02	6.32	5.96	89	5	6
89.86	6.35	2.16	1.64	97	2	2
84.74	5.56	5.59	4.11	91	5	4
83.14	5.51	3.85	7.51	89	3	7
79.59	7.41	5.86	7.14	88	5	7
74.15	8.53	6.80	10.52	83	6	11
84.17	5.38	7.27	3.18	91	6	3
84.94	5.05	8.78	1.23	92	7	1
88.26	5.98	2.78	2.98	95	2	3
77.91	4.83	9.11	8.15	84	8	8
80.51	6.92	5.73	6.84	88	5	7
70.56	5.82	11.66	11.96	78	10	12
67.74	7.05	14.13	11.08	75	13	12
82.74	6.62	6.8	3.85	90	6	4
67.74	9.58	13.17	9.50	77	13	11
74.60	5.2	9.83	10.38	81	8	10
82.17	5.57	7.09	5.18	89	6	5
75.46	6.59	8.44	9.5	83	7	10
Ave						
79.89	6.24	7.34	6.53	87.0	6.3	6.7

Calculation of oxide weight percent for Mn-Al-Si phase assuming that pyrophanite ($MnTiO_3$) forms as the titanium rich phase.

TABLE 3.14 INCLUSION COMPOSITION SAW F296

ATOMIC PERCENT				OXIDE WEIGHT PERCENT		
Mn	Ti	Al	Si	MnO	Al_2O_3	SiO_2
83.25	5.87	3.75	7.13	90	3	7
84.07	5.10	2.91	7.92	90	2	8
86.84	4.38	2.36	6.42	92	2	6
84.90	4.68	3.11	7.31	90	3	7
85.75	8.66	2.36	8.23	95	2	3
79.72	7.93	3.69	8.66	88	3	9
93.50	6.01	0.31	0.18	100	0	0
91.23	5.45	0.98	2.34	97	1	2
91.13	8.30	0.57	0.00	100	0	0
87.93	3.55	3.53	4.99	93	3	5
84.85	7.07	3.49	4.58	92	3	5
81.49	9.32	2.93	6.26	91	3	7
90.95	6.01	1.63	1.40	97	1	1
90.81	5.17	1.38	2.64	96	1	3
72.33	16.01	3.48	8.18	85	4	11
87.69	5.88	1.44	4.99	94	1	5
83.98	8.78	1.79	6.45	92	2	6
87.71	6.78	1.36	4.15	95	1	4
76.02	13.29	3.75	6.98	88	4	8
83.70	11.14	1.78	3.38	95	2	4
76.59	16.25	3.59	3.57	92	4	5
64.63	20.41	4.57	10.39	79	6	16
Ave						
84.50	8.46	2.49	4.55	92.4	2.1	5.5

Calculation of oxide weight percent for Mn-Si-Al phase assuming that pyrophanite ($MnTiO_3$) forms as the titanium rich phase.

TABLE 3.15 INCLUSION COMPOSITION GMAW AR COVER GAS

ATOMIC PERCENT					OXIDE WEIGHT PERCENT		
Mn	Ti	Al	Si	S	MnO	Al_2O_3	SiO_2
36.47	58.62	1.69	3.22	-	-	-	-
92.74	2.75	0.85	3.67	-	95	1	3
68.18	5.25	0.99	0.03	25.55	99	1	0
66.72	26.39	3.56	3.33	-	88	6	6
82.69	4.84	2.70	9.77	-	88	2	9
62.70	6.06	0.68	1.85	28.72	96	1	3
64.73	8.38	2.37	2.67	21.85	93	3	4
88.67	2.65	1.03	7.64	-	92	1	7
82.17	6.78	10.59	0.46	-	90	9	0
74.44	17.21	4.23	4.13	-	90	5	5
57.34	0.91	1.46	1.98	38.31	95	2	3
74.42	7.30	1.42	7.58	9.28	90	1	9
69.82	4.73	0.42	0.15	24.88	100	0	0
38.61	41.34	4.13	0.86	15.06	-	-	-
61.67	15.16	0.51	1.73	20.92	96	1	3
80.04	5.60	0.46	0.49	13.41	99	0	1
71.84	11.56	2.42	2.84	11.33	93	3	4
69.91	7.79	0.44	0.37	21.49	99	1	0
76.03	0.98	0.44	0.41	22.13	100	0	0
Ave							
69.43	12.33	2.13	2.80	13.31	94.6	2.0	3.4

Calculation of oxide weight percent for Mn-Al-Si phase assuming that pyrophanite ($MnTiO_3$) forms as the titanium rich phase and adjusted for those inclusions containing MnS. Some oxides have no value because titanium dominated the inclusion.

TABLE 3.16 INCLUSION COMPOSITION GMAW M2 COVER GAS

ATOMIC PERCENT				OXIDE WEIGHT PERCENT		
Mn	Ti	Al	Si	MnO	Al_2O_3	SiO_2
60.54	22.13	10.18	7.15	74	14	12
59.04	14.53	14.12	12.31	68	16	16
73.52	19.72	2.47	4.30	91	3	6
62.32	25.04	8.62	4.03	80	13	7
65.31	16.35	10.24	8.10	77	12	11
66.38	18.15	11.39	4.09	81	14	6
57.61	22.78	10.48	9.12	70	15	15
62.77	22.65	8.40	6.17	78	12	10
56.02	21.79	14.60	7.58	67	21	13
72.01	15.38	5.45	7.16	85	6	9
62.02	20.54	9.96	7.48	75	13	12
73.90	13.34	10.75	2.01	87	11	2
66.32	14.30	10.41	8.97	78	11	11
71.77	16.47	4.77	6.99	86	5	9
74.63	11.62	8.01	5.74	85	8	7
72.99	15.85	6.53	4.63	87	7	6
71.68	16.3	9.97	2.05	86	11	3
69.30	9.25	10.60	10.85	78	10	12
55.45	11.91	14.50	18.14	63	15	22
37.70	32.96	26.21	3.12	18	72	10
Ave						
64.56	18.06	10.38	7.00	75.7	14.3	10.0

Calculation of oxide weight percent for Mn-Al-Si phase assuming that pyrophanite ($MnTiO_3$) forms as the titanium rich phase.

TABLE 3.17 INCLUSION COMPOSITION GMAW MIDPT COVER GAS

ATOMIC PERCENT				OXIDE WEIGHT PERCENT		
Mn	Ti	Al	Si	MnO	Al_2O_3	SiO_2
67.32	15.79	9.61	7.28	80	11	10
65.24	20.56	8.52	5.67	80	11	9
56.43	5.30	13.13	25.14	62	12	26
55.15	25.68	9.64	9.53	66	16	18
61.39	20.15	9.99	8.47	74	13	13
59.37	23.83	7.96	8.84	73	12	15
55.57	24.48	9.47	10.47	66	15	19
66.79	20.04	6.79	6.38	82	9	9
68.62	24.63	4.55	2.19	90	7	4
66.77	17.13	10.10	6.0	80	12	8
63.05	26.90	7.87	2.18	83	13	4
61.24	19.83	9.58	9.35	74	12	14
63.15	22.64	10.68	3.53	79	15	6
65.46	18.56	6.11	9.87	79	7	14
55.04	24.40	9.79	10.77	65	15	19
61.41	18.07	11.91	8.62	74	14	12
61.84	24.01	8.92	5.23	78	13	9
55.55	20.67	13.64	10.14	65	18	16
62.63	18.37	9.03	9.97	75	11	14
61.49	21.26	9.21	8.03	75	12	13
Ave						
61.63	20.61	9.33	8.43	75.0	12.4	12.6

Calculation of oxide weight percent for Mn-Al-Si phase assuming that pyrophanite ($MnTiO_3$) forms as the titanium rich phase.

TABLE 3.18 INCLUSION COMPOSITION GMAW C5 COVER GAS

ATOMIC PERCENT				OXIDE WEIGHT PERCENT		
Mn	Ti	Al	Si	MnO	Al_2O_3	SiO_2
69.33	14.19	5.58	10.90	81	6	14
71.98	5.84	5.68	16.50	79	5	17
81.23	13.34	2.16	3.27	94	2	4
75.52	12.09	7.77	7.63	83	8	9
77.60	14.34	4.85	3.21	91	5	4
80.63	13.78	1.86	3.72	94	2	4
65.35	16.15	5.9	12.6	77	7	17
82.09	8.8	2.98	6.13	91	3	6
67.06	18.81	4.63	9.51	81	6	14
81.24	4.37	3.64	10.75	87	3	10
62.87	11.89	8.31	16.93	72	8	20
70.28	14.99	5.87	8.96	82	6	11
73.40	14.73	4.19	7.68	85	4	10
67.87	5.75	9.20	17.18	75	8	17
75.31	14.54	4.22	5.93	88	4	7
81.06	9.37	3.83	5.74	90	3	5
66.01	17.54	6.77	9.68	79	8	13
71.37	13.9	4.82	9.91	83	5	12
75.35	13.48	4.48	6.68	87	5	8
78.34	12.25	4.01	5.40	90	4	6
Ave						
73.51	12.53	5.04	8.92	84.5	5.0	10.5

Calculation of oxide weight percent for Mn-Al-Si phase assuming that pyrophanite ($MnTiO_3$) forms as the titanium rich phase.

TABLE 3.19 INCLUSION COMPOSITION GMAW M4 COVER GAS

ATOMIC PERCENT				OXIDE WEIGHT PERCENT		
Mn	Ti	Al	Si	MnO	Al_2O_3	SiO_2
87.26	9.29	0.87	2.58	97	1	3
77.99	7.76	5.37	8.88	86	5	9
76.91	8.05	5.17	9.87	85	5	10
79.03	9.14	4.75	7.08	88	4	8
69.80	8.34	5.97	15.89	78	5	17
84.01	13.60	0.97	1.42	97	1	2
74.57	16.63	5.20	3.60	90	6	5
76.76	20.74	0.57	1.92	96	1	3
64.96	23.27	5.05	6.72	82	7	11
69.56	16.35	10.28	3.81	83	12	5
80.35	9.74	3.62	6.28	90	3	7
82.96	8.17	2.32	6.55	91	2	7
61.10	23.20	6.48	9.22	75	9	16
66.49	19.62	6.08	7.80	81	8	11
71.07	13.38	7.14	8.41	82	7	10
67.43	16.45	8.86	7.26	80	10	10
74.71	16.76	4.37	4.16	90	5	5
82.21	14.72	0.82	2.25	96	1	3
70.90	11.78	8.55	8.77	81	8	10
81.75	9.46	1.94	6.85	91	2	7
Ave						
74.99	13.82	4.72	6.47	86.9	5.1	8.0

Calculation of oxide weight percent for Mn-Al-Si phase assuming that pyrophanite ($MnTiO_3$) forms as the titanium rich phase.

TABLE 3.20 INCLUSION COMPOSITION GMAW M4/C10 COVER GAS

ATOMIC PERCENT				OXIDE WEIGHT PERCENT		
Mn	Ti	Al	Si	MnO	Al_2O_3	SiO_2
73.45	13.14	4.42	8.99	85	4	11
83.60	8.10	2.41	5.89	92	2	6
77.11	8.69	6.47	7.73	85	6	8
75.68	13.00	4.59	6.74	87	5	8
78.36	14.56	1.94	5.15	92	2	6
78.88	10.98	2.61	7.53	89	2	8
79.73	10.18	4.26	5.83	90	4	6
73.76	15.65	3.80	6.80	87	4	9
75.66	12.48	4.57	7.29	87	5	9
73.49	13.81	5.48	7.22	85	6	9
81.18	10.87	3.25	4.70	92	3	5
60.29	5.71	12.45	21.55	67	11	22
72.21	8.55	6.17	13.07	80	6	14
65.97	19.74	4.47	9.82	80	6	14
70.31	10.64	6.21	12.84	80	6	14
77.47	13.72	2.23	6.59	90	2	8
78.43	8.42	2.81	10.34	87	2	11
74.52	11.82	4.48	9.18	85	4	11
83.09	9.44	2.78	4.68	92	3	5
69.28	11.23	7.23	12.26	79	7	14
Ave						
75.12	11.54	4.63	8.71	85.7	4.4	9.9

Calculation of oxide weight percent for Mn-Al-Si phase assuming that pyrophanite ($MnTiO_3$) forms as the titanium rich phase.

TABLE 3.21 INCLUSION COMPOSITION GMAW C10 COVER GAS

ATOMIC PERCENT				OXIDE WEIGHT PERCENT		
Mn	Ti	Al	Si	MnO	Al_2O_3	SiO_2
75.36	13.20	4.87	6.57	87	5	8
71.48	16.30	6.48	5.74	85	7	8
74.53	15.03	4.53	5.91	88	5	7
74.83	17.60	3.87	3.70	91	4	5
71.06	14.65	6.95	7.34	83	7	9
76.58	16.18	3.21	4.02	91	3	5
78.45	15.73	3.19	2.63	94	3	3
74.99	19.59	1.89	3.53	93	2	5
59.33	18.77	9.15	12.75	70	11	19
64.84	16.59	5.39	13.18	76	6	18
74.98	17.51	1.65	5.86	90	2	8
75.99	18.81	2.36	2.84	93	3	4
69.99	15.10	6.44	8.46	82	7	11
62.40	7.83	13.01	16.77	70	12	18
70.88	18.18	5.82	5.13	86	7	7
73.99	12.68	4.83	8.50	85	5	10
78.55	16.18	2.54	2.73	94	3	3
70.65	14.97	4.09	10.29	83	4	13
77.70	13.17	4.92	4.21	90	5	5
77.74	15.47	2.41	4.37	92	3	5
Ave						
72.71	15.68	4.88	6.73	86.1	5.3	8.6

Calculation of oxide weight percent for Mn-Al-Si phase assuming that pyrophanite ($MnTiO_3$) forms as the titanium rich phase.

TABLE 3.22 INCLUSION TITANIUM-RICH PHASE COMPOSITION

SAMPLE NUMBER	ATOMIC PERCENT	
	Mn	Ti
1	56	44
2	55	45
* 3	51	49
4	53	47
** 5	53	47

* Figure 3.8

** Figure 3.9

TABLE 3.23 PERCENT ACICULAR FERRITE/COLUMNAR GRAINS

	SAMPLES	Percent columnar grains	Percent acicular ferrite
S A W	F289	29%	43%
	F292	37%	65%
	F293	26%	41%
	F295	33%	27%
	F296	29%	78%
G M A W	AR	(89%)	0% (2%)
	M2	(81%)	16% (15%)
	MIDPT	(99%)	21% (11%)
	C5	(86%)	24% (9%)
	M4	(88%)	25% (12%)
	C10	(90%)	19% (11%)
	M4/C10	(90%)	22% (13%)

Percent acicular ferrite in the weld metal calculated from a statistical analysis of 10 random photographs taken in the weld metal. A five square millimeter grid was used for calculations.

Numbers in parenthesis are acicular ferrite and columnar grain calculations for GMAW multi-pass welds for comparison to Charpy fixed energy values.

IV. ANALYSIS OF RESULTS

A. ANALYSIS OF WELD THERMAL CYCLE

The first of the factors analyzed in determining the origins of acicular ferrite in GMAW and SAW weldments was the weld thermal cycle. As discussed in sections 2E and 2G, the weld metal microstructure depends on the time to cool from 800 to 500 °C ($dt_{8/5}$) during the time the austenite to ferrite transformation is occurring. If $dt_{8/5}$ is less than 5 seconds or greater than 30 seconds then the formation of acicular ferrite would be unlikely. The general formula generated by Christensen for calculation of $dt_{8/5}$ assumes welding of thick plates with three dimensional heat flow. All GMAW and SAW weldments meet this criteria. For multi-pass welds the equation is modified to account for a longer cooling time due to the interpass temperature. The equation becomes:

$$dt_{8/5} = (5\ n\ E)/(\{650 - T_o\}/630)$$

where T_o is the interpass temperature. Using the data recorded in Table 4.1, $dt_{8/5}$ is calculated to be 6.00 seconds for GMAW bead-on-plate welds, 7.57 seconds for GMAW multi-pass welds and 16.29 seconds for SAW weldments. These results indicate that formation of acicular ferrite is possible if other conditions are optimum.

B. ANALYSIS OF WELD METAL COMPOSITION

1. Weld Metal Oxygen

A review of Tables 3.4 and 3.6 shows that oxygen concentrations in the weld metal were adequate for formation of acicular ferrite with the exception of the GMAW weldment with 100 % argon cover gas. Weld metal oxygen in this sample was 30 ppm which created a small number of large inclusions that did not support the formation of acicular ferrite. As formation of acicular ferrite was unlikely (0 % acicular ferrite found), this sample was not used for subsequent analysis. All SAW weldments contained near optimum concentration of 300 ppm oxygen (range 270 to 350 ppm) for creating an inclusion field able to nucleate large proportions of acicular ferrite. GMAW weldments contained adequate weld metal oxygen for formation of acicular ferrite, but concentrations were at the low end of the desired levels. From this analysis lower proportions of acicular ferrite are expected in the GMAW weldments as compared to the SAW weldments.

Analysis of the GMAW weldments showed that as oxygen potential in the cover gas increased weld metal oxygen concentration also increased in an apparent linear fashion. Oxygen activity potential was determined assuming 100 % activity for any oxygen added and 75 % of the oxygen from the complete disassociation of the carbon dioxide would be

effective. This assumption appeared to agree with the conclusions of several researchers, though much controversy still exists on this issue [Gibson, 1993]. The only major deviation from this linear relationship was the C5 (5% CO_2/95% Ar) cover gas weld. The fact that weld metal oxygen in this sample was the same as the C10 (10% CO_2/90% Ar) weldment and the large deviation between the six samples analyzed indicates that some atmospheric contamination may have occurred. The sample used for this investigation was at the low end (210 ppm) of the oxygen concentrations provided for the C5 weldments.

2. Weld Metal Manganese

As discussed in section 2F, manganese is important to the formation of acicular ferrite by lowering the austenite to ferrite transformation start temperature so that a acicular ferrite microstructure is favored over grain boundary and side plate ferrite morphologies. Too much manganese lowers the transformation temperature too far so that bainitic and martensitic microstructures will predominate. Therefore manganese levels in excess of 1.0 wt % and near 1.5 wt % are optimum for acicular ferrite formation. [Grong, 1986]

A review of Tables 3.4 and 3.6 shows SAW manganese levels to be nearly optimum for acicular ferrite formation (range 1.28 to 1.54 wt %). GMAW weldments have adequate manganese concentrations, but at levels near 1.0 wt % (range

1.032 to 1.193 wt %) the proportion of acicular ferrite in the GMAW weldments is expected to be small compared to the SAW weldments.

3. Weld Metal Aluminum and Titanium

As discussed in section 2F, aluminum and/or titanium concentrations in the weld metal must be high enough to form non-metallic inclusions rich in the titanium phase or galaxite ($MnO \cdot Al_2O_3$). Analysis of previous research suggested that the combination of weld metal aluminum and titanium should be near 300 ppm to be optimum for formation of acicular ferrite. Using the data in Tables 3.4 and 3.6 a graphical presentation of this analysis is presented in Figures 4.2 (SAW) and 4.3 (GMAW). This analysis shows that with the exception of SAW sample F292 all samples for this investigation fall far short of this requirement. This analysis taken alone indicates that a large percentage of acicular ferrite should exist in SAW weldment F292 and smaller amounts in the other welds.

C. ANALYSIS OF NON-METALLIC INCLUSIONS

The importance of non-metallic inclusions for the formation of acicular ferrite was discussed in detail in sections 2F and 2G. Analysis of inclusion concentrations, composition and size distributions for each weldment was conducted to determine the relative importance of each of these factors on formation of acicular ferrite. An accurate analysis for GMAW weldments was difficult because the

difference in the amount of acicular ferrite between samples was small (range 16 to 25 %). However, comparison of the GMAW samples to the SAW samples proved to be an effective analytical tool.

1. Inclusion Concentration

Analysis of the data in Tables 3.7 and 3.23 determined the influence of inclusion concentration on the formation of acicular ferrite. GMAW results were adjusted to cover the same area as the SAW samples for direct comparisons. The volume fraction of the inclusions would indicate that the GMAW samples should have better inclusion fields for the formation of acicular ferrite than the SAW samples. In reality the average inclusion size of the GMAW inclusions are much larger than the SAW inclusions resulting in a much lower concentration of inclusions. This analysis points out the reason that using inclusion volume fraction is not a good measure of an inclusion fields ability to promote the formation of acicular ferrite.

For the SAW weldments the concentration of inclusions (measured by number and size) in each of the samples is nearly the same except for sample F296. The reason for the large number of inclusions in this sample is unexplained. However based on the other analysis this data suggests that a large number of small inclusions is desirable for formation of large percentages of acicular ferrite in the weld deposit. Figure

4.4 shows that the volume fraction of inclusions had little influence on the amount of acicular ferrite formed except for sample F296.

Comparison of the GMAW and the SAW weldments shows that a larger number of inclusions in the size range from 0.3 to 1.0 microns is more important for acicular ferrite formation than inclusion volume fraction. This becomes even more apparent when comparing the inclusion composition, since the GMAW inclusions contained more of the desirable Ti-rich phase than SAW inclusions. This investigation also found that welds that exhibited the clustering seen in Figure 3.2 formed a smaller proportion of acicular ferrite. This result was true for both the GMAW and SAW weldments.

2. Inclusion Composition

Determining the composition of the inclusions and the effects of this composition on formation of acicular ferrite was a major goal of this investigation. Previous research indicated that those inclusions rich in a titanium phase or Galaxite provided angular faces that promoted the nucleation of acicular ferrite. Determination of the inclusion phases is important in that it holds the key to controlling formation of acicular ferrite and determining the mechanism of the ferrite nucleation and growth on the inclusion.

This investigation first tried to determine the composition of the titanium-rich phase. Using auger electron

microscopy, Peters had determined the titanium-rich phase to consist of TiN [Peters, 1989]. The analysis of the data from the present investigation presented in Figures 4.2 and 4.3 show a general trend that for a nearly constant weld metal nitrogen concentration, titanium concentration continues to decrease as weld metal oxygen concentration increases. This trend suggests that the titanium was forming an oxide and floating out of the molten weld pool prior to solidification. To test this theory a sample with known TiN inclusions was analyzed in the SEM with EDX analysis and compared to a GMAW inclusion. Figure 4.5 shows a micrograph of the TiN inclusion used for this analysis. Figure 4.6 is a micrograph of the GMAW inclusion with an x-ray may showing the angular phase at the inclusion edge to be titanium-rich. Figure 4.7 shows the EDX spectrum of each of these inclusions for comparison. The TiN inclusion spectrum shows a nitrogen K-series peak that is larger than the titanium L-series peak. In the GMAW inclusion spectrum of the same counts showed a nitrogen K-series peak smaller than the titanium L-series peak. This result also suggests that the titanium-rich phase is an oxide.

Working with HSLA steels with low oxygen ($\approx$ 80 ppm) and nitrogen (max = 20 ppm) concentrations, Senogles used x-ray diffraction (XRD) to find a titanium-rich phase called Pyrophanite, $MnTiO_3$, in the cast steel inclusions. The steel composition for this experiment included of 50 ppm aluminum and 50 to 150 ppm titanium. The iron matrix was disolved using

a nitric acid solution, leaving just the inclusions for XRD analysis. Average inclusion size was of the order of five microns. The current investigation was unable to reproduce this experiment because the inclusions in the weld deposit are much smaller than cast steel inclusions preventing filtering of the inclusions. [Senogles, 1994]

TEM analysis of inclusions on a carbon replica prepared sample using a LaB_6 filament energized to 120,000 volts was unable to produce a diffraction patterns due to the thickness of the inclusions. Using a HVEM energized to one million volts provided a diffraction pattern from a 0.47 micron inclusion. Figure 3.16 shows the diffraction pattern obtained at a camera distance of 2.5 meters. Analysis of this diffraction pattern was complicated by multiple phases and multiple crystals of the phases present. The complexity of the diffraction pattern prevented single crystal analysis. Plotting the ring pattern for Pyrophanite ($MnTiO_3$) on the diffraction pattern shows a majority of the spots fall on these rings (Figure 4.8). Similar analysis were conducted for iron, Manganosite, Mn_2TiO_4 and Galaxite, phases identified as possibilities by SEM EDX analysis, with few or no matches.This result strongly suggests that the diffraction pattern is for a polycrystalline Pyrophanite phase.

Another experiment to determine the composition of the titanium-rich phase was conducted in the SEM with EDX analysis. Large inclusions (one to two microns) with titanium

rich phases in the center were identified in the GMAW samples. Figures 3.7, 3.8 and 3.9 are examples of the inclusions used for this analysis and typical results.Using a LaB_6 filament energized to 20,000 volts a small spot size (seven) was used with a spot analysis (800 second count). Background due to the interaction bulb was stripped as discussed in section three. These results presented in Table 3.22 show approximately a 1:1 atomic ratio of titanium to manganese. These results support the conclusion that the titanium-rich phase in the inclusion is Pryophanite.

SEM EDX analysis of multiple inclusions from each sample are listed in Tables 3.10 through 3.21. Assuming that the titanium phase is Pyrophanite the other major constituents in the inclusion manganese, aluminum and silicon were converted to weight percent oxides and plotted on a $MnO \cdot Al_2O_3 \cdot SiO_2$ ternary phase diagram. The results of this analysis are presented in Figures 4.9 (SAW) and 4.10 (GMAW). These results indicate that the other predominant phase in the inclusions is Manganosite. When weld metal aluminum concentration reaches 200 ppm aluminum concentration in the inclusions increases so that the other dominant phase is Galaxite which has been identified from TEM diffraction patterns in previous research on weld metals with high concentrations of aluminum [Dowling, 1986].

Manganosite inclusions are spherical and therefore have been shown to be poor sites for nucleation of acicular

ferrite as compared to angular phases like Galaxite or Pyrophanite. Figure 3.6 is a micrograph of this type of inclusion. TEM EDX analysis of a carbon replica sample provided a spectrum equivalent to the SEM EDX spectrum validating the SEM results. In all cases analyzed on the TEM with carbon replica samples, the inclusions were free of iron validating the background stripping procedure and verifying that the second phase in the inclusions was a complex $MnO \cdot Al_2O_3 \cdot SiO_2$ phase.

Research on welds with low titanium concentrations (< 50 ppm) and high aluminum concentrations (> 200 ppm) by Bhatti and others showed that the level of acicular ferrite found in the weld deposit increased as the percentage of aluminum-rich inclusions increased. Aluminum-rich inclusions were most effective for acicular ferrite formation when the inclusion ratio of [wt% Mn]/[wt% Al] was less than 0.24. [Bhatti, 1984] Using TEM diffraction pattern analysis of aluminum-rich inclusions, Dowling identified the aluminum-rich phase as Galaxite ($MnO \cdot Al_2O_3$) [Dowling, 1986].

For weldments with low weld metal aluminum concentrations, Bonnet and Charpentier showed that titanium in the inclusions is important for formation of acicular ferrite. Their research showed that weld metal titanium concentrations less than 45 ppm formed almost no acicular ferrite. As weld metal titanium concentrations were increased to 140 ppm, up to 80 % of the weld metal consisted of the acicular ferrite

microstructure. [Bonnet, 1983] Evans working with weld metals low in aluminum found that the amount of acicular ferrite formed was sensitive to the ratio of manganese and titanium in the weld metal [Evans, 1993]. This suggests that an optimum manganese-to-titanium ratio also exists in inclusions to optimize inclusion composition for acicular ferrite formation.

Saggese showed results that supports the above findings (Figure 2.9). For low weld metal aluminum concentrations, titanium in the inclusions appeared to be responsible for acicular ferrite formation. As titanium levels in the inclusions increased, so did the amount of acicular ferrite formed. For constant concentrations of titanium, as weld metal aluminum concentration increases the amount of acicular ferrite formed also increases. However the rate at which acicular ferrite percentage in the weld metal increases is much less for those welds that contained significant levels of titanium. [Saggese, 1983] This suggests that the titanium-rich phase in the inclusions is more effective for nucleation of acicular ferrite than the Galaxite.

Composition analysis in the present research indicates that as aluminum concentrations in the weld metal reach 200 ppm, The angular phase Galaxite is formed in the inclusions as reported by Bhatti and Dowling [Bhatti 1984, Dowling 1986]. For lower aluminum concentrations the complex $MnO \cdot Al_2O_3 \cdot SiO_2$ phase is predominately composed of MnO, Manganosite. In titanium-containing weldments the inclusion composition

appears to be a combination of Pyrophanite/Manganosite or Pyrophanite/Galaxite depending on the aluminum concentration. Both Galaxite and Pyrophanite are angular phases which have been shown to be a requirement for nucleation of acicular ferrite on the inclusion. Galaxite has a melting temperature of 1800 °C and would form in the molten weld pool. Manganosite is a glassy phase with a melting temperature in the range of 1600-1800 °C depending on the aluminum and silicon concentrations which also forms in the molten weld pool. Pyrophanite remains molten after the steel has solidified, but Manganosite or Galaxite can exist inside this molten inclusion as solid particles. This idea is supported by the HVEM micrograph in Figure 3.16 which shows a two phase inclusion with heavier particles existing in a lighter matrix (e.g. Manganosite in Pyrophanite). At about 1400 °C the Pyrophanite solidifies as angular inclusions generating a large strain field in the surrounding matrix which would assist in nucleating acicular ferrite. This could explain why the titanium-containing inclusions are more effective than the Galaxite-containing inclusions for forming acicular ferrite as shown in Figure 2.9.

Weld metal aluminum and titanium was plotted against inclusion aluminum and titanium for each of the GMAW and SAW weldments to determine if a correlation existed. These results are presented in Figures 4.11 through 4.14. The GMAW samples with low oxygen levels show a wide range of inclusion

compositions for the same or similar weld metal composition. However as weld metal oxygen concentration increases similar concentrations of weld metal titanium result in higher inclusion titanium levels. SAW samples with optimum concentrations of weld metal oxygen show a more identifiable trend of increasing inclusion titanium and aluminum content with increasing weld metal concentrations. This trend exists for all SAW samples except F296 which has a much higher number of inclusions than the other samples. These results suggest that control of inclusion composition through weld metal composition requires optimum concentrations of oxygen in the weld metal.

3. Inclusion Size Distribution

The results of the investigation into inclusion size distribution are presented in Tables 3.7, 3.8 and 3.9. From the discussion in section 2F it was expected that the GMAW inclusions would be smaller than the SAW inclusions due to a higher heat input in the SAW samples, lowering the cooling rate, allowing more time for inclusion growth prior to solidification. For our investigation GMAW inclusions are larger because in the multi-pass SAW weldments the larger inclusions have had multiple opportunities to float out of the weld pool during reheat from subsequent passes. Although a detailed study of the inclusion field of the GMAW multi-pass weldments was not conducted, the reduction in acicular ferrite

from the single pass welds is probably due to a similar phenomena resulting in a less dense inclusion field. This phenomena was documented in the research conducted by Douglas [Douglas, 1989].

Each of the GMAW inclusion fields exhibit a s-shaped size distribution indicative of low weld metal oxygen concentrations. Size distributions for the GMAW M4 cover gas (220 ppm oxygen, 25% acicular ferrite) and Ar cover gas (30 ppm oxygen, 0 % acicular ferrite) are plotted in Figure 4.15.

Each of the SAW inclusion fields exhibit the c-shaped size distribution indicative of high concentrations of weld metal oxygen. Size distributions for SAW samples F296, F292 and F295 are plotted in Figure 4.16. Sample F296 (78 % acicular ferrite) has a large number of inclusions with moderate amounts of titanium in the inclusions. The large number of inclusions is very favorable for formation of acicular ferrite. From size distribution information only, it would appear that sample F295 would be better for formation of acicular ferrite than sample F292. In reality sample F292 (65% acicular ferrite) has more acicular ferrite than sample F295 (27 % acicular ferrite). Table 4.2 provides various factors for comparison between these two samples. The difference that stands out between these samples is the amount of aluminum and titanium in the inclusions of the samples. This result suggests that inclusions rich in galaxite and/or pyrophanite are more effective at nucleating acicular ferrite. These

conclusions indicate that the amount of acicular ferrite can be controlled by controlling weld metal composition, ensuring adequate concentrations of oxygen, aluminum and titanium are present.

D. FRACTURE TOUGHNESS

An analysis to determine the effectiveness of the acicular ferrite microstructure on improving fracture toughness was conducted as part of this investigation. This analysis identified four factors that interact to control weld toughness; weld metal Mn concentration, tensile strength, percent columnar grains and percent acicular ferrite.

In general, as tensile strength increases, weld fracture toughness decreases due to the increase in strength resulting from microstructures more susceptible to brittle fracture. This trend is clearly shown in Figure 4.17. The GMAW weldments have large amounts of columnar grains, similar weld Mn concentrations and similar amounts of acicular ferrite. Using Charpy fixed energy as a measure of fracture toughness, the trend of decreasing fracture toughness for increasing strength is clearly identified. Figure 4.18 shows little change in fracture toughness for the range of weld manganese concentrations associated with the GMAW weldments. These figures also show that fracture toughness decreases more for the argon cover gas with no acicular ferrite, suggesting that

even small amounts of acicular ferrite in the weld deposit (10%) can improve fracture toughness.

The same analysis for the SAW weldments shows the interactions between the four factors controlling weld toughness. These factors are represented in the plots in Figures 4.19 and 4.20. Figure 14.19 shows that a weld with high tensile strength can have good fracture toughness if the weld has a low percentage of columnar grains and high percentages of acicular ferrite. Figure 4.20 shows the interactions between Mn concentration, percent columnar grains and percent acicular ferrite. Sample F296 has excellent fracture toughness due to near optimum Mn concentration, low amount of columnar grains and large amounts of acicular ferrite even though tensile strength is high. Sample F292 has a lower fracture toughness due to a significant increase in columnar grains and small decrease in acicular ferrite even though tensile strength is much lower. Sample F289 has less acicular ferrite and lower Mn concentration with similar fracture toughness as sample F292. This is due to a decrease in both columnar grains and tensile strength. Sample F293 shows the importance of maintaining optimum weld metal manganese content. With all other factors similar, the ductile to brittle transition temperature (DBTT) is higher by 22 °F (-62 °F vice -84 °F). This data suggests that the reduction in fracture toughness occurs due to the lower manganese content in the weld metal creating a coarser microstructure, reducing

fracture toughness. Sample F295 shows that fracture toughness is poor even if Mn concentration is optimum and strength is low if a low percentage of acicular ferrite exists in the weld deposit.

This analysis concludes that weld deposits with high fracture toughness can be created even at high tensile strengths if large proportions of the weld metal microstructure are acicular ferrite. Toughness can also be improved by minimizing the fraction of columnar grains in the weld deposit and maintaining a low tensile strength. Controlling manganese concentrations improves fracture toughness by refining the microstructure and promoting the formation of acicular ferrite.

E. GENERAL REVIEW

The reason for generating a weld deposit microstructure that consists of acicular ferrite is to create a high strength weld with good fracture toughness. For high strength steels used in Naval construction programs this can be achieved in SAW weldments by using a flux with a high basicity index (BI near three) together with a weld filler wire of appropriate composition. For the fluxes used for this investigation, those with the higher basicity indexes had higher proportions of acicular ferrite in the weld metal (Table 4.3). The Lincoln MIL800 flux, with the highest BI of the fluxes tested (BI = 2.97),used in sample F296 was the best flux for promoting the

formation of acicular ferrite (78%) and creating a high strength weld (825 MPa) with good fracture toughness (DBTT = -108 °F). This flux created an inclusion field consisting of a large number of medium sized inclusions (average size = 0.423 microns, ≈ five times as many inclusions as other fluxes). This appears to have been caused by more of the weld metal oxygen existing as oxides rather than as dissolved oxygen. As other weld metal conditions were bounded by the other fluxes used, the reason for this phenomena is unclear and requires more research. The Oerlikon OP121TT (Houston) flux used for weldment F292 (BI = 2.83) also provided a high strength weld (752 MPa) with good fracture toughness (DBTT = -85 °F) by forming a large proportion of acicular ferrite in the weld deposit. In this case the reason for acicular ferrite formation is due to a weld metal composition that contained optimum concentrations of oxygen, manganese, titanium and aluminum. This created inclusions that contained large proportions of the angular phases, pyrophanite and galaxite, which were effective nucleation sites for promoting the formation of acicular ferrite. Further research may show that F296 is a better choice especially if it generates large amounts of appropriate inclusions everytime it is used.

The results of the investigation into GMAW weldments of high strength steels showed that the present cover gases and welding procedures are not adequate to produce high strength welds with good fracture toughness properties. In general,

oxygen concentrations in the weld metal were not high enough to form the number of inclusions required for producing large amounts of acicular ferrite. For those weldments where higher oxygen potential existed in the cover gas produced higher weld metal oxygen concentrations, subsequent losses of titanium and aluminum limited the effectiveness of the inclusions for nucleating acicular ferrite. In addition, limitations of heat input into the weld reduced the effectiveness of reheat from subsequent weld passes for refining the grains creating large proportions of columnar grains in the weld deposit (80 to 99%). Both of these conditions are detrimental to fracture toughness.

More acicular ferrite could be produced if GMAW weldments had weld metal compositions that contained near 300 ppm oxygen, 1.0 wt % manganese and a combined concentration of titanium and aluminum near 300 ppm. These conditions could be created by increasing the oxygen potential of the cover gas to six to eight weight percent (6% oxygen or 15% carbon dioxide) and choosing a weld wire higher in aluminum and/or titanium and manganese to account for losses due to losses of these elements in the molten weld pool. However this solution for acicular ferrite does nothing to reduce the amount of columnar grains formed in the weld deposit.

The use of a flux-cored weld wire may be a more appropriate choice for GMAW weldments. This type of weld wire would not only create the desired weld composition, but also

provide more heterogeneous nucleation sites for solidification in the molten weld pool creating a more equiaxed grain structure. This should reduce the amount of columnar grains found in the weld deposit and dramatically improve fracture toughness in GMAW weldments. More research should be conducted on this topic.

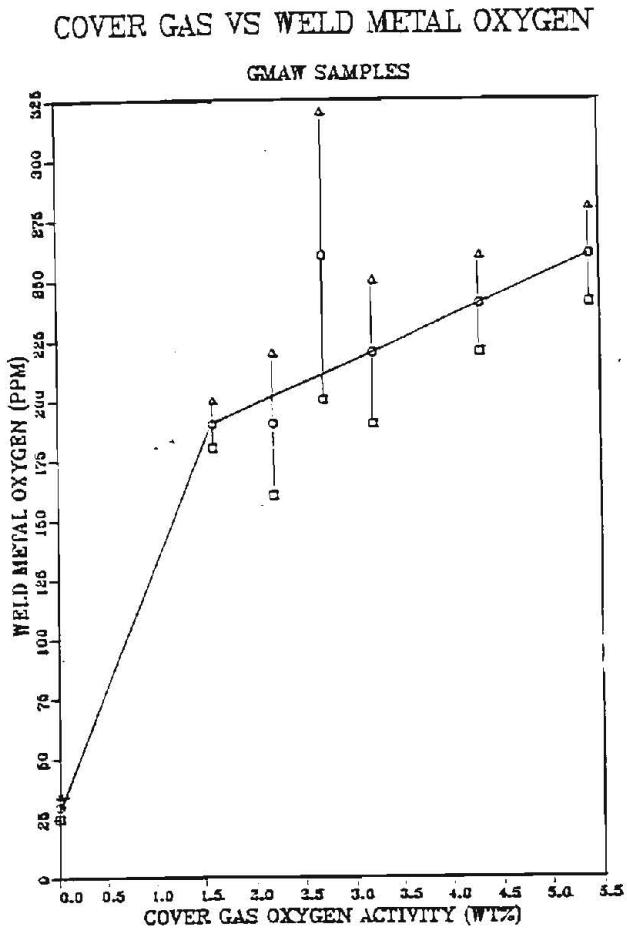

SAMPLE	COVER GAS (Vol%)	Calculated oxygen potential (wt%)
Ar	100% Ar	0
M2	98% Ar/2% O_2	1.6
MIDPT	33.3% Ar/C10/M4	2.1
C5	95% Ar/5% CO_2	2.8
M4	96% Ar/4% O_2	3.2
C10/M4	50% C10/M4	4.4
C10	90% AR/10% CO_2	5.6

Figure 4.1
GMAW Cover Gas Oxygen vs Weld Metal Oxygen

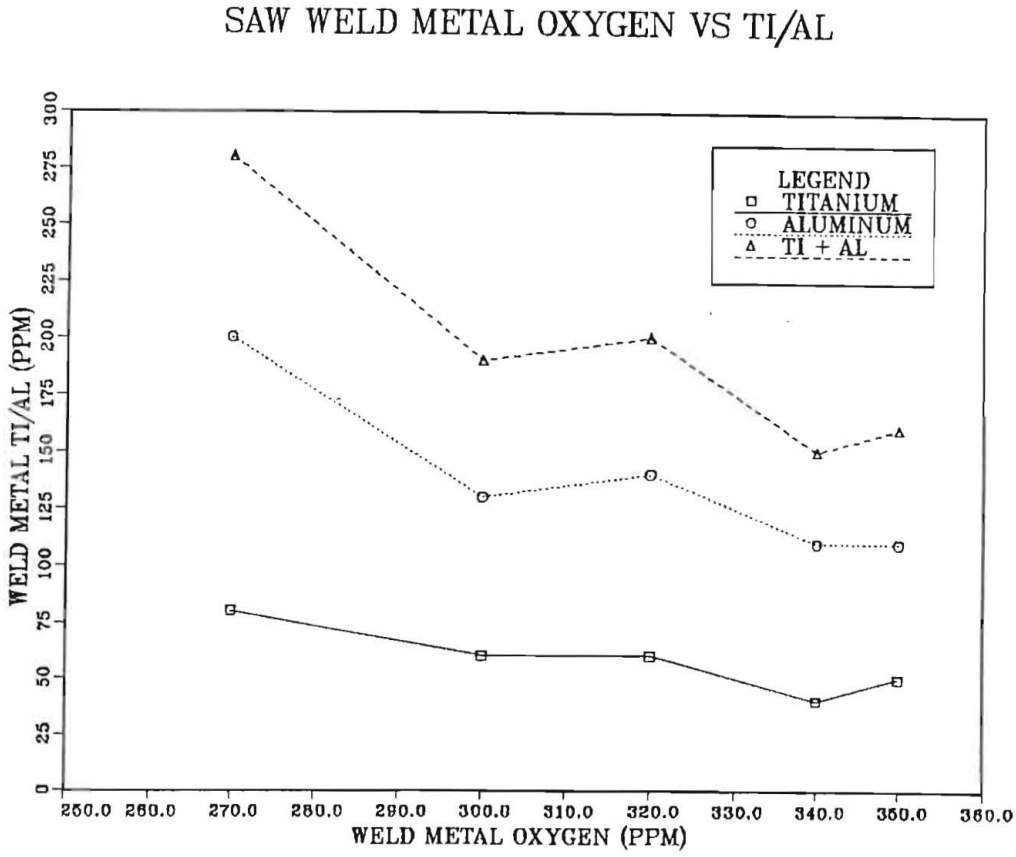

SAMPLE	OXYGEN	Ti	Al	Ti + Al
F292	270	80	200	280
F289	300	60	130	190
F296	320	60	140	200
F293	340	40	110	150
F295	350	50	110	160

Figure 4.2
SAW Weld Metal Oxygen vs Ti/Al

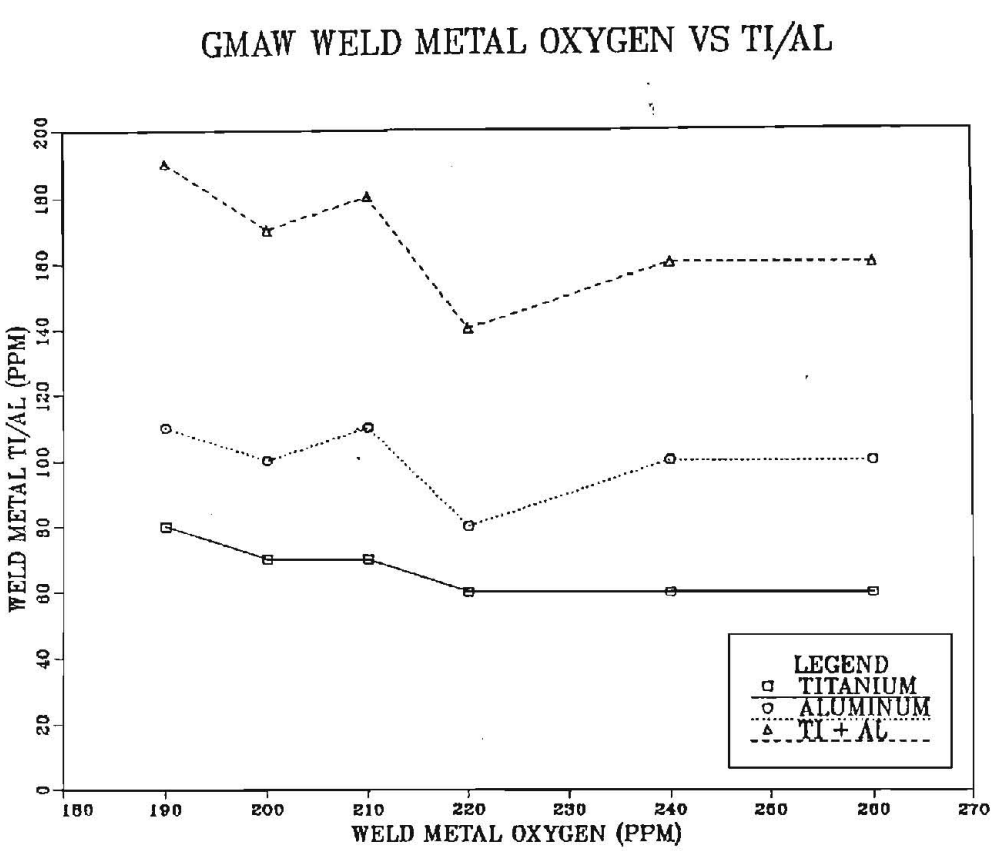

SAMPLE	OXYGEN	Ti	Al	Ti + Al
M2	190	80	110	190
MIDPT	200	70	100	170
C5	210	70	110	180
M4	220	60	80	140
C10/M4	240	60	100	160
C10	260	60	100	160

Figure 4.3
GMAW Weld Metal Oxygen vs Ti/Al

SAW % AF VS INCLUSION VF

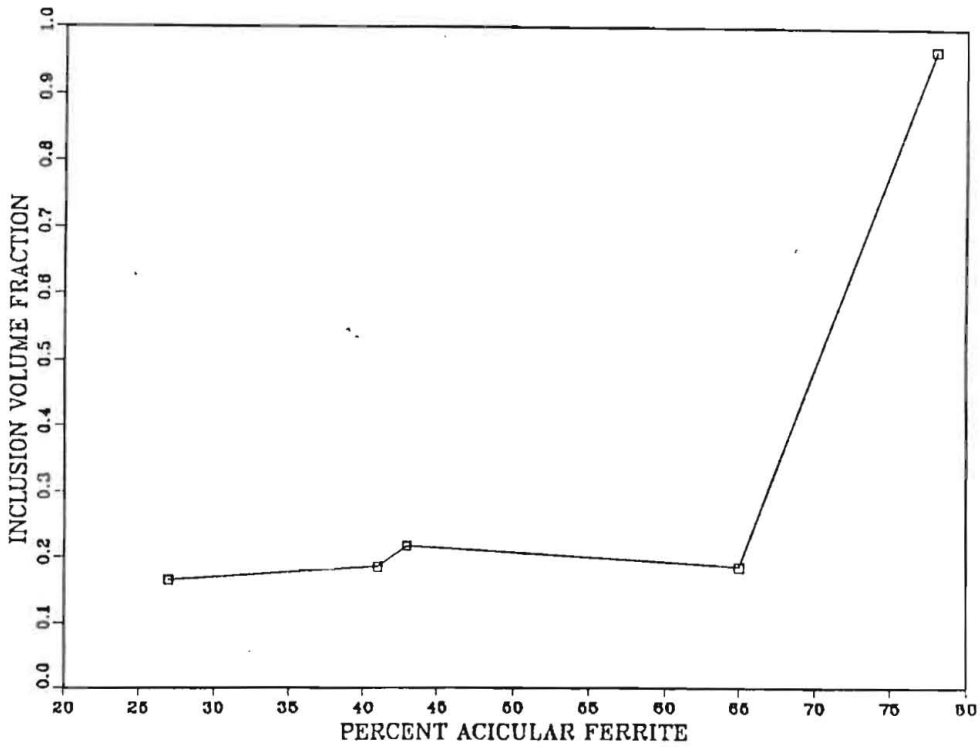

SAMPLE	% AF	INCLUSION VF	# INCL	AVE SIZE (microns)
F295	78	.165	364	.323
F293	65	.185	408	.322
F289	43	.216	483	.320
F292	41	.185	297	.378
F296	27	.966	1237	.423

Figure 4.4
SAW Acicular Ferrite vs Inclusion Volume Fraction

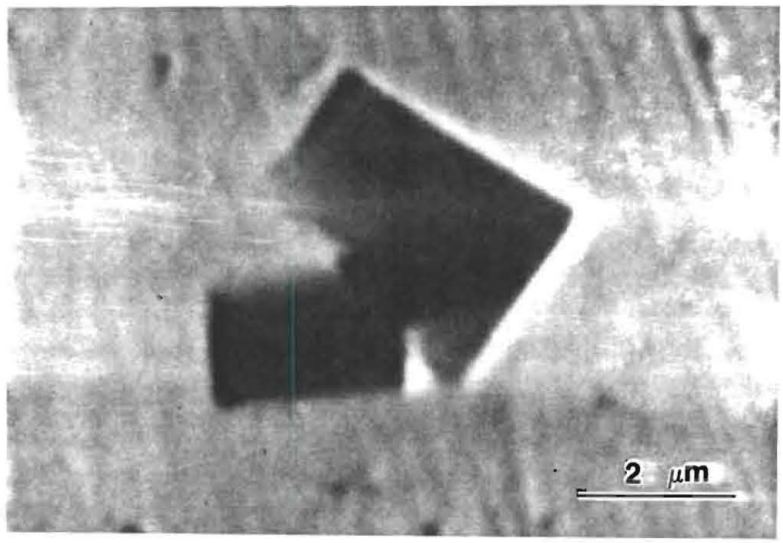

Figure 4.5
TiN Inclusion in HY-80 steel (11.1 Kx)

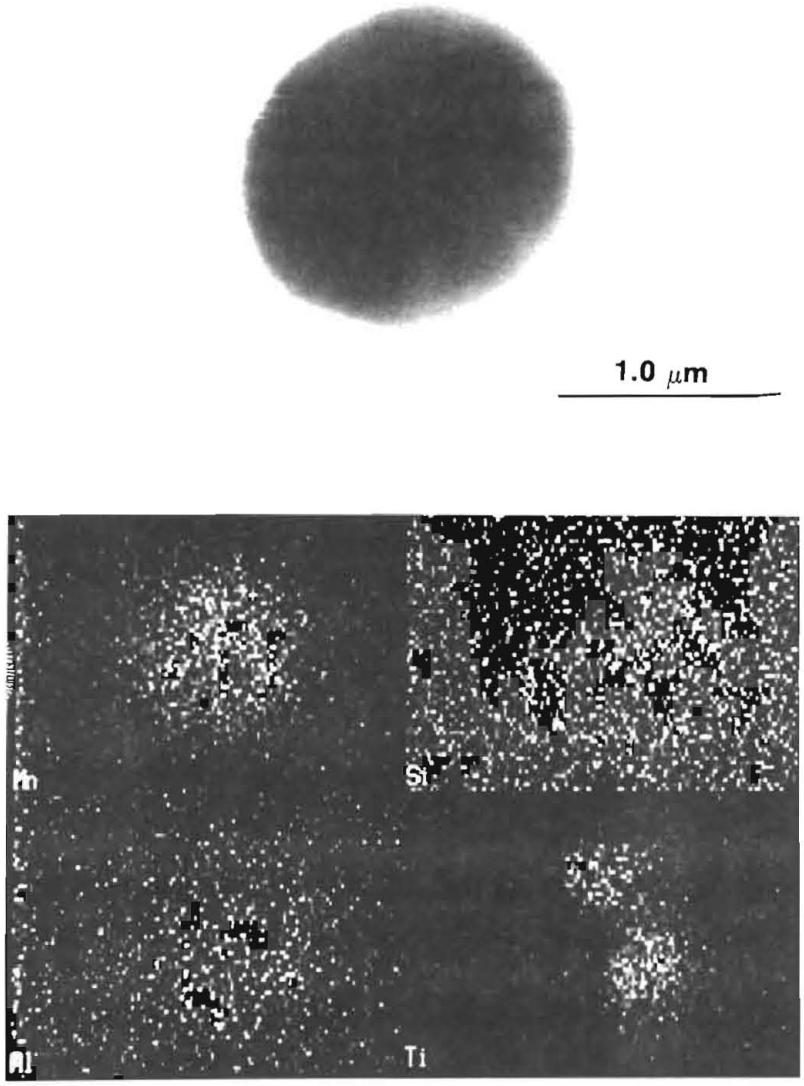

Figure 4.6
GMAW Inclusion (31.3 Kx)(top), x-ray map showing titanium-rich phase (bottom).

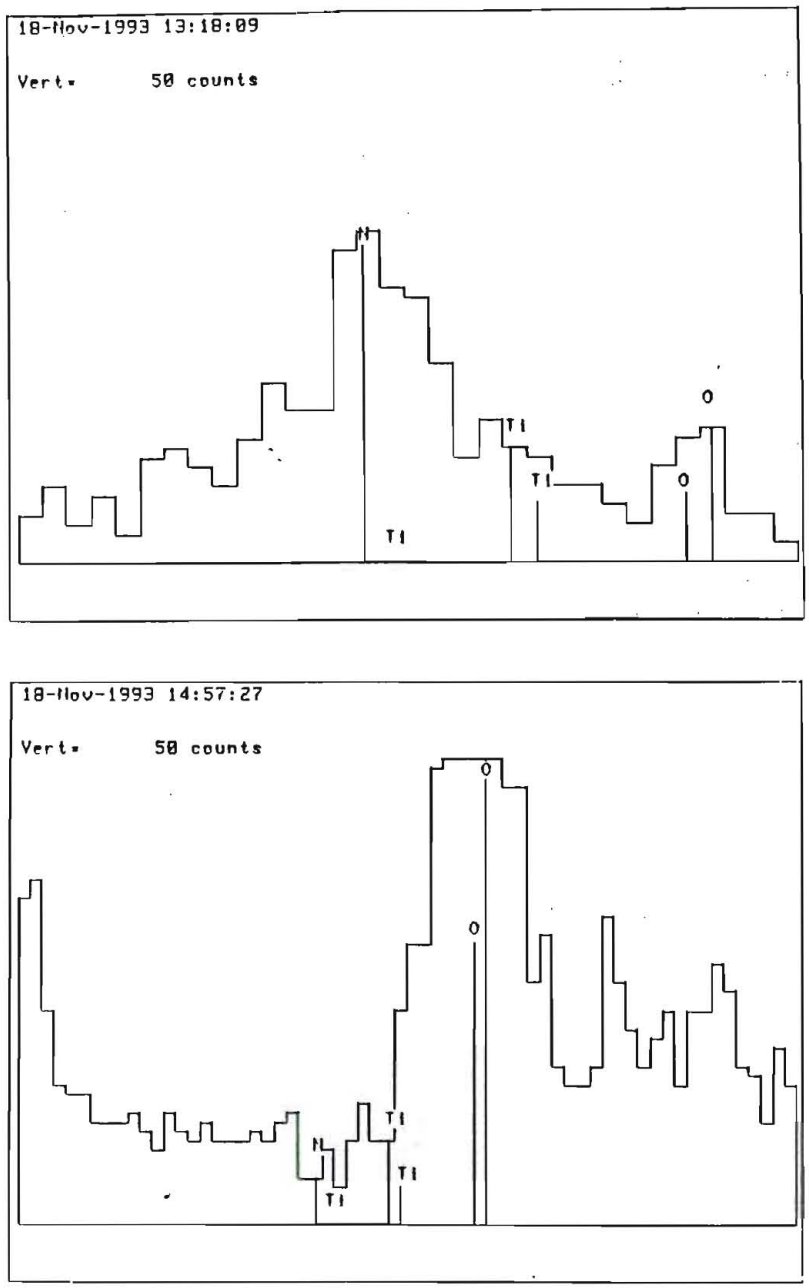

Figure 4.7
SEM EDX Spectrums in the vicinity of the oxygen and nitrogen K-lines, TiN inclusion (top), GMAW inclusion (bottom).

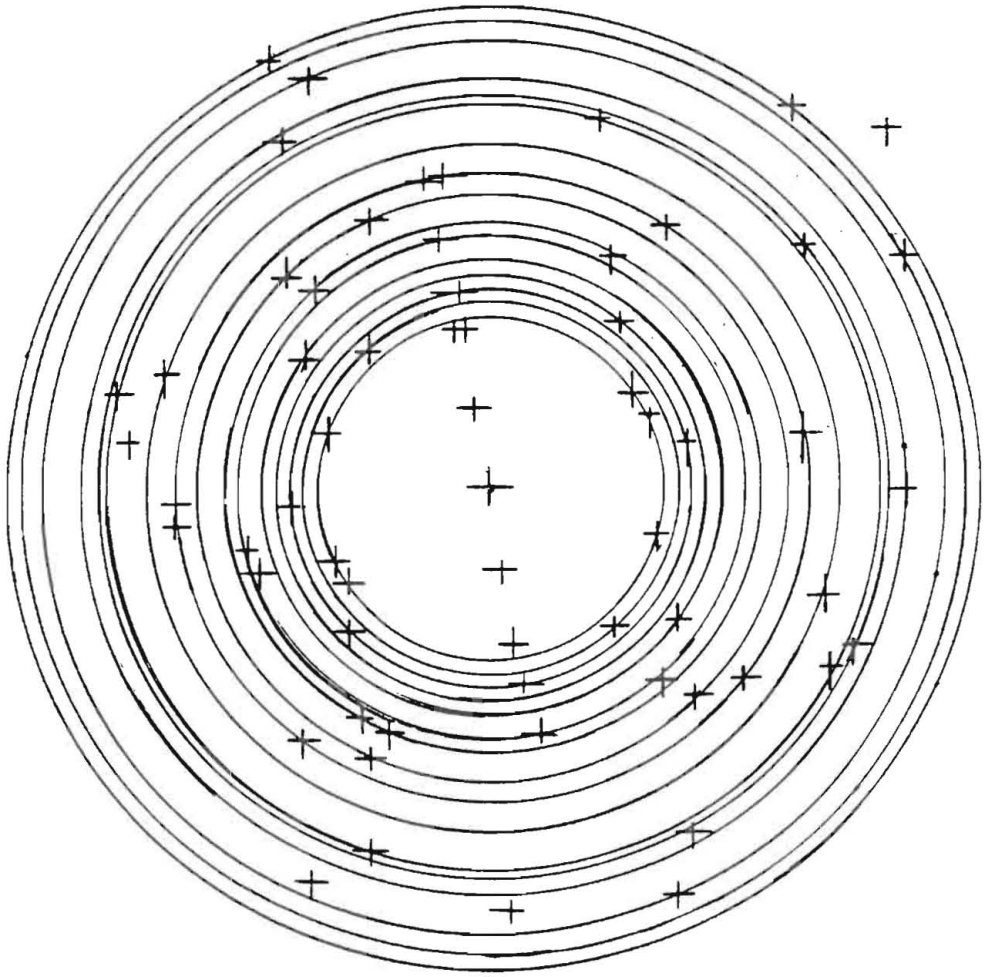

Figure 4.8
Pyrophanite ring pattern superimposed on an HVEM diffraction pattern taken from a titanium-containing oxide inclusion in a SAW weldment.

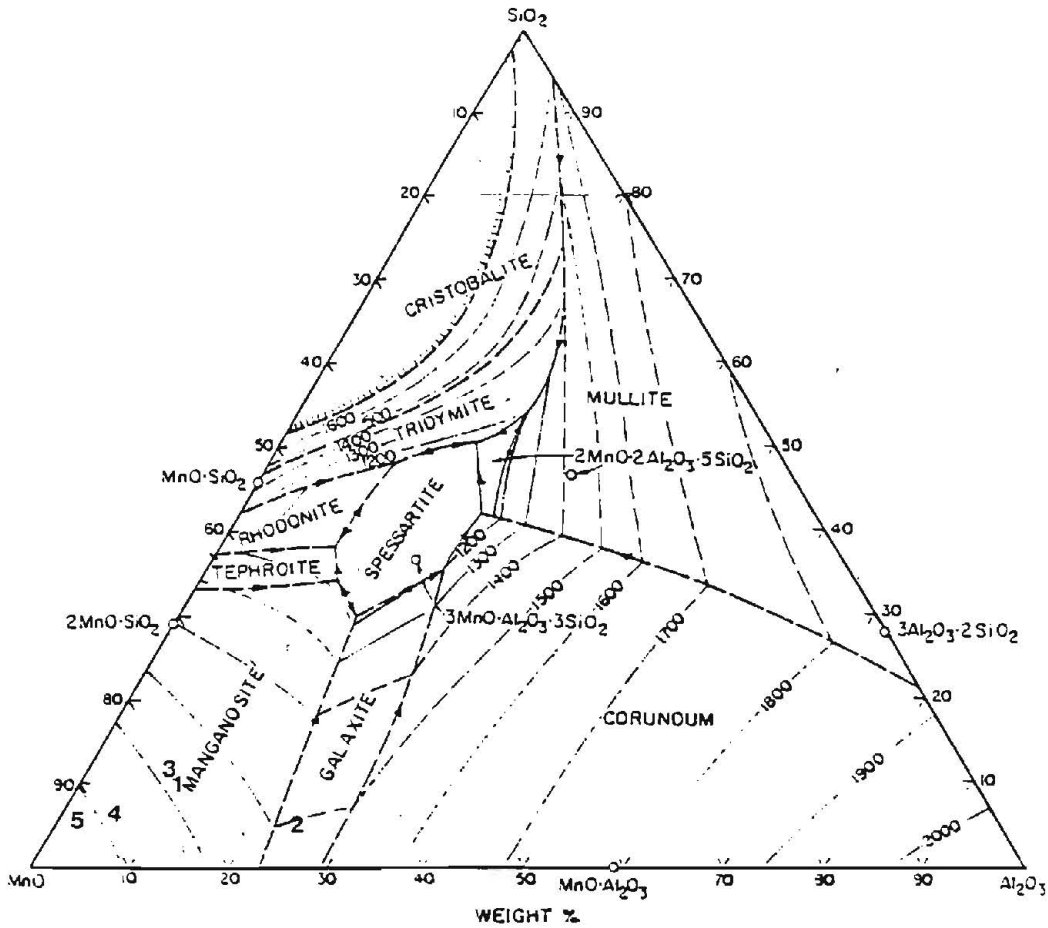

NUMBER	SAMPLE	AVERAGE wt% $MnO-AL_2O_3-SiO_2$
1	F289	80.0-10.8-9.2
2	F292	70.4-24.6-5.0
3	F293	80.5-8.4-11.1
4	F295	87.0-6.3-6.7
5	F296	92.4-2.1-5.5

Figure 4.9
SAW Inclusion Oxides [Mori, 1981]

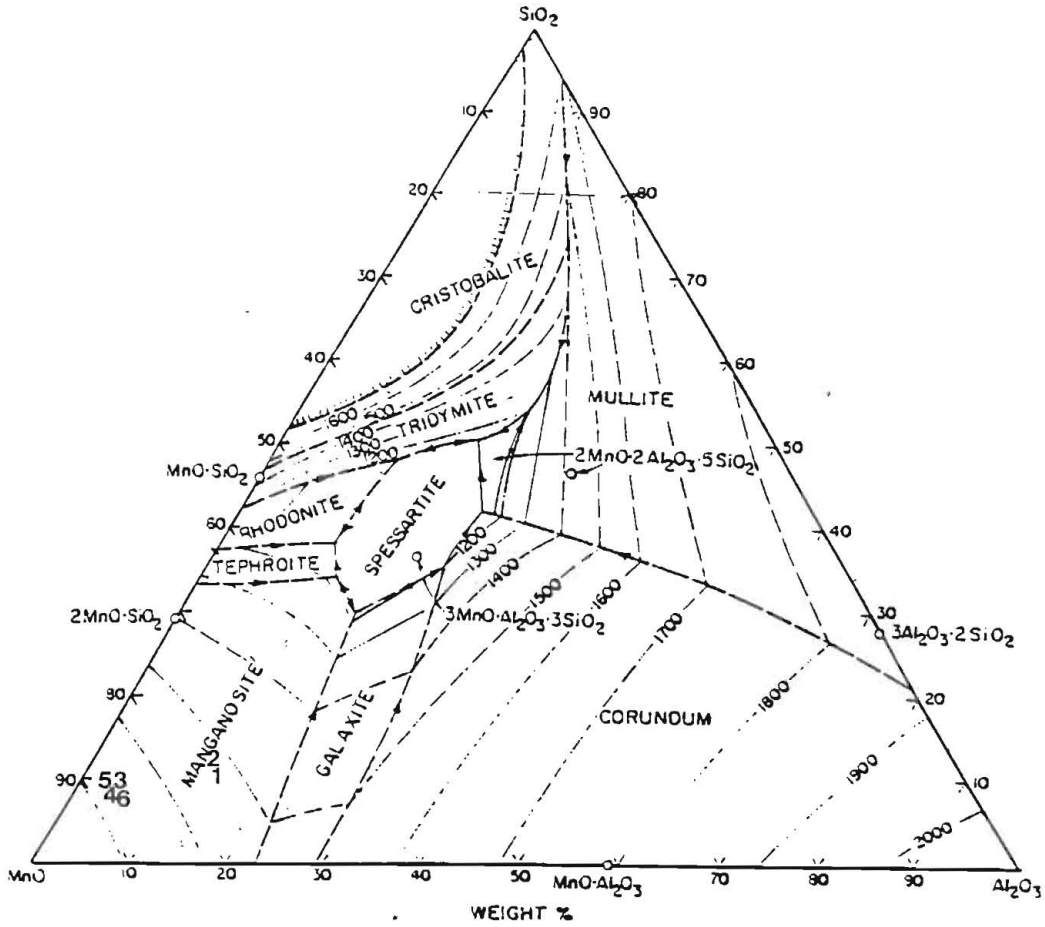

NUMBER	SAMPLE	AVERAGE wt% $MnO-AL_2O_3-SiO_2$
1	M2	75.7-14.3-10.0
2	MIDPT	75.0-12.4-12.6
3	C5	84.5-5.0-10.5
4	M4	86.9-5.1-8.0
5	C10/M4	85.7-4.4-9.9
6	C10	86.1-5.3-8.6

Figure 4.10
GMAW Inclusion Oxides [Mori, 1981]

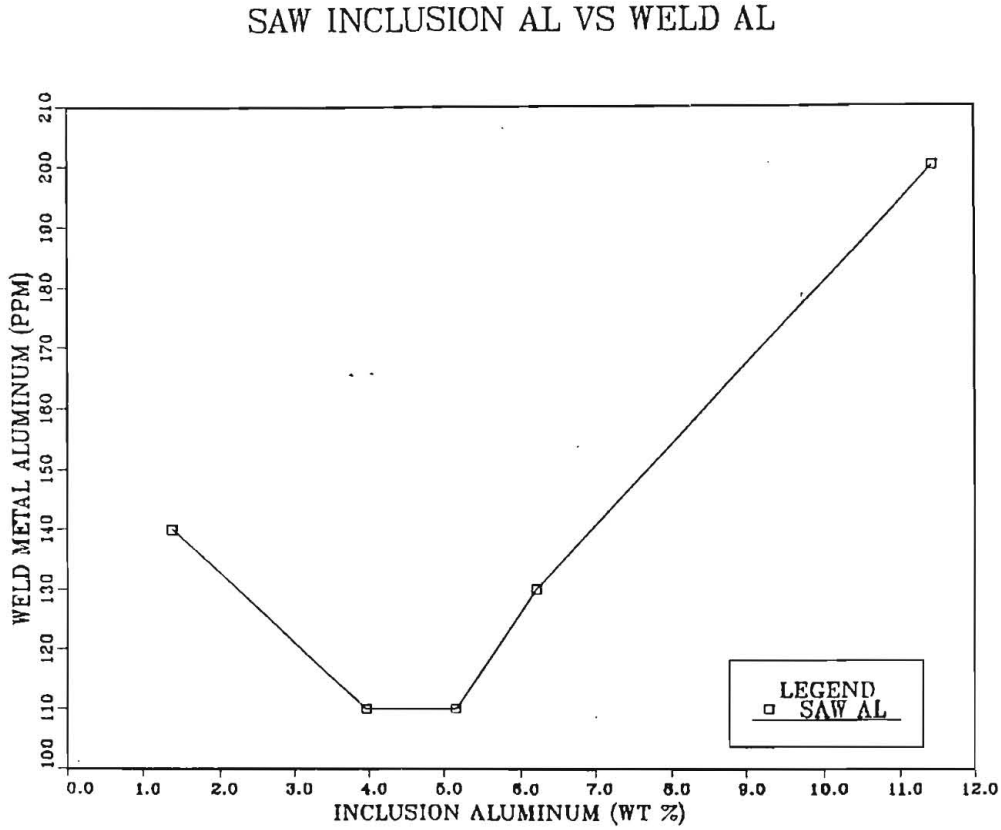

SAMPLE	INCLUSION Al	WELD METAL Al
F296	1.38	140
F295	3.96	110
F293	5.16	110
F289	6.21	130
F292	11.43	200

Figure 4.11
SAW Inclusion Al vs Weld Metal Al

SAW INCLUSION TI VS WELD TI

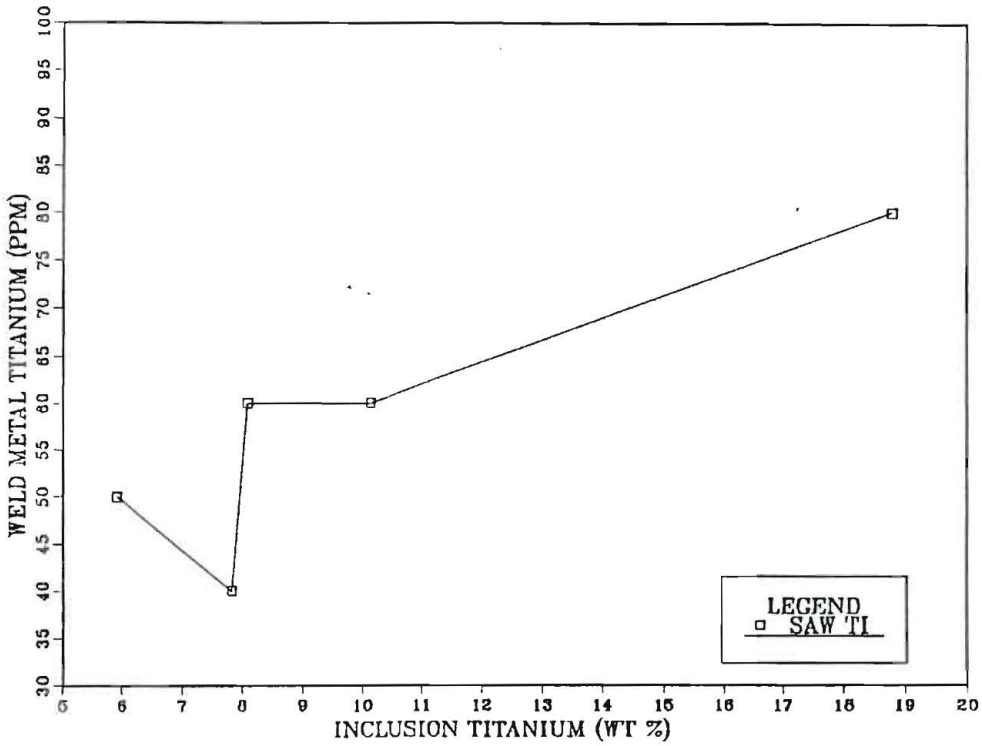

SAMPLE	INCLUSION Ti	WELD METAL Ti
F295	5.92	50
F293	7.83	40
F296	8.09	60
F289	10.13	60
F292	18.79	80

Figure 4.12
SAW Inclusion Ti vs Weld Metal Ti

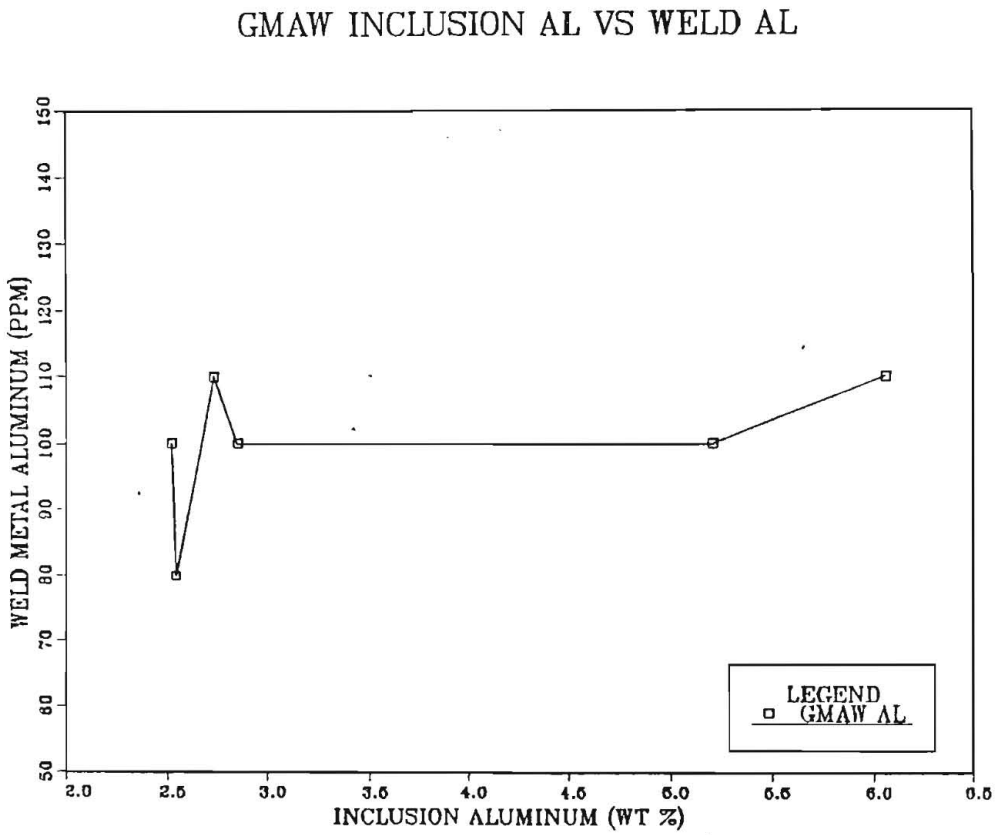

SAMPLE	INCLUSION Al	WELD METAL Al
C10/M4	2.52	100
M4	2.54	80
C5	2.73	110
C10	2.85	100
MIDPT	5.21	100
M2	6.06	110

Figure 4.13
GMAW Inclusion Al vs Weld Metal Al

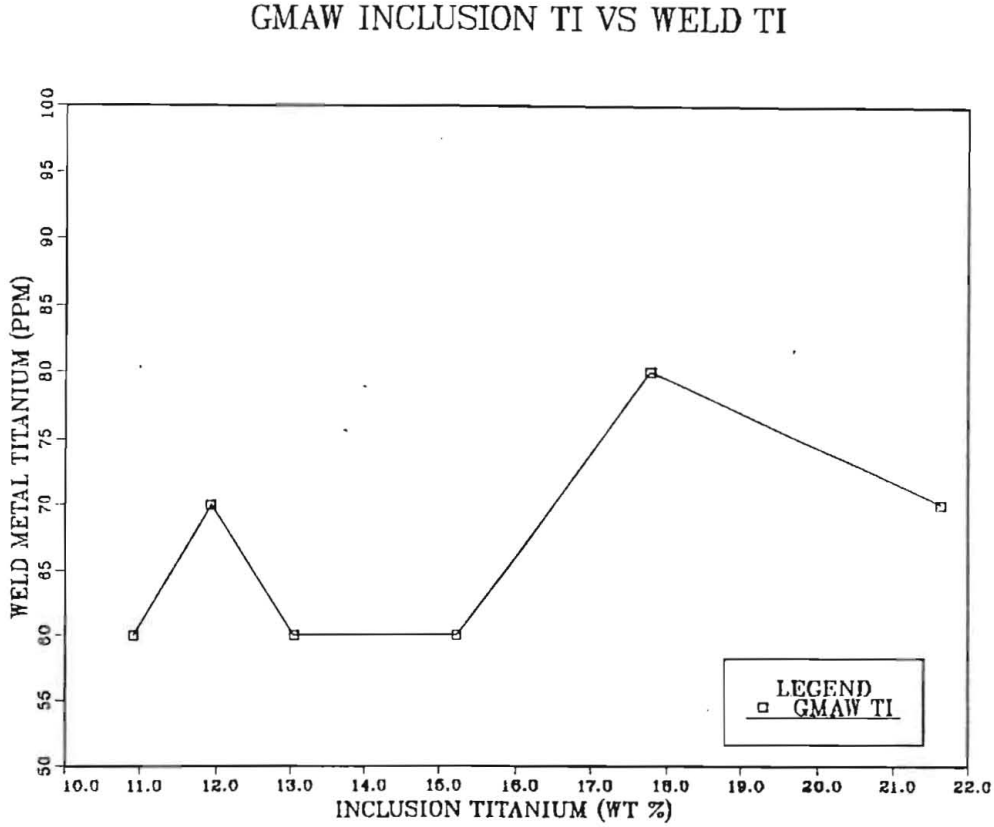

SAMPLE	INCLUSION Ti	WELD METAL Ti
C10/M4	10.92	60
C5	11.93	70
M4	13.05	60
C10	15.23	60
M2	17.79	80
MIDPT	21.64	70

Figure 4.14
GMAW Inclusion Ti vs Weld Metal Ti

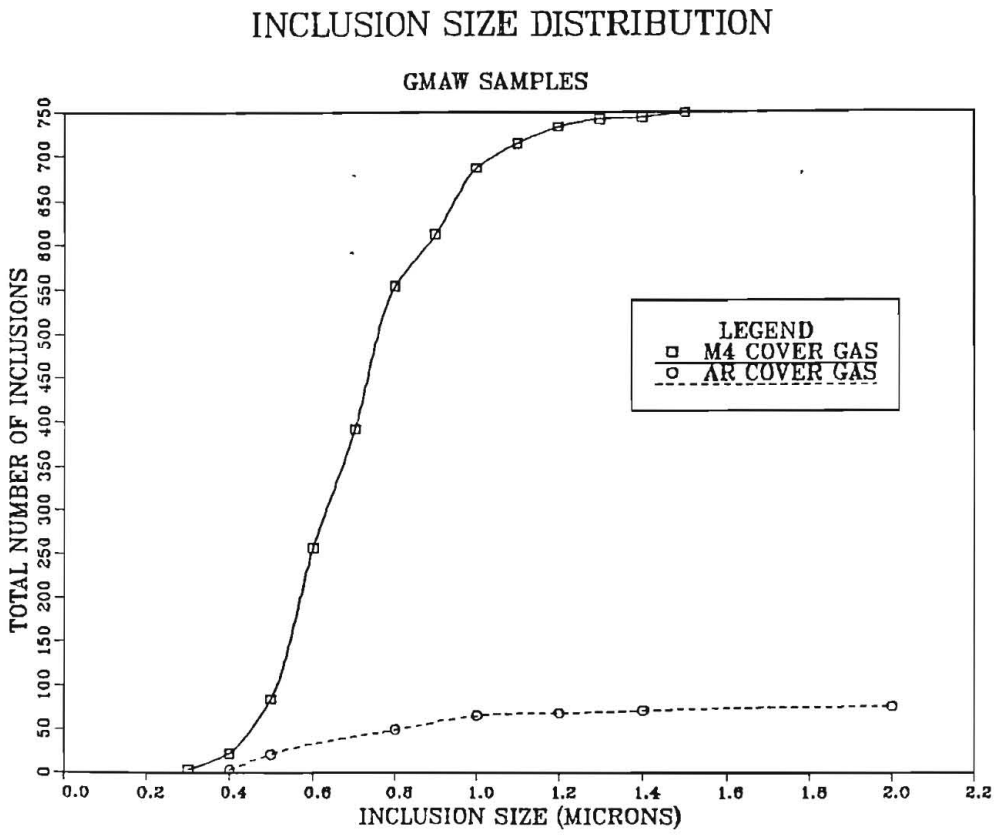

Figure 4.15
GMAW Size Distribution (data in Table 3.9)

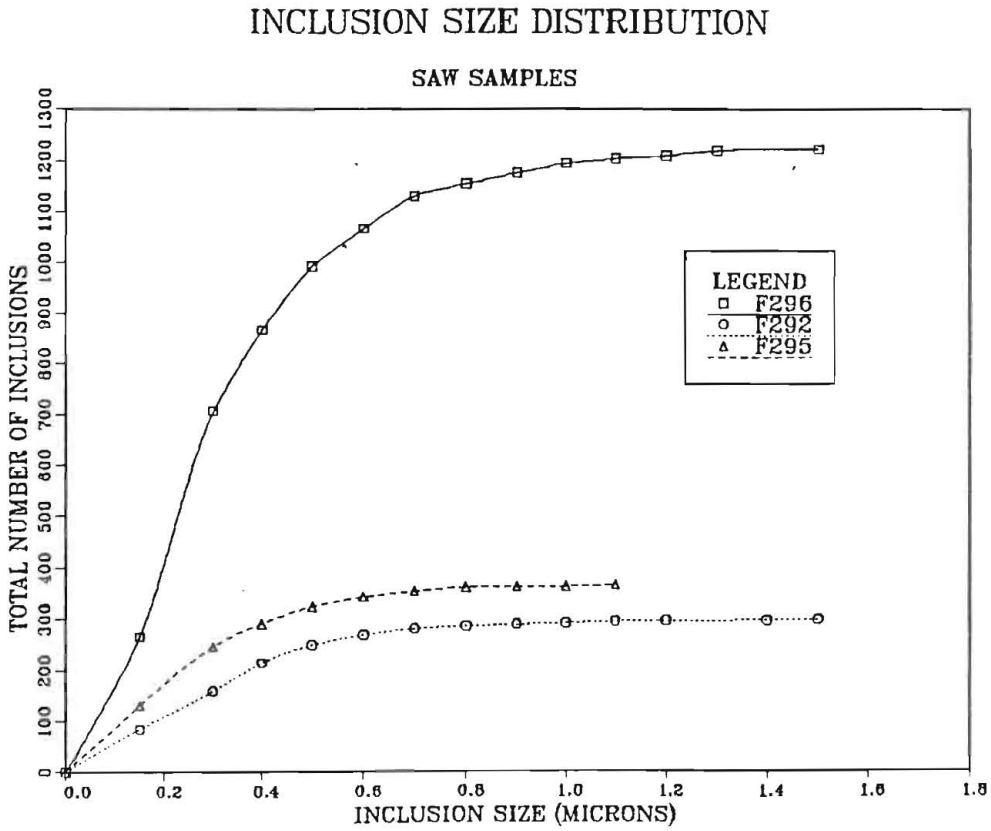

Figure 4.16
SAW Size Distribution (data in Table 3.8)

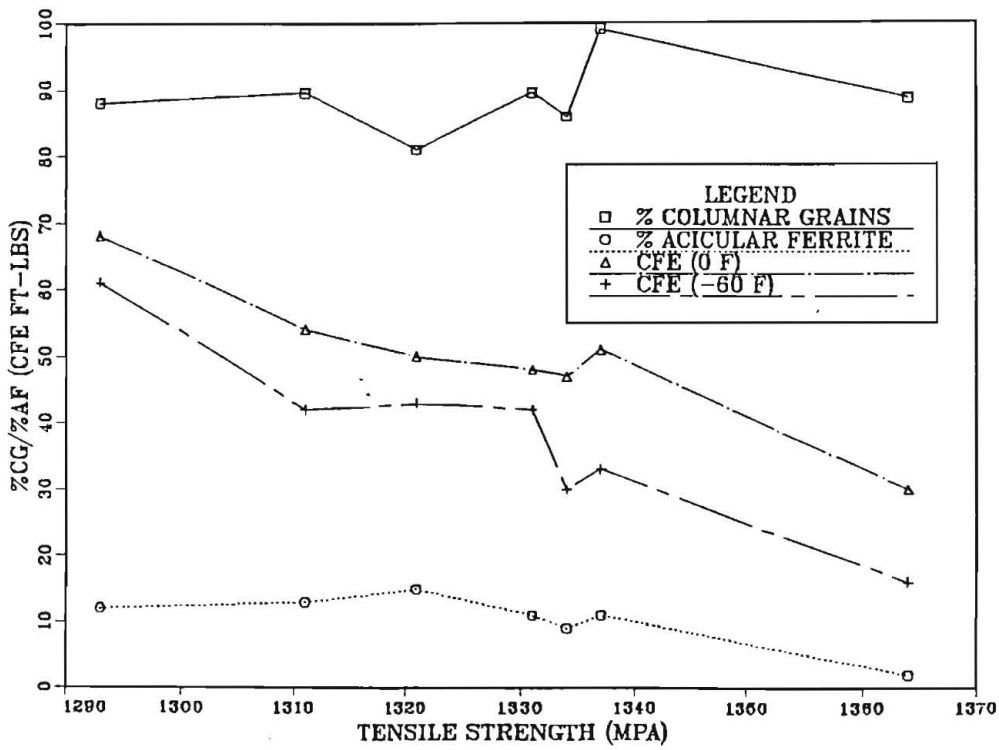

SAMPLE	TS (MPa)	%CG	%AF	CFE (0°F)	CFE (-60°F)
M4	1293	88	12	68	61
C10/M4	1311	90	13	54	42
M2	1321	81	15	50	43
C10	1331	90	11	48	42
C5	1334	86	9	47	30
MIDPT	1337	99	11	51	33
Ar	1364	89	2	30	16

$$TS\,(MPa) = 15.4\{16 + 125\,(C) + 15\,(Mn+Cr) + 12\,(Mo) + 6\,(W) + 8\,(Ni) + 4\,(Cu) + 25\,(V+Ti)\}$$ [Pickering, 1987]

Figure 4.17
GMAW Strength vs % Columnar Grains/ % Acicular Ferrite/ Charpy Fixed Energy

GMAW WELD MN VS %CG/%AF/CFE

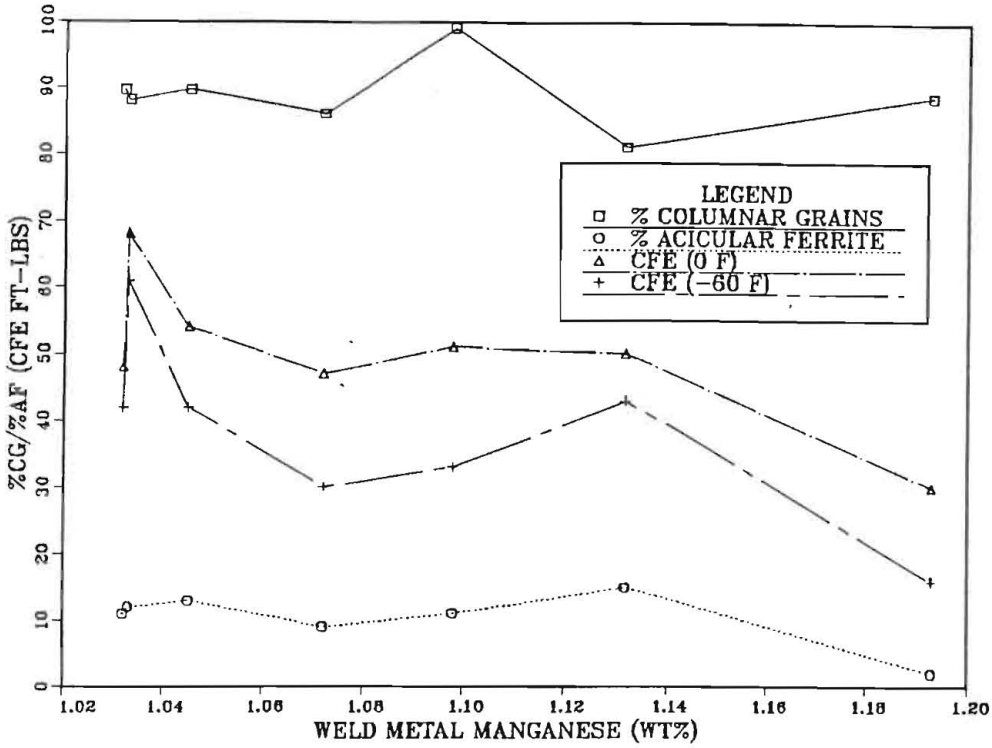

SAMPLE	Mn (wt%)	%CG	%AF	CFE (0°F)	CFE (-60°F)
C10	1.032	90	11	47	42
M4	1.033	88	12	68	61
C10/M4	1.045	90	13	54	42
C5	1.072	86	9	47	30
MIDPT	1.098	99	11	51	33
M2	1.132	81	15	50	43
Ar	1.193	89	2	30	16

Figure 4.18
GMAW Weld Mn vs % Columnar Grains/ % Acicular Ferrite/ Charpy Fixed Energy

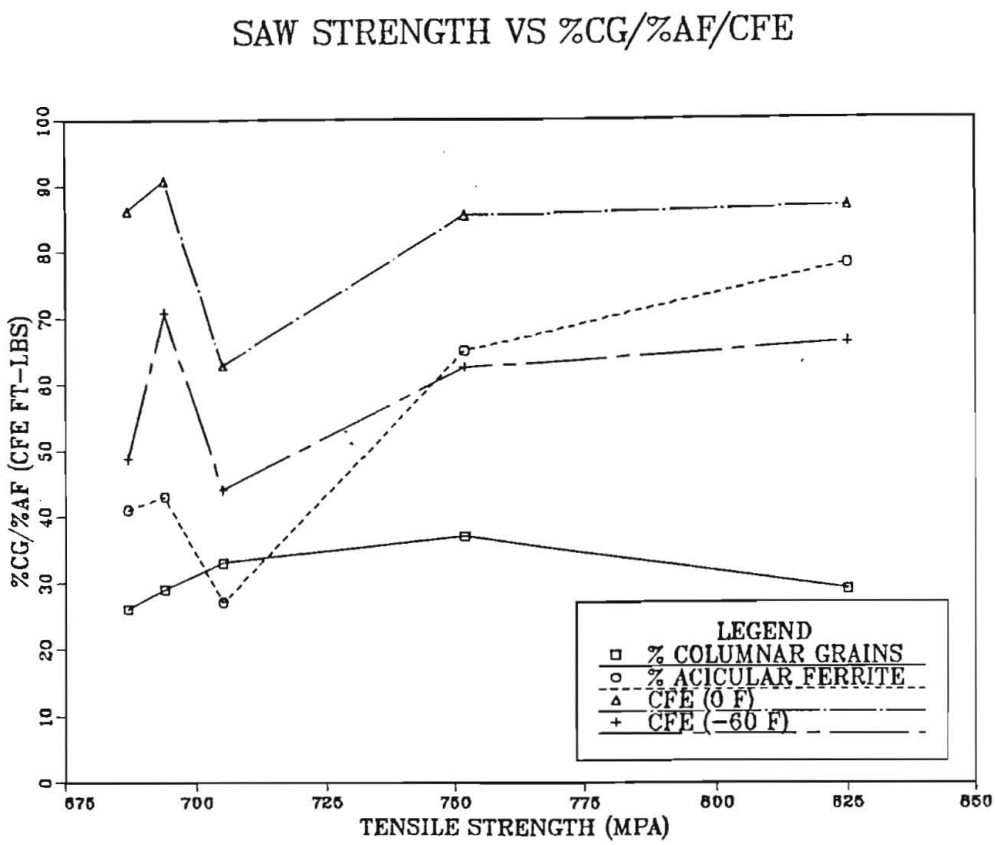

SAMPLE	TS (MPa)	%CG	%AF	CFE (0°F)	CFE (-60°F)
F293	687	26	41	86.1	48.7
F289	694	29	43	90.6	70.7
F295	705	33	27	62.8	44
F292	752	37	65	85.3	62.5
F296	825	29	78	86.6	66.2

Figure 4.19
SAW Strength vs % Columnar Grains/ % Acicular Ferrite/ Charpy Fixed Energy

SAW DBTT VS CG/AF/WELD MN

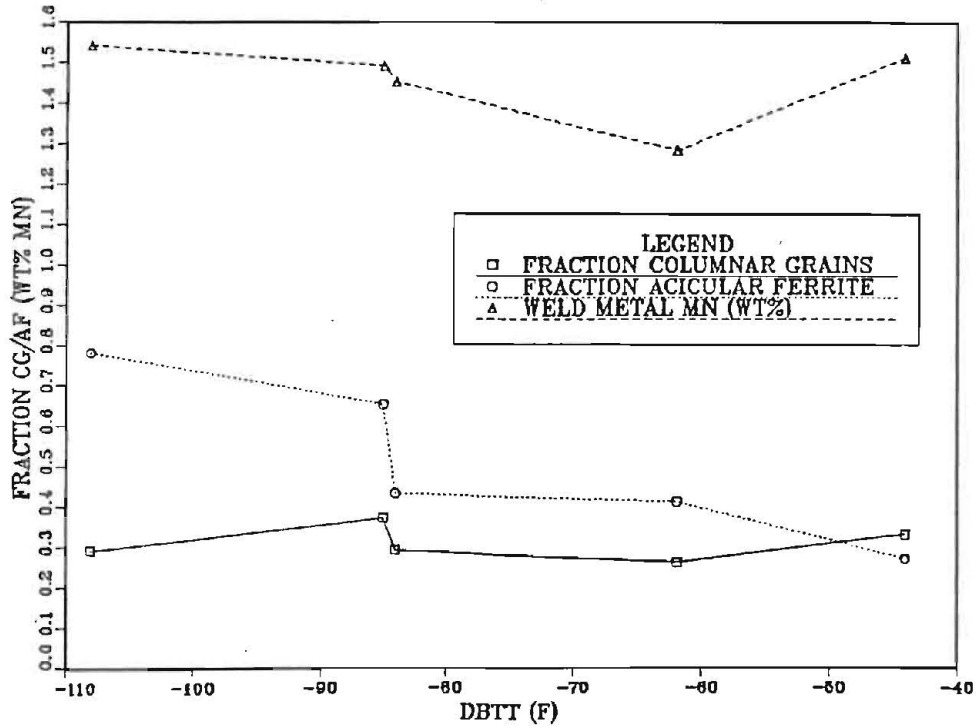

SAMPLE	DBTT (°F)	CG	AF	WELD Mn	TS (MPa)
F296	-108	.29	.78	1.54	825
F292	-85	.37	.65	1.49	752
F289	-84	.29	.43	1.45	694
F293	-62	.26	.41	1.28	687
F295	-44	.33	.27	1.51	705

Figure 4.20
SAW DBTT vs % Columnar Grains/ % Acicular Ferrite/
WELD Metal Mn

TABLE 4.1 WELD THERMAL CYCLE

	GMAW bead-on-plate	GMAW multi-pass	SAW multi-pass
efficiency (n)	.7	.7	.95
power input (E) (KJ/mm)	1.717	1.717	2.177
interpass temp (T_o)	RT	150	250
$dt_{8/5}$ (sec)	6.00	7.57	16.29

TABLE 4.2 SAW SAMPLE COMPARISON

SAMPLE	F292	F295
% ACICULAR FERRITE	65	27
# OF INCLUSIONS	297	364
AVE INCL SIZE (microns)	.378	.323
INCL VOL FRACTION	.185	.165
BI	2.83	2.63
WELD OXYGEN (wt%)	.027	.035
WELD Mn (wt%)	1.49	1.51
WELD Al (wt%)	.020	.011
WELD Ti (wt%)	.008	.005
INCL Al (wt%)	11.40	3.95
INCL Ti (wt%)	18.79	5.92

TABLE 4.3 FLUX BASICITY INDEX/ACICULAR FERRITE

[Kettel, 1993]

SAMPLE	FLUX	BI	% ACICULAR FERRITE
F289	Oerlikon OP121TT (Eisenberg)	2.65	43
F292	Oerlikon OP121TT (Houston)	2.83	65
F293	Kobe PFH80AK	2.75	41
F295	L-TEC 651 VF	2.63	27
F296	Lincoln MIL800	2.97	78

V. SUMMARY

A. CONCLUSIONS

Volume fraction of non-metallic inclusions in the weld deposit is not a good measure of the inclusion field's ability to promote the formation of acicular ferrite. The number and size distribution of the inclusions combined with the titanium and aluminum content of the inclusions provides better data for analyzing inclusion field effectiveness.

To enhance the ability of the inclusion field to promote the formation of acicular ferrite, inclusions should contain large amounts of aluminum or titanium to form angular phases such as Galaxite or Pyrophanite. Inclusion composition can be controlled by controlling weld metal composition if oxygen concentrations in the weld metal are optimized near 300 ppm. Achieving a total weld metal composition that contains 300 ppm oxygen, 1.5 weight percent manganese (SAW) or about 1.0 manganese (GMAW) and a combined titanium plus aluminum concentration of near 300 ppm appears optimum for formation of large proportions of acicular ferrite in the weld deposit.

For the steels studied in the present work the inclusions are composed of two primary phases. A titanium-rich phase Pyrophanite, $MnTiO_3$, is an angular phase that is a requirement for nucleation of acicular ferrite on the inclusions. The

second phase is a complex Mn-Al-Si oxide that exists as Manganosite for low concentrations of aluminum in the weld metal (< 200 ppm) or Galaxite for higher aluminum concentrations. Manganosite forms spherical inclusions that are not good sites for nucleation of acicular ferrite. Galaxite forms more angular inclusions and has been shown to be an effective site for nucleation of acicular ferrite like the titanium-rich phase, Pyrophanite.

Pyrophanite is more effective for promoting the formation of acicular ferrite than Galaxite. This appears to be a result of the formation temperature of the phases. Galaxite forms in the molten weld pool at 1800 °C. Pyrophanite forms after the weld metal has solidified, at 1400 °C, creating a much larger strain field in the surrounding matrix. This strain field could provide the energy required for the nucleation of the acicular ferrite on the inclusion.

A large volume fraction of inclusions generated by a large number of medium sized inclusions, average size 0.3 to 0.5 microns, is effective for producing large proportions of acicular ferrite in the weld deposit, even if inclusion composition is not optimum. This conclusion is generated by the results of SAW weldment F296 which contained the largest proportion of acicular ferrite in the weld metal. Both strength (825 MPa) and fracture toughness (DBTT = -108 °F) were the best of the five samples analyzed. However, the

reason that such an optimum inclusion field was generated could not be explained.

Weld filler wire and/or flux must be chosen carefully to maintain an optimum concentration of manganese in the weld metal. This optimum concentration appears to be about 1.5 weight percent in SAW weldments and 1.0 weight percent in GMAW weldments. This optimum manganese concentration enhances fracture toughness by promoting the formation of acicular ferrite (lowers austenite to ferrite transformation temperature) and generally refining the final microstructure of the weld deposit. Low concentrations of manganese restrict the amount of acicular ferrite formed. High concentrations of manganese increase hardenability and strength to the point that loss of fracture toughness from these factors overshadows any benefits.

Fracture toughness of the weld deposit is controlled through the interaction of four variables. High tensile strength welds tend to have lower fracture toughness due to the microstructures providing the strength (bainite and martensite) being susceptible to crack propagation. An optimum manganese concentration is required to promote the formation of acicular ferrite and refine the microstructure of the weld deposit. High proportions of acicular ferrite in the weld deposit are good for both strength and fracture toughness. Columnar grains in the weld deposit are detrimental to fracture toughness. High strength welds with excellent

fracture toughness can be achieved by maintaining optimum weld manganese concentration, low percentage of columnar grains and high percentages of acicular ferrite.

In general SAW weldments will have better fracture toughness than GMAW weldments. This condition exists because the low heat input of the GMAW weldments does not refine the previous weld passes as effectively as the SAW weldments with higher heat inputs. This creates large amounts of columnar grains in the weld deposit which are detrimental to fracture toughness.

B. RECOMMENDATIONS

The large number of medium sized inclusions in SAW sample F296 proved optimum for formation of acicular ferrite. Weld metal composition and other weld parameters seemed to be in the middle of the range of the other samples tested. It appears that more of the oxygen in the weld metal is contained in the inclusions as oxides rather than as dissolved oxygen. No feasible explanation for this phenomena could be found during this investigation. Due to high strength and excellent fracture toughness, this weld should be reexamined to see if the same inclusion field can be recreated and studied to determine the reason for its occurrence.

Without fully understanding the reasons for the conditions existing in SAW sample F296, Naval construction programs should use the flux used for SAW sample F292 for SAW

weldments(Oerlikon OP121TT). This flux produced a high strength weld (752 MPa) with good fracture toughness properties (DBTT = -85 °F) by providing optimum conditions for the formation of acicular ferrite.

GMAW weldments have poor fracture toughness due to a low percentage of acicular ferrite in the weld deposit and large percentage of columnar grains. To improve fracture toughness, one or both of these conditions must be improved. To promote the formation of more acicular ferrite a weld composition containing more titanium and/or aluminum and more oxygen must be achieved. Due to the limitations of heat input in the GMAW process, other means to promote the formation of more equixaed grains in the weld deposit. The use of a flux cored weld wire could improve fracture toughness by creating welds with higher oxygen, titanium and aluminum concentrations thus forming more acicular ferrite and providing more heterogeneous nucleation sites in the weld pool to reduce the amount of columnar grains formed.

LIST OF REFERENCES

Abson D.J., Investigation Into the Role of Non-metallic Inclusions on Ferrite Nucleation in Carbon Steel Weld Metals, The Welding Institute Members Report 67, 1978.

Abson D.J. and Pargeter R.J., Facyors Influencing As-Deposited Strength, Microstructure and Toughness of Manual Metal Arc Welds Suitable for C-Mn Steel Fabrications, pp 142-148, 152-165, 174-178, International Metals Review, v.31, No. 4, 1986.

Bhatti A.R., Saggese M.E., Hawkins D.N., Whiteman J.A. and Golding M.S., Analysis of Inclusions in Submerged Arc Welds in Microalloyed Steels, pp 224s-230s, Welding Research Supplement, July 1984.

Bonnet C. and Charpentier F.P.,Effect of Residual, Impurity and Microalloying Elements on Weldability and Weld Properties, Proc. International Conference, London, The Welding Institute, Paper 8, November 1983.

Court S.G. and Pollard G., Microanalysis of Weld Metal Inclusions, pp 427, Journal of Materials Science Letters 4, 1985.

Czyryca E.J., Link R.E., Wong R.J., Aylor D.M., Montemarano T.W. and Gudas J.P., Development and Certification of HSLA-100 Steel Products, pp 64-65, Naval Engineers Journal, v.102,no.3, May 1990.

Department of the Navy Military Specification MIL-E-23765/2D(SH) Amendment 1, Electrodes and Rods - Welding, Bare, Solid or Alloyed Cored, Low Alloy Steel, pp 9, 23 October 1990.

Dolby R.E., Factors Controlling Weld Toughness - the Present Position, The Welding Institute Members Report 14, 1976

Douglas B.A., Nonmetallic Inclusions in HSLA Steel Weldments, Masters Thesis, Naval Postgraduate School, Monterey, Ca., 1989.

Dowling J.M., Corbett J.M. and Kerr H.W., Inclusion Phases and the Nucleation of Acicular Ferrite in Submerged Arc Welds in High Strength Low Alloy Steels, pp 1611-1622, Metallurgical Transactions A, v.17A, September 1986.

Edmonds D.V. and Cochrane R.C., Structure-Property Relationships in Bainitic Steels, pp 1533, Metallurgical Transactions A, v.21A, June 1990.

Evans G.M., The Effect of Titanium in Manganese Containing SMA Weld Deposits, pp 447s-454s, Welding Research Supplement, March 1993.

Farrar R.A. and Watson M.N., Effects of Oxygen and Manganese on Submerged Arc Weld Metal Microstructures, pp 285-286, Metal Construction, 1979.

Harrison P.L. and Farrar R.A., Influence of Oxygen Rich Inclusions on the Delta Ferrite to Austenite Phase Transformation in HSLA Steel Weld Metals, pp 2218, Journal of Materials Science, 1981.

Flax R.W., Kieth R.E. and Randall M.D., Welding the HY Steels, pp 2, ASTM Special Technical Publication 494, 10 May 1971.

Gibson H., Influence of Shielding Gas Composition on Alloy Recovery During Gas Metal Arc Welding, Masters Thesis, Massachusetts Institute of Technology, Cambridge, Ma., 1993.

Graville B.A., Proceeding Welding of HSLA (Microalloyed) Structural Steels (ROMS), pp 29, Metals Park, 1978.

Grong O. and Matlock D.K., Microstructural Development in Mild and Low-alloy Steel Weld Metals, pp 27-46, International Metals Reviews, v.31, 1986.

Haddock J.T., An Investigation of a New Magnesium Based Reagent for the Ladle Treatment of Steel, pp 6-10, PHD Thesis, University of Wolverhampton, United Kingdom, 1988.

Kettell K.W., Correlation of Flux Composition and Inclusion Characteristics with Submerged Arc Weld Metal Properties in HY-100 Steel, Masters Thesis, Naval Postgraduate School, Monterey, Ca., 1993.

Kirkwood P.R., Microstructural and Toughness Control in Low Carbon Weld Metals, pp 260-264, Metal Construction, May 1978.

Kou S., Welding Metallurgy, pp 16-18, John Wiley and Sons, 1987.

Metals Handbook, pp 114, 155, 9th edition, American Society for Metals, v.1 and 6, 1983.

Mori N., Homma H., Okita S. and Wakabayashi M.,Mechanism of Notch Toughness Improvement in Ti-B Bearing Welds,

International Institute of Welding, IIW Document 1196-81, 1981.

Olson D.L., Dixon R. and Liby A.L., Welding Theory and Practice, pp 123-129, 134-146, North-Holland, 1990.

Pargeter R.J., Investigation Into Submerged Arc Weld Metal Inclusions, The Welding Institute Members Report 151, 1981.

Peters D.J., Submerged Arc Welding Comsumables for HSLA-100 Steel, Masters Thesis, Massachusetts Institute of Technology, Cambridge, Ma., 1989.

Philbrook W.D., pp 187-201, International Metals Review, v.22, 1977

Pickering F.B., Physical Metallurgy and the Design of Steels, pp 106, Applied Science Publishers LTD, London, 1978.

Ramsay C.W., Matlock D.K. and Olson D.L., Influence of Weld Metal Inclusion Type, Content and Size Distribution on the Microstructure and Properties of High Strength Steel Weld Metal, pp 21, 37-52, Final Technical Report 15, October 1988.

Saggese M.E., Hawkins D.N. and Whiteman J.A., Effect of Residual, Impurity and Microalloying Elements on Weldability and Weld Properties, The Welding Institute paper 15, November 1983.

Senogles D.J., PHD, University of Leeds, United Kingdom, 1994.

Seraiva R.A., The Study of Single-Pass GMA Welds with Different Cover Gas Compositions on GSLA-100 Steel, Masters Thesis, Naval Postgraduate School, Monterey, Ca., 1993.

Shackleton D.N., The Welding of HY100 and HY130 -- Literature Review, pp 287, The Welding Institute, 1972.

Terashima H. and Hart P.H.M., Effect of Residual, Impurity and Microalloying Elements on Weldability and Weld Properties, Proc. International Conference, London, The Welding Institute, Paper 27, November 1983.

Yang J.R. and Bhadeshia H.K.D.H., Thermodynamics of the Acicular Ferrite Transformation in Alloy-Steel Weld Deposits, pp 187-191, International Conference on Trends in Welding Research, ASM International, 1989.

INITIAL DISTRIBUTION LIST

		No. Copies
1.	Defense Technical Information Center Cameron Station Alexandria VA 22304-6145	2
2.	Library, Code 052 Naval Postgraduate School Monterey CA 93943-5002	2
3.	Naval Engineering Curricular Office, Code 34 Naval Postgraduate School Monterey CA 93940-5000	1
4.	Department Chairman, Code ME Department of Mechanical Engineering Naval Postgraduate School Monterey CA 93940-5000	1
5.	Dr. Alan G. Fox, Code ME/FX Department of Mechanical Engineering Naval Postgraduate School Monterey CA 93940-5000	2
6.	Mr. Gene Franke Naval Surface Warfare Center Carderock Division, Annapolis Detachment Code 615, 3A Leggett Circle Annapolis MD 21402-5067	1
7.	Mr. R. Wong Naval Surface Warfare Center Carderock Division, Annapolis Detachment Code 615, 3A Leggett Circle Annapolis MD 21402-5067	1
8.	Mr. Michael G. Vassilaros Naval Surface Warfare Center Carderock Division, Annapolis Detachment Code 615, 3A Leggett Circle Annapolis MD 21402-5067	1
9.	Daniel G. Brothers 2450 SW 38th Street #73 Ocala FL 32674	2